A Comparative Experimental Study on Natural Organic Matter Degradation by Electrochemical Oxidation on Boron Doped Diamond and Mixed Metal Oxide Electrodes

by

Shasvat Rathod

A thesis

presented to the University of Waterloo

in fulfilment of the

thesis requirement for the degree of

Master of Applied Science

in

Mechanical and Mechatronics Engineering

Waterloo, Ontario, Canada, 2020

Author's Declaration

I hereby declare that I am the sole author of this thesis. This is a true copy of the thesis, including any required final revisions, as accepted by my examiners.

I understand that my thesis may be made electronically available to the public.

Abstract

Natural organic matter (NOM) pollutants have complexified water treatment facilities and their direct methods for water disinfection. Furthermore, untreated NOM in water networks can lead to property damage in water plumbing and drainage systems, taste and odor challenges, color, bacterial growth in the water distribution systems, and formation of carcinogenic disinfection by-products. Electrochemical treatments, through the production of oxidative species such as OH·, can mineralize organic pollutants. Additionally, electrochemical treatments are useful for the removal of various new age (growing prominent in the last 20 years) pollutants such as phenolic compounds, synthetic dyes, pesticides and drugs, surfactants, and industrial wastewater. In recent years, BDD electrodes have received considerable attention for nonselective NOM removal. Nonetheless, due to the difficulties of NOM characterization and lack of universal standards of measurements for NOM degradation, BDD electrodes have lagged behind for large scale applications. The adoption of an electrochemical technology as an effluent treatment must consider some aspects in order to make its implementation feasible, such as but not limited to performance of anode material and energy consumption. Therefore, a detailed study of NOM removal by BDD electrodes is necessary for long-term goals with BDD anode electrochemical treatment.

Firstly, this study directly compares BDD electrode performance for NOM oxidation to widely documented mixed-metal oxide anodes (MMO, dimensionally stable anodes). Three treatment setups were tested in batch mode, recorded as (M1) BDD anode and BDD cathode, (M2) BDD anode and stainless-steel cathode, and (M3) MMO anode and stainless-steel cathode. In an attempt to provide a complete discussion, several NOM characterization methods were utilized: total organic compound (TOC), chemical oxygen demand estimated by peCOD (COD), ultraviolet at the 254 nm wavelength (UV_{254}), specific ultraviolet absorbance (SUVA), specific energy

consumption, and COD/TOC ratio. The performance was successfully gauged under several parameters such as initial pH, duration of electrolysis, and applied current density.

Secondly, a 2nd order box-benkhen design (BBD) was employed to optimize and investigate the effects of process variables. The response surface methodology (RSM) optimized the following operating conditions: initial pH (6.5 – 8.5), electrolysis time (30 – 120 mins), and applied current density (10 – 30 mA cm^{-2}). All the statistical analyses were performed by Stat-ease Design Expert 8.0.7.1 statistical software package (Stat-Ease Inc., Minneapolis, USA).

Although the MMO electrode had better performances at lower current densities of 10 mA cm^{-2} between the 0 to 30-minute range, the removal efficiencies concretely determined that BDD electrodes exhibited higher oxidation under a broader range of operating conditions such as higher current density, increased duration, and broader pH ranges. Additionally, BDD electrodes consumed energy efficiently and outperformed MMO electrodes at higher current densities and pH, reaffirming its low capacitance and electrochemical stability. Furthermore, peCOD/TOC ratios and SUVA values determined BDD electrodes are more effective at NOM breakdown.

Derringer's optimization techniques from the BBD configuration presented electrolysis time and applied current density to have a significant effect on the electrochemical process. Whereas initial pH was confirmed to have a minimal effect on NOM removal. Pareto analysis of variance suggested peCOD estimations were not indicative for NOM and, TOC along with SUVA, provided a stronger estimation. 3D contour plots identified different mechanisms dictated NOM removal based on electrode type and pollutant. M1 and M2 (BDD anodes) were largely unaffected by initial pH, whereas longer electrolysis duration and larger applied current densities drastically improved NOM removal. On the other hand, M3 (MMO anodes) reduced in performance, at higher pH, after

an electrolysis duration of 60 minutes, and reached maximum SUVA at low applied current density.

In summary, the electrooxidation process shows promise for large scale applications to treat NOM wastewater with high removal efficiencies by monitoring electrochemical electrolysis duration and applied current density. However, the lack of a universal method of NOM characterization proposes difficulties for NOM monitoring. TOC, COD, and SUVA predicted different trends as NOM involves a complex matrix of aromatic compounds, molecular weights, and organic macromolecules. Therefore, research for a comprehensive NOM characterization method will propel the application of BDD anodic electrochemical oxidation. Additional studies to research BDD behavior under a more extensive range of operating conditions are required to maximize the removal of organics in water.

Acknowledgments

Firstly, I would like to thank Professor Norman Zhou for unparalleled support and patience in my work. Furthermore, the opportunity to access to his CAMJ research group and resources.

Secondly, I would like to thank Professor Mark Servos, and all involved in the Water Group for access to the laboratory.

Most importantly, I would like to thank Dr. Robert Liang for his guidance, advice, assistance, and there is a lack of words for the amount of help he provided.

I would like to thank all my cohort and friends in the CAMJ group. I would like to thank my parents, Amrut and Kala, who always supported and encouraged me to pursue my dreams.

Dedication

To my family

List of Figures

List of Tables

List of Equations

List of Abbreviations

AOPs: Advanced oxidation processes

BDD: Boron-doped diamond

CVD: Chemical Vapour Deposition

DBP: Disinfection by-products

DET: Direct electron transfer

DOC: Dissolved organic carbon

DSA: Dimensionally stable anodes

EAOPs: Electrochemical advanced oxidation processes

EC: Electrochemical processes

EO: Electrooxidation

MMO: Mixed-metal oxides

OH: Hydroxyl radicals

SUVA: Specific Ultraviolet Absorbance

TOC: Total organic carbon

Chapter 1. Introduction

Water, although abundant and vital to animal and plant life, is exposed to pollution as a product of human industrialization and urbanization [1]–[3]. The introduction of new chemical compounds has further intensified the adverse stressors aquatic ecosystems face, such as nutrient pollution, leaching of toxins into surface waters, and oxygen depletion. Furthermore, conventional and existing water treatment methods cannot fluidly adapt to treat new synthetic pollutants [4]. Therefore, the advancement of existing treatment approaches and the development of novel, innovative treatments are paramount to protect the environment and delicate water cycles.

Pollution by natural organic compounds has become more predominant in recent years. Although the effects of organic load on human health are relatively unknown, water utilities and treatment facilities face critical challenges from carbon-based compounds [5], [6]. Natural organic matter (NOM), when present in surface and groundwater supplies, has a significant influence on the selection, design, and operation of water treatment processes [7]. The presence of organic compounds, which include, but are not limited to, aromatics, proteins, polysaccharides, and humic substances, increase capital and ongoing costs [8][9]. Likewise, high concentrations of NOM from seasonal variability induce process control complications. Also, for water utilities, inadequate NOM removal leads to taste and odor challenges, the formation of carcinogenic disinfection by-products (DBPs), and deterioration of natural pathogen inactivation capabilities[10]. Currently, traditional methods of NOM removal processes involve coagulation and flocculation, followed by sedimentation and filtration. On the other hand, novel albeit expensive options includes magnetic ion-exchange resin techniques, activated carbon filtration, and advanced oxidation processes (AOPs)[11]–[13].

However, conventional selective techniques are not able to altogether remove all toxic and refractory organic pollutants. As a result, electrochemical advanced oxidation processes (EAOPs) have cemented themselves as promising technologies for the destruction of complex waste streams. Electrochemical techniques (EC) are innovative, inexpensive, and effective in purifying industrial influent and effluent waters before discharge or recycling[14]–[18]. Coupled with little to no chemical requirements and classified as "green" technologies that provide sustainable advantages over traditional methods[19][20]. Lastly, EAOPs degrade organics through reactive hydroxyl radicals (OH·), formed at the anode surface via oxidation, which unselectively reacts with a wide range of recalcitrant organics as highlighted in equation 1.1 [21].

Equation 1-1: Anodic surface reaction to form OH radicals

$$H_2O \rightarrow OH^- + H^+ + e^-$$

Various electrodes have been applied to EAOPs, wherein common materials include doped-SnO_2, PbO_2, and the relatively newer boron-doped diamond (BDD). Composite materials are often studied and introduced to strengthen useful semiconducting electrode materials. Diamond, as a magnetic isolating material, has the necessary characteristics to enable anodic oxidation in electrochemical water treatment[22]. Through Chemical Vapour Deposition (CVD), the development of thin synthetic diamond films can be deposited on suitable surfaces to strengthen overpotential and, thus, maximize radical hydroxyl production[23]. The continued evolution of CVD techniques has introduced ultra-thin boron-doped diamond electrodes on different substrates. Furthermore, BDD electrodes possess different electrochemical properties from traditional allotropic carbon electrodes[20]. Most importantly, it exhibits larger electrochemical potential windows in aqueous media, enhanced chemical and mechanical stability, higher overpotential for OH· production, and high corrosion resistance[24].

However, there is a limiting body of knowledge on the effectiveness of EAOP electrodes for NOM oxidation[21]. Since NOM encompasses a wide variety of chemical compounds, the understanding of specific mechanisms is instead inferred as opposed to studied in-depth. Several findings suggest BDD electrodes are competitive with traditional AOPs and dimensionally stable anodes (DSA) such as mixed-metal oxides (MMOs) and carbon-based anodes [19][25], [26]-[27]. Nonetheless, an extensive literature survey shows that research has not identified or optimized EC processes using BDD electrodes to treat NOM. To date, most studies on BDD electrodes on wastewater treatment processes have focused on traditional one-factor analysis without direct comparisons to DSAs[28]–[31].

1.1. Research Objective

The broad objective of this research was to ascertain the BDD electrode's ability for NOM degradation. Through comparison to MMO electrodes, the effects of electrode material on NOM devolution were studied. Conditional effects of initial pH, current density, and electrolysis time were studied by quantifying NOM through TOC, DOC, and UV_{254} absorbance. Lastly, a statistical model, Box-Behnken response surface design (BBD), was used to optimize and investigate the influence of key process variables on NOM removal.

1.2. Thesis Organization

This thesis is organized into five chapters, including a literature review.

- **Chapter 1: Introduction**

The introduction provides (1) an overview of the main objectives of the research question, and (2) a schematic outline of the thesis breakdown.

- **Chapter 2: Literature Review**

The literature review contains a summary of (1) electrochemical processes and mechanisms, (2) diamond film electrodes, (3) natural organic matter characterization and treatments in water, and (4) statistical response surface methodology (RSM) for modeling complex systems.

- **Chapter 3: Removal of Natural Organic Matter in water through EC oxidation using BDD and MMO electrodes**

Chapter 3 highlights the research and findings of NOM removal from synthetic water experiments using BDD and MMO electrodes, studied by comparatively observing TOC, COD, and UV_{254} removal efficiencies.

- **Chapter 4: Process optimization using BBD statistical modelling**

Chapter 4 presents the research and findings of BBD statistical model fitting to investigate the effects of parameters such as initial pH, current density, electrode material, and electrolysis time (independent variables) on TOC, COD, and UV_{254} removal efficiencies. A general goal to optimize process conditions for large-scale applications.

- **Chapter 5: Conclusions and Recommendations**

The conclusion outlines general takeaways from this thesis as well as future research needs in the area of BDD enabled EAOPs.

Chapter 2. Literature Review

2.1. NOM characterization

NOM refers to complex organics present in natural and synthetic waters. Although predominant in most source waters, large concentrations harm aspects of water treatment. Processes such as coagulation, flocculation, and adsorption, incur reduced effectiveness under variable NOM qualities. Furthermore, untreated NOM leads to taste and odor challenges, biological growth in the effluent, and possible formations of hazardous disinfection by-products [20], [32] [33].

Studies have introduced NOM reduction through various means; however, quantifying all aspects of NOM is nearly impossible. Therefore, surrogate measures are often utilized, such as dissolved organic carbon (DOC), DBP production, and total organic carbon (TOC) [34]–[38]. NOM is divided into humic and nonhumic substances, where the former is hydrophobic. The latter is less hydrophobic, comprised of hydrophilic acids, proteins, amino acids, and carbohydrates [33], [39]. Chemically, humic substances provide more challenges to water treatment facilities and require extensive monitoring. Nonetheless, the undefined makeup of humic substances has halted any direct analytical techniques. Consequently, surrogate measures of organic carbon content characterize humic substances (DOC and COD), and the ability to absorb UV light (at 254 wavelengths), or potential to generate DBPs. Characterization of NOM plays a significant role in treatment selection; firstly: higher carboxylic acid concentrations are more challenging to coagulate chemically [33]. Secondly, molecules of lower charge densities are more natural to adsorb onto activated carbon. Although humic fractions of NOM reduce the effectiveness of water treatments, nonhumic substances lead to DBP formation and a more significant proportion of

biodegradable organic growth. Therefore, treatment systems which can regularly degrade various NOM qualities, without system overhauls are paramount for future water treatment facilities [33], [40].

2.1.1. Methods of Characterisation

The main methods of representation are total organic carbon (TOC), dissolved organic carbon (DOC), adsorption of UV-light (UV_{254}), and chemical oxygen demand (COD)[41]. Furthermore, visual indicators such as a yellow hue in water samples can indicate their presence. However, these analyses provide limited information on the character of NOM and only estimate the amount[41], [42][43].

2.1.1.1. Ultraviolet and visible (UV-Vis)

UV-Vis spectroscopy measures the reflection beam from a sample surface. The concentration of an analyte measured by absorbance at defined wavelengths through Beer-Lambert Law. Through experimentation, wavelengths ranging from 220 – 280 nm are concluded to be NOM predictors. Specifically, absorbance at 220 nm denotes carboxylic and aromatic chromophores, whereas 254 nm identifies aromatic groups with multiple degrees of activation (closer as a potential surrogate measure for DOC)[41], [44].

Ratios between wavelengths such as UV_{254} / UV_{204}, UV_{254} / $UV_{436,}$ or UV_{254} / UV_{203} can provide additional insight on NOM characterization. For example, UV_{254} / UV_{203} correlates with the formation of DBPs. Nonetheless, absorbance loses accuracy under the presence of nitrates and sulfates[44].

2.1.1.2. Total organic carbon (TOC) / dissolved organic carbon (DOC)

Total organic carbon is the amount of particulate, including dissolved organic carbon, in a sample. DOC is defined as the organic matter in a sample after filtration through a 0.45 μm filter. TOC and

DOC are the most convenient and accepted measures of overall NOM content. Additionally, an oxidizing agent can be added to a solution (and consequently measured) to express the concentration of carbon present through COD [41], [45].

2.1.1.3. Specific UV-absorbance (SUVA)

SUVA is UV absorbance of a sample at 254 nm divided by the DOC concentration. In addition to content, the ratio describes the hydrophobicity and hydrophilicity of NOM. SUVA greater than 4 indicates mainly hydrophobic material (humic), whereas SUVA values less than 3 suggest hydrophilic material (nonhumic)[46]. Several studies have confirmed a concrete correlation between NOM quality and SUVA metrics. Additionally, SUVA can predict aromatic carbon in NOM and the potential for DBP production[41].

2.1.1.4. Fluorescence

Fluorescence involves measuring the emitted radiation of excited analyte molecules by irradiation. Compared to UV-Vis, fluorescence provides better sensitivity and selectively. Furthermore, it shows potential as a monitoring technique[41].

2.1.1.5. Fractionation

Generally unique and classified by physical and chemical properties, NOM is often isolated into separate groups of molecules with similar properties. Previously applied methods of fractionation include precipitation, solvent extraction, and adsorption chromatography[47].

2.1.1.6. Resin and Membrane fractionation

A standard method of isolating fulvic and humic acids, adopted by the International Humic Substances Society (IHSS), uses commercially available synthetic resin to distinguish adsorption between hydrophobic and hydrophilic NOM. XAD-4 and XAD-8 resin, predominately used in

fractionation, favor the isolation of hydrophobic and aromatic NOM. On the other hand, hydrophilic fraction does not adsorb onto the resin[41], [48].

Mechanical isolation of NOM is preferably performed through membrane filtration with a 0.45 µm paper filter. RO filters are used as an alternative, as well. NOM, especially aquatic humus, is a mixture of organic matter with different sized molecules, which could be bracketed by different sized filters. Although relatively simple to perform, results are affected by flow restriction, in which deposition of macromolecules results in gel layers forming deterring resistance to flow[41].

2.1.1.7. DBP formation

General reaction for DBP formations is summarized by,

$$Precursor + Disinfectant \rightarrow DBPs$$

DBPs are formed by organic (NOM) or inorganic (bromide) precursors formed by chemical disinfectants (chlorine, ozone) [49].

2.1.1.8. Chlorination

NOM reacted with halogen born products to produce DBP, such as chloroform. Whereas some are oxidation-by products. In 1985, a simplified conceptual model was introduced for halide formation. DBP formation begins with a β-diketone moiety (R' – CO – CH_2 – CO – R) with a chlorine substitution on the middle carbon. Followed by rapid hydrolysis, provided if the remaining "R" chain is a hydroxyl group, the reaction promptly completes. Otherwise, the structure is further oxidized to form DBPs such as chloroform or trichloroacetic acid. The conceptual model is transferable to any halogen, including bromine. Bromine ions are easily oxidized, which, in turn, reacts with NOM to form Bromo- and Bromochloro- DBPs. Brominated DBPs pose a higher health risk than chlorinated forms [50].

2.1.2. Conventional NOM Removal and Water Treatment

In the present treatment, NOM removal is categorized into separation and transformation processes. Separation processes remove NOM intact, without any modifications to the chemical and physical properties. On the other hand, transformation processes modify NOM properties [51].

2.1.2.1. Coagulation

Historically, most water treatment plants apply some form of coagulation for NOM treatment in North America schematically similar to figure 2-1 [52]. Coagulants tend to isolate higher molecular weight NOM more effectively, as well as nonpolar NOM. Recently, with the discovery of DBPs, coagulation has been linked to reducing precursors that form DBP. In addition to initial TOC and NOM characterization, coagulation efficiency is affected by coagulant dose and pH. The most significant and cheapest NOM removal utilized ferric salts and alum as coagulants, respectively[51]–[53].

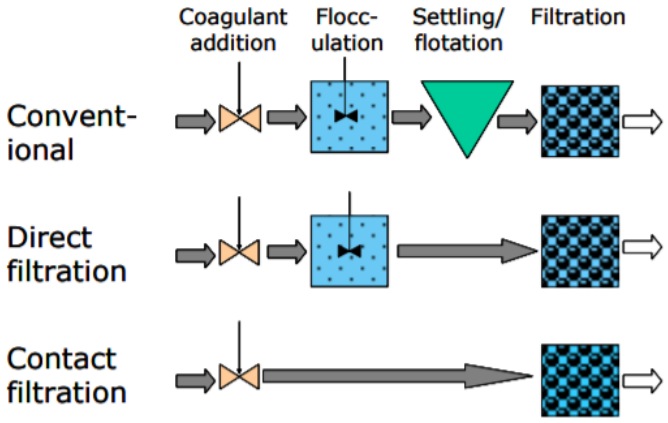

Figure 2-1: Coagulation treatment schematic adapted from NOM Removal technologies [51]

Primarily carried out with the addition of alum, NOM coagulation mechanisms are (1) complexation of NOM with metal coagulants, (2) precipitation of metal-NOM solid phases, (3) complexation of NOM with dissolved coagulant species, (3) adsorption of complexed materials onto metal (hydroxyl) solids, and (4) direct adsorption of NOM onto precipitated solid surfaces.

Sub-optimal coagulation conditions (pH and dosage) represent operational challenges. Firstly, process efficiencies are reduced from high residual metal content as well as reduce quality levels. Secondly, variable NOM conditions could result in inadequate coagulant dosages, which leads to shorter equipment life, increased maintenance costs, reduced base consumption, increased sludge production, and increased backwater consumption [51].

2.1.2.2. Membrane (nano) filtration

While 1982 introduced membrane filtration as a method of humic substance removal, the first full-scale plants were put into operation immediately by 1990 with a process design outlined in figure 2-2. Typical pore sizes of membranes range from 1 – 5 nm, operated at a pressure of 4 – 8 bar [54].

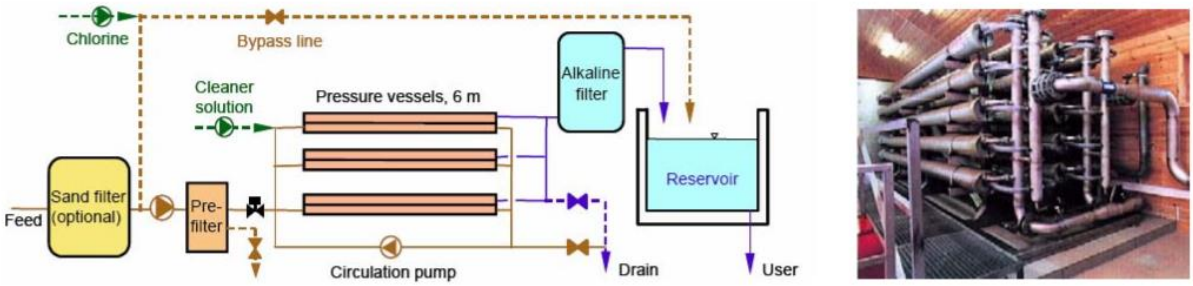

Figure 2-2: Membrane nano-filtration flow scheme adapted from NOM removal technologies [51]

Raw water initially passes through pre-treatment to remove large colloidal particles. Afterward, sieve openings guide flow under increased operating pressure to a circulation pump. Cross-flow filtration through the membrane produced two effluent streams: (1) permeate and (2) concentrate. In addition to NOM, calcium and bicarbonate concentrations are also reduced by 15 – 30%. Nanofiltration processes are great performers when NOM content is high, and turbidity is low.

Nonetheless, membranes are subjected to fouling and require cleaning procedures: (1) a frequent daily cleaning and (2) central cleaning performed twice a year. The capacity loss caused

by fouling can reduce by controlling a particle size range of about 0.1 – 3 µm. NOM removal can reach 70% with specialized membranes[53]–[55].

Alternative filter configuration includes two-media anthracite/sand filters. Coarser grains provide increased filter depth and work amicably for more substantial NOM qualities[55].

2.1.2.3. Ozonation and Biofiltration

Ozone, as an unstable gas, comprised of three oxygen radicals, is highly reactive. In addition to effectiveness against bacteria and viruses, its oxidizing properties can reduce NOM and eliminate taste and odor problems[54].

Ozonation results in products that are more biodegradable than humic substances that were not complexed in addition to NOM removal. Therefore, biofiltration is often paired up with ozonation to remove organic ozonation by-products, as identified in figure 2-3 [54], [56], [57].

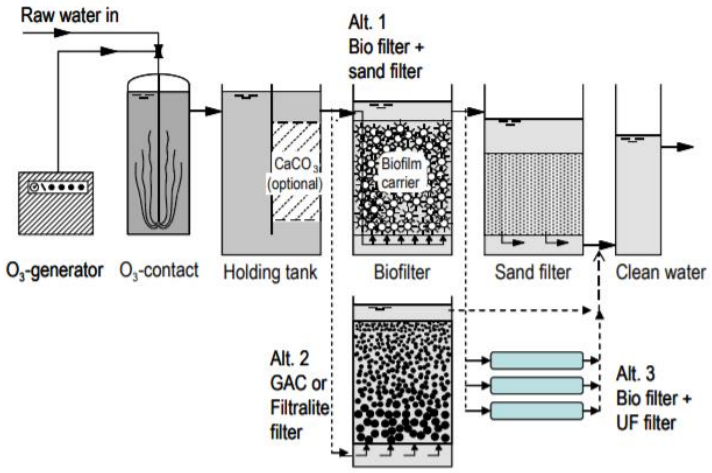

Figure 2-3: Biofiltration with Ozone tank flow scheme adapted from [51]

Plants in Norway incorporate activated carbon filters after the ozonation of NOM waters. Furthermore, granular activated carbon filters achieve a higher life due to the biological regeneration provided by ozonation. Biofilters can also consist of packed bed plastic carriers, sand filters for biomass separation, combined filter medium (anthracite, sand, and calcium carbonate).

Nevertheless, TOC removal remains relatively low at around 20 – 30 % even though color removal is high at 70 – 80 %[54].

2.1.2.4. Electrochemical advanced oxidation processes (EAOPs)

EAOPs emerged as promising technologies for NOM and complex waste stream treatment. Hydroxyl radicals are formed through the oxidation of water on the anode surface through[21],

$$H_2O \rightarrow \cdot OH + H^+ + e^-$$

The most common facilitating anodes include SnO_2, PbO_2, and BDD. Ideally, high overpotential is necessary to induce O_2 production over secondary reactions. Additionally, since water is not oxidized on EAOPs until 2 V SHE, there is a large potential window for direct electron transfer (DET). DET reactions further oxidize organics through a surface reaction[58]–[60],

$$R \rightarrow (R^{\cdot})^+ + e^-$$

DET reaction pathways are a critical rate-limiting step for the oxidation of organic compounds resistant to hydroxyls. As a result, multiple studies have highlighted EAOPs are effective at mineralizing: phenolic compounds, perfluorinated organics, chlorinated organics, DBPs, landfill leachates, pharmaceuticals, endocrine disruptors, human waste, and industrial waste streams [21], [61].

2.1.2.5. AOPs

Traditional AOPs produce hydroxyl radicals through the Fenton process. UV light or ozone facilitates the activation of H_2O_2 for effective water treatment. Naturally, AOPs subject high capital and operating costs; however, they are frequently studied as an alternative to conventional treatment technologies. AOPs can tackle organics resistant to conventional treatments such as coagulation.

EAOPs have several advantages over AOPs such as (1) chemical-free disinfection, (2) DET reactions can act as secondary mineralization mechanisms, (3) energy recovery potential by capturing hydrogen gas from cathodic reactions, and cheaper operation[21].

2.2. Application of diamond electrodes on electrochemical advanced oxidation processes (EAOPs)

Electrochemical film studies to gauge the performance and effects of diamond thin films have flourished since the mid-1980s [64], [65]. Although initial studies were devoted to driving technologies for diamond film fabrication, recent papers searched to understand better the relationship between the semiconductor and structural properties of diamonds[66][67].

Diamond electrodes are grown by energy-assisted (plasma) Chemical Vapour Deposition (CVD) on various substrates such as silicon, titanium, niobium, and carbon. Substrate selection plays a crucial role in diamond film electrode performance due to material drawbacks. Silicon substrates are brittle, whereas niobium and titanium are too expensive. Lastly, the stability of diamond layers on carbon substrates is volatile because internal cracks on the carbon surface cause diamond film detachment during long-term electrolysis[38], [68].

Boron atoms, depending on the concentration, allows diamond films to conduct. For moderate doping, 10^8 boron atoms per cm^3, the electrode behaves as a semiconductor. Notably, BDD electrodes exhibit several fundamental properties that provide advantages over DSA (MMO) electrodes[69]–[71].

BDD electrodes provide a higher potential window in aqueous electrolytes. In high-quality diamond films, hydrogen evolution commences at -1.25 V and oxygen evolution at +2.3 V[72]. BDD electrodes are less susceptible to corrosion in aggressive media. Diamond morphology is stable in long-term cycling from hydrogen to oxygen evolution in acidic media. BDD electrodes

have an inert surface with low adsorption properties. Therefore, a strong tendency to resist deactivation [73]–[76].

2.3. Boron-doped Diamond Anodic Water treatment

Electrochemistry, although an alternative to traditional methods of treating wastewater, is dependent on many factors, particularly the nature of electrode material. Several electrodes tested for water treatment fell victim to surface fouling (carbon), low selective oxidation (Iridium), and limited service life (tin)[77][78]. Whereas BDD, coupled with its high anodic stability and fuller potential window, is proven to be an excellent material for organic oxidation in water treatment. BDD electrodes perform organic oxidation under two mechanisms (1) direct electron transfer under low applied potential, and (2) indirect oxidation through hydroxyl radicals above a potential region of oxygen evolution[79]. Under direct electron transfer, BDD electrodes have active sites for adsorption and thus reduce the electrocatalytic activity of aliphatic alcohols, carboxylic acids, and secondary oxidations. Studies have demonstrated, at a potential above 2.3 V, current densities increase with carboxylic acid concentrations, which suggests the presence of oxygen evolution (an indirect mechanism) above 2.3 V[18][80].

Through experimentation, a mechanism of organic oxidation is through the following mechanism, where organic oxidation and oxygen evolution co-occurs [81][81]:

$$BDD + H_2O \rightarrow BDD(OH\cdot) + H^+ + e^-$$

$$BDD(OH\cdot) + R \rightarrow BDD + mCO_2 + nH_2O$$

Organic evolution occurs in competition with side reaction of hydroxyl radical to discharge O_2,

$$BDD(OH\cdot) \rightarrow BDD + \frac{1}{2}O_2 + H^+ + e^-$$

Experiments have confirmed the secondary mechanisms do not participate in the anode surface, where the formation of hydroxyl radicals occur. Summaries of previous papers have highlighted, BDD electrodes promote large mineralization percentages of organic pollutants with electrogenerated OH radicals, as observed in table 2-1.

Table 2-1: Pollutant oxidation by electrochemical oxidation; BDD anode and DSA cathode

Pollutant	***Experimental Conditions***	***Average Efficiency***	***Ref.***
Carboxylic Acids	i = 30 mA cm^{-2}; T = 30 °C; 1 M H_2SO_4	Efficiency: 70–90%	[79], [80], [82]
Polyacrylates	i = 1–30 mA cm^{-2}; 1 M $HClO_4$	Efficiency: 100%	[82]
Industrial wastewaters	i = 7–36 mA cm^{-2}; initial COD 1500–8000 mg/l	Efficiency: 85–100%	[83]
Carwash wastewater	i = 15–60 mA cm^{-2}	Efficiency: 40%	[66], [84], [85]
Wastewater from automotive industry	i = 30–50 mA cm^{-2}; initial COD 2500 mg/l	Efficiency: >90%	[86]

BDD anodic behavior observed mineralization was inflated with higher applied currents and hindered by initial concentrations. Notably, at high organic concentrations, COD decreases linearly, indicating a kinetically controlled process. Whereas at low organic concentrations, COD decreases exponentially, suggesting a mass-transport driven reaction [18][87], [88].

COD trends and current efficiency for electrochemical combustion are predicted with astute precision, based on a kinetic model:

Equation 2-1 limiting current efficiency formula for kinetic based COD removal

$$i_{lim} = 4F\mathrm{k}_m COD$$

Where i_{lim} is the limiting current density, 4 is the number of electrons exchanged for oxygen evolution, F is faraday's constant, k_m is the average mass transport coefficient, and COD is the chemical oxygen demand.

Likewise, diamond electrodes have been entertained as efficient electrochemical processes for water disinfection for household/domestic water treatment. High overpotential for water electrolysis allows reliable disinfection, without any added chemicals [89]–[91].

2.3.1. Electrocoagulation

Electrocoagulation, commonly associated with electrooxidation, institutes generation of coagulants in-situ by dissolving aluminum and iron ions from respective electrodes. Additionally, hydrogen gas is produced at the cathode along with metal ions at the anode, which can help propagate particulates out of waters through flocculation[92]. Although aluminum and iron anodes are predominately used, titanium and tin electrodes have shown feasibility to product metal coagulants.

The chemical anodic reactions are:

$$M \rightarrow M^{n+} + ne^-$$

At alkaline conditions,

$$M^{n+} + nOH^- \rightarrow \mathrm{M(OH)_3}$$

At acidic conditions,

$$M^{n+} + nH_2O \rightarrow \mathrm{M(OH)_3} + nH^+$$

In parallel, oxygen evolution occurs at the cathode,

$$2H_2O + 2e^- \rightarrow H_2 + 2OH^-$$

Hydrolyzed metal ions can form large chains of M – O – M – OH to chemically adsorb electronegative and organic pollutants such as F^- and carboxylic acids [92], [93]. Compared to

conventional techniques, electrocoagulation predicts high particulate removal efficiency, low cost, and complete automation[18][92].

Current density directly determines the production of metal ions from the respective electrodes. Larger currents often require smaller coagulation units. However, excess current leads to wasted electrical energy in the form of heating. As a result, large current densities result in decreases in current efficiency. Also, initial pH, temperature, as well as flowrate, dictate current efficiency. In terms of current efficiency, aluminum electrodes reach 120% efficiency attributed to pitting and corrosion effects, in the presence of halogens. Quality of coagulation treatment depends on ions produced as a product of current and time[18][94].

Additionally, the conductivity of water treated increases with the presence of salts and anions. Chloride ions mainly increase coagulation propagation through the reduction of other secondary anion production, such as sulfates and carbonates. Since sulfates and carbonates lead to precipitations of calcium and magnesium ions, which form insulating layers on the electrode surfaces, protruding the production of active coagulants. Thus, the addition of salts such as NaCl or organics that generate chlorine increased water disinfection through coagulation. When chlorine ions are present, additional reactions take place, exacerbating pollutant removal[95]–[97]:

$$2Cl^- \rightarrow Cl_2 + 2e^-$$

$$Cl_2 + H_2O \rightarrow Cl^- + H^+ + HOCl$$

Furthermore, unlike electrooxidation, which harbors a steady current efficiency over broader pH ranges, electrolyte pH affects the solubility of metal hydroxides and thus profoundly affects electrocoagulation efficiencies. Treatment performances of aluminum, iron, and titanium coagulant electrode systems concluded the best pollutant removal at neutral pH[18][95].

2.3.2. Electroflotation

Electroflotation (EF) floats pollutant to the surface using tiny hydrogen and oxygen bubbles generated through electrolysis [98], [99]. Therefore, staple reactions are hydrogen evolution and oxygen evolution at the cathode and anode, respectively. Despite sharing similar electrochemical reactions with EC and EAOPs, Pollutant removal through EF is significantly dependant on the size of bubbles formed as opposed to applied potential and current density. Nevertheless, it currently plays a minimal role in particle sizes. A general decrease in gas bubble sizes propagated with increasing current density. Furthermore, bubble size deviates under non-neutral pH; wherein size increases with pH[100].

Although mineral recovery is the primary use of EF, water, and wastewater treatments can utilize EF for separations of oil and low-density suspended solids[98].

2.3.3. Electrooxidation (EO)

Indirect EO uses chlorine and hypochlorite generated anodically to degrade pollutants in the electrolytic solution. Although many inorganic and organic pollutants are unselectively reducing, larger molecular sizes are more natural to reduce. However, the formation of chlorinated organic intermediates and final gases hinders more extensive applications of EO. Furthermore, pollutants are significantly reduced by electrochemically generated hydrogen peroxide in addition to hydroxyls and chlorides[18], [93], [101]–[103].

Another advancement of EO includes adding mediators, or metal ions, from oxidized anode surfaces to increase the reactivity of the electrolyte. Typical mediators include silver, titanium, iron, carbon, and nickel. Mediated ions operate efficiently under acidic conditions [18][104]–[106].

On the other hand, direct EO of pollutants occurs at the anode surfaces. Physically adsorbed oxygens (absorbed hydroxyl radicals) causes complete combustion of organic compounds (R)[107]:

$$R + MO_x(OH*)_z \rightarrow CO_2 + zH^+ + ze^- + MO_x$$

$$R + MO_{x+1} \rightarrow RO + MO_x$$

Generally, hydroxyls are more useful for pollutant oxidation than MO_{x+1}. In summary, direct oxygen evolution coincides with indirect EO, and high overpotential is required to produce O_2 evolution at the anodes. Anodic surface oxidation, synonymous with direct EO, requires fewer chemicals to wastewaters with minimal tendencies to produce secondary pollution. Specifically, these comparative advantages to EC, EF, and indirect EO make anodic oxidation more fruitful for application. However, anode films such as platinum, iron, titanium, and diamond provide both activity and stability[18], [108].

The formation of oxygen dictates the performance of specific anodes in EO. Table 2-2 summarizes extensively investigated anode materials and their overpotential tendencies.

Table 2-2: Anodes used for electrochemical oxidation and their respective overpotentials

Anode	***Overpotential (V)***	***Ref.***
Pt	1.3	[86]
Pt	1.6	[109]
IrO2	1.6	[110]
Graphite	1.7	[109]
PbO2	1.9	[111]
SnO2	1.9	[112]
Pb–Sn (93:7)	2.5	[113]
Ebonex® (titanium oxides)	2.2	[114][115]
Si/BDD	2.3	[116]

Ti/BDD	2.7	[117]

BDD films on silicon and titanium surfaces encompass the highest overpotential and, thus, high current efficiencies with minimal side reactions.

2.3.3.1. BDD electrodes in EO

Diamond exhibits high strength, hardness, resistance to thermal shock, and infrared transmissivity. Stabilized by cubic lattice sp^3-hybridized arranged carbon atoms, the structure is fundamentally resistant to anodic wear. As a result, diamond includes important properties to EO, such as high thermal conductivity, wide bandgap, high electron, high hardness, and chemical inertness [18], [118].

Additionally, doping boron significantly improved the conductivity of diamond. Boron powder or Boron gas is introduced in the doping gas stream and deposited along with diamonds on the substrates through CVD. O_2 evolution for Si/BDD electrodes is 2.3 V, 0.4 V higher than isolated tin, and lead electrodes. Furthermore, BDD film provided the most anodic activity for degradation of organic, and priority pollutants such as ammonia, cyanide, phenol, dyes, surfactants, and landfill leachate [18], [31], [119]–[121].

2.4. Electrode types

EAOP electrodes are inactive electrodes, which during the electrochemical reactions, do not change oxidation states,

$$M^n(\,) + H_2O \rightarrow M^n(OH\cdot) + H^+ + e^-$$

Where $M^n(\,)$ denotes electrode surface sites in an oxidation state n, M^n (·OH) indicates a hydroxyl radical physically adsorbed on the surface site[21], [107].

Additionally, oxygen evolution on inactive electrodes occurs between H_2O and M^n (OH·) to form O_2,

$$M^n(OH\cdot) + H_2O \rightarrow M^n(\,) + 3H^+ + 3e^- + O_2$$

Although the exact mechanism of the oxygen reaction is unknown, BDD electrodes speculate H_2O_2 production. In contrast, active electrodes cycle oxidation states of substrate sites. M^n (OH·) is further oxidized to higher M^{n+1}

$$M^n(OH\cdot) \rightarrow M^{n+1}(O) + H^+ + e^-$$

On active anodes, the formation of OH is lower than on inactive, and thus a majority of the substrate oxidation occurs though oxygen transfer reactions[21],

$$M^{n+1}(O) + R \rightarrow M^n(\,) + RO$$

2.4.1. Doped SnO_2 electrode

In order to function as an effective EAOP electrode, tin must be doped to increase the conductivity. Even though deemed toxic by the EPA, antimony is the most common doping element for tin oxides. Therefore, alternative dopants such as Ar, B, Bi, F, P increase electrode effectiveness for water treatment procedures[21]. Mechanisms of deactivation include (1) formation of nonconductive Sn hydroxide layers on the outer anode surface and (2) passivation of the Ti substrate. Tin oxide electrodes may influence DET reactions, but further research is required[21], [63].

2.4.2. PbO_2 electrode

Lead electrodes confirm the facilitation of hydroxyl radical production on anodic surfaces; however, the mechanism is not fully understood. Studies have insinuated OH formation occurs on a Pb oxide gel layer that forms on the outside anodic surface. An equilibrium zone is postulated[68], [122],

$$PbO_2 + H_2O \leftrightarrow PbO(OH)_2$$

Subsequent reactions with water neutralize the lead active site charges into:

$$Pb(OH^+)(\cdot OH) + H_2O \leftrightarrow PbO(OH)_2[\cdot OH] + H^+$$

Although weakly adsorbed OH is available in equilibrium gel layers, studies have confirmed similar efficiencies to BDD electrodes. Additionally, dopants increase crystal grain sizes, which in turn, increase surface area for lead electrodes. However, slow leaching of lead ions leads to a limited appeal of usage in water treatment applications. Furthermore, EPA standards are applied to lead electrodes for toxicity[21], [122]–[126].

2.4.3. BDD electrodes

Most promising and recently studied electrode for EAOPs, BDD electrodes are produced relatively inexpensively through CVD. Boron, the most common dopant, substitutes for the carbon atoms to give p-type semiconductor properties[21], [70].

At low doping levels (~10^{12} atoms), the diamond incurs semiconductor properties with a hole hopping mechanism. At higher doping levels (~10^{20} atoms), the diamond follows semi-metallic conductivity. Likewise, the electrochemical performance of redox species differs as a function of crystal size and synthesis method. Smaller sizes indicate larger grain boundary proportions, which may lead to higher corrosion rates of edge sites.

BDD electrodes are renowned for extreme stability due to the sp^3 hybridization. Nonetheless, BDD films are prone to failure when exposed to high current densities and regular wear and tear. Different substrates are introduced for BDD films, including Ta, Nb, W, and Zr. However, the most common substrate Si is non-ideal for industrial applications due to its frailty. Multiple methods are studied to improve adhesion on Si substrates, such as: roughening the substrate through bead blasting. Increasing the stability of BDD/Ti electrodes is primarily the focus for BDD synthesis, as Ti is more desirable due to its conductive and robustness advantages over Si films[21].

Research confirms boron dopants aggregate at grain boundaries, crystal edges, and other defects. Therefore, more dislocation sites could increase the performance of BDD electrodes as the electrochemical activity is concentrated at BDD dislocation sites. Furthermore, electrochemical surface area was strongly correlated with boron-doping levels[21], [70], [79], [109], [127]–[129].

Figure 2-4 highlights the charge transfer mechanism on BDD electrode sites.

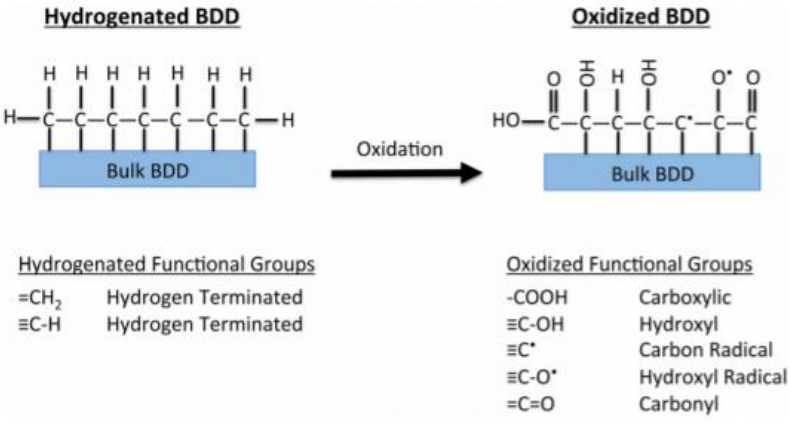

Figure 2-4: BDD electrooxidation mechanism for site-based electron transfer [21]

Oxygenated functional groups are further oxidized to carbon radicals and deprotonated hydroxyl radical sites. Functional groups on the BDD surface have a substantial effect on the charge transfer, which facilitates reaction mechanisms such as hydrophobic, dipole, and catalytic interactions[21][70]. Although relatively unknown, the mechanism of OH· production links to the functional groups present at the electrode surface. Studies indicate that over-potential for water oxidation decreases upon oxidation of the BDD surface. Therefore, results indicate that functional groups on the anode surface can be investigated in more detail, as the BDD surface was considered inert previously[21].

2.4.3.1. Oxidation Pathways

EAOP electrodes exhibit different reaction pathways depending on the compounds in question. Select chemical classes are reviewed, primarily focused on relevant compounds with different molecular properties such as phenols, aliphatic acids, and perfluorinated organic compounds. Phenols are the most common in waste streams, with varying hydrophobicity and acidity due to the substituents, and oxidizing ability by both DET and OH oxidation pathways. Aliphatic acids exhibit hydrophilic properties and are standard products of both AOP and EAOP, due to low reactivity with ODs. PFCs are hydrophobic and completely non-reactive with OHs[21].

2.4.3.1.1. Phenols

Commonly found in industrial waste streams of oil refineries, dyes, textiles, and pharmaceuticals. EAOP electrodes provide an alternative to biological treatment. Three pathways guide the oxidation of phenolic compounds as identified in figure 2-5 [21], [122], [130].

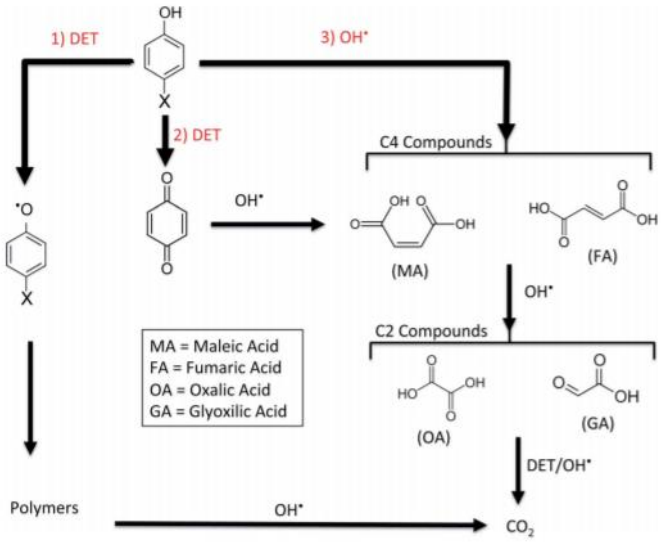

Figure 2-5: Phenol oxidation mechanism through BDD DET oxidation pathways [21]

Pathway 1 is dominant at lower anodic potentials and requires significantly less OH· formations. The DET mechanism produces phenoxy radicals. Studies suggest the phenoxy radicals produce passivating films on the anode surface.

Pathway 2 performs an additional DET reaction on the phenoxy radical to form a phenoxenium (phenol functional group). Subsequently, the phenoxenium ion is converted to benzoquinone through a nucleophilic attack, consuming a hydroxyl radical and releasing a stable organic. EAOP electrodes complete mineralization of phenolic compounds.

Pathway 3 utilizes an adsorbed OH· at the electrode surface or diffused in a surface layer. This mechanism is dominant at higher applied potentials, which produces OH·. Although studies have tried to determine the location of OH· on the electrode surface, exact locations are difficult to model and vary based on location, substituent type, quantity, and electrode type. Flurries of OH· attack reduce phenols to C4 (aliphatic) carbon compounds and C2 compounds, and ultimately, reduced to CO_2 through a combination of DET and OH reactions[12], [21], [58], [130]–[133].

2.4.3.1.2. Aliphatic acids

As introduced in pathway three above, studies have suggested complete mineralization of aliphatic acids is possible at high electrical charges and reaction times, through EAOPs. Nonetheless, this often increases the cost of electrochemical treatment. EAOP electrodes, however, are more reactive than AOPs as a result of an additional DET pathway reaction. Aliphatic compounds cause biological growth in water samples, specifically oxalic and acetic acids [21].

Acetic acid adsorbs to the BDD surface readily. However, adsorption of acetic acid at the electrode surface inhibits displacement of water at the anode surface and, thus, a decrease in OH production. Likewise, oxidation of other compounds that undergo DET reactions.

Oxalic acids are removed by the DET mechanism using BDD, SnO_2, PbO_2, and TiO_2 electrodes. Similarly, oxalic acid is sensitive to surface functional groups at the BDD surface[21], [134]–[137].

2.4.3.1.3. Perfluorinated organic compounds

PFCs are regular effluent wastes in metal plating processes, semiconductor manufacturing, and household cleaner productions. PFCs are resistant to traditional AOPs because of the high stability of carbon-fluorine bonds[21].

Figure 2-6 presents the perforate oxidation mechanism. Lower anodic potential for oxidation at BDD anodes compared to Sn-Bi/Ti is observed. Additionally, several carbon atoms influence the anodic potential required to oxidize PFCs. A higher carbon to fluorine ratio reduces the energy required for direct electron transfer. [21], [85], [138], [139]

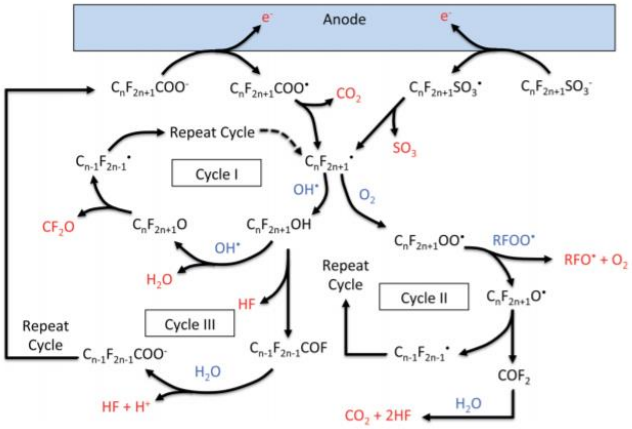

Figure 2-6: Perfluorinated oxidation method through BDD DET oxidation mechanism [21]

Cycle 1 is the preferred pathway for PFC reduction. The compound reacts with OH formed on the anode to release water and shorter chained perfluorinates.

Cycle 2, through the detection of shorter chained perfluoro acids, indicates an additional reaction mechanism. The pathway releases HF, which and shorter chained perfluorinates.

Cycle 3 introduces a secondary mechanism after cycle 1; PFCs react with dissolved O_2 to form peroxy radical species. Studies have highlighted complete TOC removal for PFCs; however, mass balances of F limit removal to 75-90 %[21], [138]–[142].

2.4.3.1.4. By-product formation

2.4.3.1.4.1. Perchlorate formation

Recent studies have highlighted oxidation of chloride on BDD to form ClO_4^- and chlorinated organic compounds. The formation of perchlorate is linked to severe health risks and problematic in oxidation as it is the final product of chlorinated organic compounds. Perchlorates form through the oxidation pathway[21], [143],

$$Cl^- \rightarrow OCl^- \rightarrow ClO_2^- \rightarrow ClO_3 \rightarrow ClO_4^-$$

Conversion of ClO_3^- to ClO_4^- on BDD electrodes follows a two-step DET reaction on the electrode surface.

$$ClO_3^- \rightarrow ClO_3^* + e^-$$

$$ClO_3^* + *OH \rightarrow HClO_4$$

Unfortunately, ClO_4^- on BDD electrodes is approximately 50 – 100 times higher than Pt. and MMO, due to the fact active electrode materials do not form OH radicals at higher quantities. Controlling reactor conditions to limit kinetic mass transfers can limit the production of perchlorates[143].

2.4.3.1.4.2. Halogenated organic compounds

HOCs are products of organic oxidation in landfill leachates. Instead of being final products, HOC formation continuously forms during electrolysis, and after the elimination of halogen ions, it is oxidized to inorganic end-products[21]. Additionally, the formation of HOCs is diverse, ranging from trihalomethanes, haloacetonitriles, haloketones, and especially chloroform,

which makes up 55% of total HOC concentrations. Increasing pH applied current densities and chloride concentrations, respectively, increase HOC formation.

Formation of DBPs, such as chloroform, during electrolysis, is a good indicator of chlorinated by-product formation as a surrogate to represent NOM changes in water samples[21], [144]–[146].

Performance comparison

BDD electrodes, compared to AOPs, can mineralize organic compounds without the accumulation of refractory compounds. Furthermore, EAOP oxidation increased at higher contaminant concentrations. Lastly, the cost of oxidation for BDD electrodes was less than ozonation and comparable to Fenton AOPs[21].

2.4.3.2. Synthesis of Diamond films

CVD

Three main stages encompass synthesis: (1) activation of gas mixtures, (2) gas-phase reactions, and (3) diffusion of gas species onto the substrate surfaces[24].

The single crystalline diamond film is obtained when gas species adhere to the surface before structural defects form. Lastly, when gas species do not settle into equilibrium positions, they form nanocrystalline diamond structures. Popular synthesis methods for diamond films are shown in table 2-3.

Table 2-3: Common CVD techniques and their production details

CVD Technique	***Technique Details***
Hot Filament Chemical Vapor Deposition	• Refractory metal (tungsten) is heated to 2000 with methane and hydrogen, passed over got the filament • Diamond is deposited on a substrate • Suitable for industrial purposes
Oxy-Acetylene Torch	• Combustion flame assisted diamond CVD • Welding torch to oxidize a mixture of acetylene and oxygen gases

	• Simple and cost-effective • Difficult to control the growth rate
Microwave plasma	• Hydrogen concentrations increased using a DC plasma ignited by an electrical discharge • Another pathway to dissociate molecular hydrogen into atomic hydrogen • Microwave frequency used to ignite plasma oscillates the electrons in the gas mixtures used to deposit diamonds • A substrate typically about 2-3 cm in diameter is placed on a holder in a tube reactor (quartz or steel) • Microwaves enter the reaction chamber from a proprietary antenna that converts microwave signal into a circular one • Under suitable conditions of gas pressure, microwave power, gas mixture ratio, gas flow rates of different gases, substrate temperature, the diamond film grows on the substrate
DC plasma CVD	• DC plasma used to activate the gas source • Activation of the gas phase is achieved via collisions of high-energy electrons with the neutral gas species, resulting in the dissociation of the gas species, and the generation of the diamond-forming reactive gas species • Diamond deposited at a meager rate • Jet method → gas injection nozzle consisting of a cathode rod surrounded by an anode tube • Thick diamond films are obtained on a routine basis • DC plasma jet CVD produces Boron or phosphorus-doped diamond film

2.4.3.3. Diamond Nucleation

The nucleation process affects film thickness, grain sizes, homogeneity, morphology, defects, and surface roughness.

Scratching the surface with abrasive powder has been common and powerful to achieve nucleation sites on the substrate. The diamond powder has been the most effective. Likewise, the density of nucleation growth is proportional to scratching time. Scratching with powder creates surface dislocations, which are considered chemically active sites. Adsorbing diamond-forming gas species due to enhanced bonding at high-energy intersecting surfaces with a high density of unsaturated bonds and low coordination numbers[24].

2.5. Response Surface Methodology (RSM)

RSM is a collection of statistical and mathematical techniques for developing, improving, and optimizing processes[147].

In technical fields, common modeling problems aim to predict a response variable y (output) with a set of predictor variables x_1, x_2, …, and x_k. In most cases, the exact relationship between the two variables is not fully understood. In statistical models, the empirical model is denoted as,

$$y = f(x_1, x_2, \dots, x_k) + \varepsilon$$

Where e represents the error in the model, and f is the unknown response surface. Generally, first-order or second-order polynomial models are best described with f.

$$y = \beta_0 + \sum_{j=1}^{k} \beta_j x_j + \ \varepsilon$$

$$y = \beta_0 + \sum_{j=1}^{k} \beta_j x_j + \sum_{j=1}^{k} \beta_{jj} x_j^2 + \sum_{j=1}^{k} \sum_{i=1}^{i<j} \beta_{ij} x_i x_j + \ \varepsilon$$

The first-order model describes a flat surface, whereas the second-order model describes a curved surface. For electrochemical reactions, second-order models, also known as quadratic models, provided the best fit[147], [148].

2.5.1. Derringer's desirability function

The desirability function approach, proposed by Derringer in 1980, is the most prominent method in the industry for the optimization of multiple response processes. It measures operating conditions "x" that provide the most desirable results, by designating other operating conditions outside of the desired limits[149][150].

For a response Y_i (x), a desirability function d_j (Y_i) assigns numbers for Y_i such that d_j (Y_i) = 0 for undesirable functions, and d_j (Y_i) = 1 for desirable functions.

Overall, for all factors,

$$D = \left(d_1\left(Y_1\right) d_2\left(Y_2\right) \ldots\ d_k\left(Y_k\right)\right)^{\frac{1}{k}}$$

Desirability function for maximizing a response

$$d_i\left(Y_i\right) = \begin{cases} 0 & ,\hat{Y}_i < L_i \\ (\hat{Y}_i(x) - L_{\ i})/(T_{\ i} - L_{\ i}))^s & ,\ T_i \leq \hat{Y}_i \leq L_i \\ 1 & ,\hat{Y}_i > L_i \end{cases}$$

Where Li, Ui, and Ti are the lower, upper, and target response values, respectively.

The desirability approach consists of: (1) fitting response values for all k responses, (2) Define individual desirability functions for each response, (3) Maximize overall desirability for all controllable factors [149], [151], [152].

2.5.2. Hierarchical Design

Hierarchical models incorporate a design where lower-level units used a hierarchy of successive higher-level units. A survey outlining the wage gap between men and women provides an example of the hierarchical design shown in figure 2-7 [153].

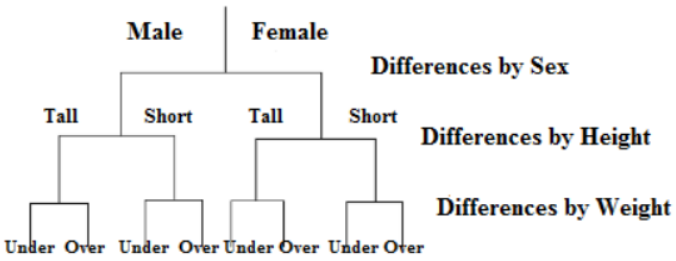

Figure 2-7: Hierarchical design example adapted from [153]

Inherently, statistics with hierarchical models allow the showcase of interferences between quantities. In linear models, observations are considered independent.

2.5.3. Behnken Design (BBD)

Chemometric tools such as RSM are often applied in analytical chemistry. Although most models evaluate the effect of factors, RSM can identify the interaction effects between the factors using a hierarchical structure. Previous successful applications of optimization were used in flow injection analysis, capillary electrophoresis, electroanalysis, and electrocoagulation process to treat grey wastewater in batch mode (can be extrapolated to all EC systems in batch mode to high precision)[150].

BBD is a second-order design based on three-level factorial designs, as presented by figure 2-8.

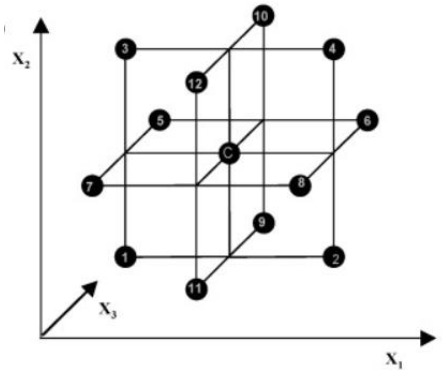

Figure 2-8: BBD design geometry for three factors

The number of experimental runs required for a complete BBD is:

$$N = 2k(k-1)$$

Significantly less than full factorial designs.

In summary, Box-Behnken is an adequate design for response surface methodology because: (1) it allows good estimation of parameters in a quadratic model, (2) detection of lack of fit is readily available, and (3) it can allow the use of blocks[150][154]–[156].

2.5.4. Applications of RSM and BBD

Gilpavas et al. applied RSM to gauge the effect of operating parameters of electrocatalytic degradation of wastewater using a multifactorial BBD. The goal was to optimize operating conditions to maximize color and organic matter oxidation. Although variables were considered, such as characteristic of wastewaters, temperature, and pollutant concentrations, their model tested the effects of pH, current density, and cathode area. The study maximized operating conditions using COD, color, and TOC degradation efficiency for EO processes. Regression analysis showed a high coefficient of determination with a second-order regression model[148], [151].

Coking wastewater was subjected to a BBD design to optimize performance by Zhu et al. A regression model of TOC removal efficiency of Fenton and electro-Fenton processes was developed and validated by ANOVA. Process variables tested were initial pH, reaction time, and current density. Successful application of BBD and RSM produced two quadratic models with a highly significant and high coefficient of determinations. Additionally, the model predicted linear effects and interaction of critical variables regarding TOC removal from coking wastewater[151], [156], [157].

Additionally, Wu et al. applied RSM based on BBD methodology to investigate the effects of three independent variables on response functions: applied current, initial pH, and initial TC concentration. The proposed model was an excellent second-order regression fit for experimentation. Lastly, the results of the adequacy check, through the determination of coefficients and ANOVA, confirmed that the second-order regression model was accurate to analyze variables in EAOPs[157], [158].

Lastly, Khuri et al. investigated to optimize operating conditions such as initial pH, current density, electrode distance, and electrode time on electrocoagulation processes. Four factors RSM

with BBD utilized with a significant correlation with experimental data. Quadratic models to predict COD, TS, and FC removal, had a high coefficient of determination. Therefore, second-order polynomial models fit electrocoagulation processes statistically[154], [157].

Chapter 3. Comparative study of natural organic matter removal using BDD and MMO electrodes

3.1. Introduction

NOM, due to its complicated constituents, is often evaluated through DBPs. DBPs consist of halogenated organic, nonhalogenated organic, and inorganic halogen oxide compounds. Treatment utilities specifically combat numerous pollutants such as heavy metals (Cd, Cr, Cu, Pb, Hg, Zn) and dissolved suspended solids including, but not limited to benzene, toluene, xylene, phenol, aromatic halogens, and trichloroethylene [159][160][161].

Toxicity and carcinogenic effects, subjugated by NOM DPBs, can cause harm to human health and the environment. Although, in the last few years, electrochemical technology has advanced in research and application as an alternative for NOM elimination, concrete evidence, and control of electrochemical reactions for NOM removal are not well documented [13], [41], [51], [162]–[165]. A wide variety of electrode materials have often obtained different organic matter efficiencies; however, no comparative benchmark between electrode materials exists for NOM removal[21].

Electrode materials leading the charge in electrochemical technology innovation are BDD and dimensionally stable anodes such as Ti/IrO_2-Ta_2O_5 and MMO. Different reaction mechanisms highlight their different organic matter efficiencies: non-active anodes such as BDD are direct oxidative species which induce oxidation via hydroxyl radicals, and DSAs such as MMO, promote hypochlorite mediated oxidation in addition to hydroxyl radicals (when chlorine and chloride are present). BDD electrodes have shown excellent results in effluent matrices involving NOM such as textile dyes, dairy, herbicides, pharmaceuticals, and heavy metals [161], [166]–[169].

Therefore, the objective of this chapter is to evaluate the performance of BDD electrodes comparatively to MMO electrodes, during the treatment of synthetic NOM water employing electrolytic batch cells.

In order to encapsulate the data, for nonselective and efficient NOM monitoring, a combination of TOC, COD, and UV absorption data at 254 nm is best for concentration assessment.

Firstly, TOC is an indirect measure of organic molecules present in waters, in which up to 80% of humic and fulvic substances are easily recognizable through TOC analysis. US Environmental Protection Agency (USEPA)[170] mandates that water utilities monitor TOC to reduce DBP precursors.

Secondly, compounds that contribute to COD are biodegradable organic compounds, non-biodegradable compounds, and inorganic oxidizable compounds. Additionally, it is an indicator of pollution in the effluent discharges of wastewater, which coincide with NOM content. Under the Clean Water Act, COD is used as a regulatory method to gauge overall treatment plant efficiencies[170].

Lastly, SUVA is defined as the susceptibility of water to enhance coagulation and oxidation. NOM's tendency to undergo coagulation and oxidation is heavily dependent on functional group content, molecular weight, and hydrophobic content. Moreover, SUVA is a reliable indicator of aromaticity, where NOM in high-SUVA waters tend to have lower hardness and higher TOC concentrations[171].

EAOP, as identified in the literature review, can effectively combat NOM concentrations in surface waters. Furthermore, an application system using BDD electrodes could offer an efficient solution for NOM treatment through controlled electrochemical oxidation-reduction

processes. BDD electrode performance by comparing NOM removal to MMO electrodes, using quantifiable TOC, COD, UV_{254} absorbance.

3.2. Materials and methods

3.2.1. Synthetic water preparation

Synthetic water was produced in the lab with Suwannee River NOM. Wherein Suwannee River NOM is an established end-member of natural organic matter from an aquatic system used in several papers as reference material of the International Humic Substances Society[172]. Additionally, alginic acid and inorganic ions dissolved in deionized water were added to create a synthetic water matrix-like natural water outlined by Rosenfeldt and Linden [173], [174]. All chemicals were purchased from Sigma Aldrich.

Table 3-1: Synthetic NOM water matrix solution contents

S1 [1 L solution]	0.001539 M $CaCl_2$
	0.004110 M $MgCl_2*6H_2O$
	0.0004847 M KNO_3
	0.001716 M $CaSO_4*2H_2O$
	0.00025 M NaOH
	0.0001336 M $C_6H_{11}NO_6$
	0.0015 M $NaHCO_3$
	0.01024 g Suwannee River NOM
S2 [1 L solution]	0.001539 M $CaCl_2$
	0.004110 M $MgCl_2*6H_2O$
	0.0004847 M KNO_3
	0.001716 M $CaSO_4*2H_2O$
	0.00025 M NaOH
	0.0001336 M $C_6H_{11}NO_6$

	0.0015 M $NaHCO_3$
	0.01024 g Suwannee River NOM
	0.0000003125 M NaOH

Table 3-2: Synthetic NOM matrix initial NOM bulk measured through TOC/DOC, UV_{254}, SUVA, and pH

Parameter	*Units*	*Synthetic 1*	*Synthetic 2*	*River Water*
TOC and DOC	Mg L^{-1}	6.2483	7.0270	5.0
UV_{254}	cm^{-1}	0.161	0.175	0.14
SUVA	L mg-M^{-1}	2.3	2.9	2.8
pH	--	6.5	8.5	8.2

3.2.2. Electrochemical Setup

NOM degradation was carried out in a batch system with three unique electrode configurations in order to highlight BDD electrode performance over MMO electrodes. All tests for TOC, COD, and SUVA analyses used a two-electrode setup with a volume capacity of 300 mL of the synthetic solutions. The setups include (M1) BDD anode and BDD cathode electrochemical system, (M2) BDD anode and stainless-steel cathode electrochemical system, and (M3) MMO anode and stainless-steel cathode electrochemical system. The system(s) were mechanically stirred for the duration of the experiment at 400 rpm. Additionally, the psychical properties of the electrodes were machined to have the same surface areas [10 mm x 10 mm x 1 mm]. Furthermore, the distance between electrodes was kept constant at 3 mm in the synthetic NOM water.

Batch tests were run uninterrupted, and the overall TOC, COD, and UV_{254} measurements were taken at the end of the allotted duration(s) at (1) 30 minutes, 60 minutes, and 120 minutes. TOC and COD evolution as a function of time was mapped by equation 3-1 and 3-2 [175]:

Equation 3-1: Electrochemical efficiency of NOM removal measured through TOC efficiency

$$E_{TOC}\ (\%) = \frac{(TOC_0 - TOC)}{TOC_0} * \ 100$$

Equation 3-2: Electrochemical efficiency of NOM removal measured through COD efficiency

$$E_{COD}\ (\%) = \frac{(COD_0 - COD)}{COD_0} * \ 100$$

Where $(TOC_0 - TOC)$ and $(COD_0 - COD)$ are the changes in total organic carbon concentration and chemical oxygen demand measured in [mg L^{-1}]. Where TOC_0 and COD_0 are initial NOM concentrations surrogated with TOC and COD measurements.

SUVA, in addition to TOC and COD removal, was assessed to strengthen the conclusions extrapolated by the respective removals[53], [176]. Equation 3-3 measures SUVA of solution.

Equation 3-3: Electrochemical efficiency of NOM removal measured through SUVA

$$SUVA = \frac{UV_{254}}{DOC}$$

Where UV_{254} is the absorbance at wavelength 254 nm [cm^{-1}], and DOC is dissolved oxygen content measured in [mg L^{-1}]. DOC is measured by filtering a sample through a 0.45 µm filter, afterward, analyzed by the TOC system.

3.2.3. Measurement of TOC, COD, and UV_{254}

TOC values were delivered using Shimadzu© TOC-L total organic carbon analyzer with a Shimadzu ASI-L autosampler. Specifically, the equipment utilized a 680˚C combustion catalytic

oxidation detection method. Although the combustion catalytic oxidation method subjects and identifies low molecular-weight organics, larger harder to decompose insoluble and macromolecular organic compounds are resistant[177].

MANTECH PeCOD© Analyzer determined COD. The primary mechanism is advanced oxidation through photocatalysis with titanium dioxide (TiO_2). As the reaction proceeds on a small volume of sample, the electrical charge generated is plotted over time as exampled in figure 3-1. Wherein, the area under the curve, is proportional to the COD of the sample[178].

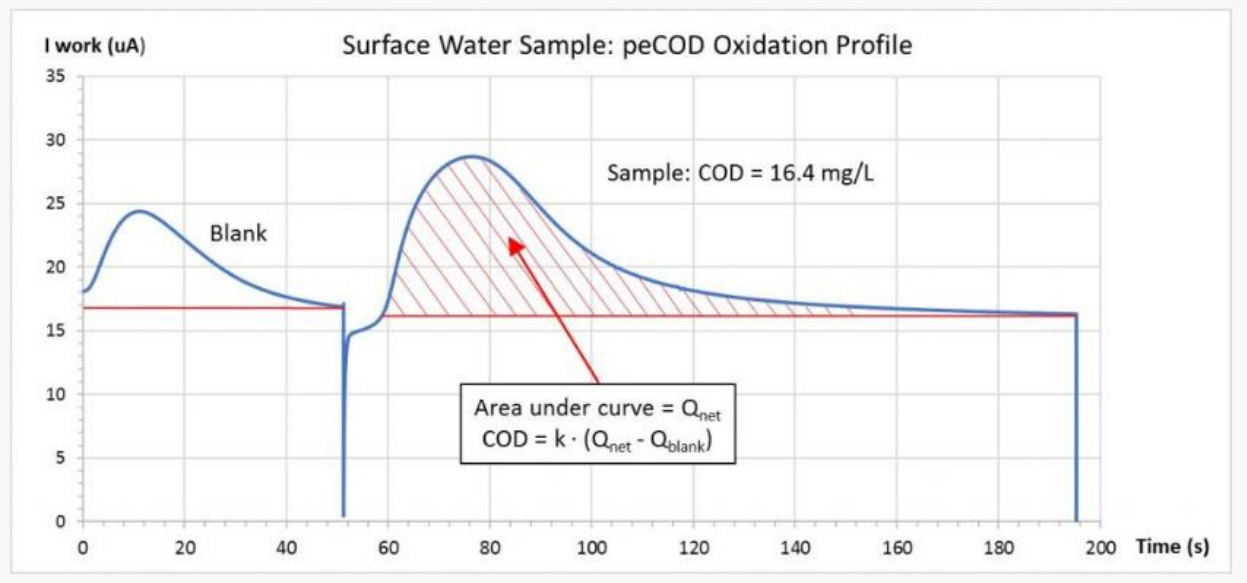

Figure 3-1: PeCOD analyzer work vs. time adapted from [178]

UV_{254}, and consequently, SUVA values were measured using a fluorescence plate reader (spectral max M3, Molecular Devices) set with a 254 nm. UV light at 254 nm, shined through a water sample in a quartz cell, identifies aromatic rings or unsaturated carbon bonds by looking at the change in intensity of the UV wavelengths[179].

3.3. Results

3.3.1. TOC Efficiency

Electrode material played a significant role in electrochemical disinfection. BDD electrodes, as inactive electrodes, do not change the oxidation state during their electrochemical reaction pathway [21]. However, the MMO electrodes cycle oxidation states that during oxidation of substrates [26]. BDD electrodes, known for their extreme stability, have been previously investigated for water disinfection [21], [94], [123], [125], [185]–[187]. In this experiment, TOC removal was mapped as a function of treatment time for M1, M2, and M3 treatment setups. Furthermore, electrode setup behaviors under three key operating factors were assessed. This includes the initial pH (6.5 – 8.5), current density (10 – 20), and electrolysis time (30 – 120 min) on TOC removal.

Figure 3-2 illustrates TOC removal as a function of time. The figures highlighted performance at 6.5 and 8.5 pH, in separate applied current densities of 10 mA cm^{-2} and 20 mA cm^{-2}. For all treatment systems, the highest TOC removal was experienced at 120 minutes and, thus, used for quantitative comparisons below. Moreover, BDD anodes displayed an increase in TOC content at lower electrolysis duration, which could be a product of partial oxidations of NOM. Nonetheless, increasing the duration further oxidized the carbon chains to CO_2 and H_2O.

At 6.5 pH and 10 mA cm^{-2}, TOC removal was maximized in setup M3, with an MMO anode and stainless steel (SS) cathodes at 65.8 %, whereas M1 and M2 showed low removals of 2.4 and –0.7 % respectively. Likewise, at 8.5 pH and 10 mA cm^{-2}, M3 once again exhibited the largest TOC removal at 43.2 %. On the other hand, M1 and M2 performed poorly at 1.9 and 8.8 %, respectively. MMO electrodes showed a higher affinity for chlorine and hypochlorite production, reflected by a more significant TOC removal. Additionally, M3 systems introduced agglomerates to the solution, which increased the floc size of the NOM. TOC and COD testing equipment failed to

recognize the larger flocs, which [may have] inflated TOC removal (%) for MMO electrode systems.

Additionally, low current densities of the experimental design account for comparatively low removal percentages to previous studies [19], [26], [27], [166]. Increasing the current density to 20 mA cm^{-2} sharply increased the rate of TOC removal. At 6.5 pH and 20 mA cm^{-2}, M1 showed the greatest removal growth, flatlined at 33.6 %. M3 removal reduced to 30.8 %. Lastly, M2 exhibited a TOC removal of -23.2 %. Increasing the current density had mixed results with BDD electrodes at low pH. However, at high pH, M1 and M2 universally presented the greatest TOC removal at 40.2, 40.1, and 34.9 % for M1, M2, and M3, respectively. Therefore, a greater TOC removal was observed by BDD electrodes at high pH and high current densities.

Overall, the magnitude of NOM removal was lower than other entertained methods, such as UV advanced oxidation processes [18], which attributed to the low current densities of the experimental setup. Other researchers achieved a removal efficiency of 81 % using a Titanium-BDD electrode system with a current density of 38 mA cm^{-2} [8], [12][18]. Raising the current density to 20 mA cm^{-2} increased the TOC removal significantly and omitted the initial increases in partial oxidated carbon chains in TOC analyses, as shown in figure 3-2. It was observed that the current density profoundly influenced organic matter oxidation.

Current density: 10 mA cm^{-2} Current density: 20 mA cm^{-2}

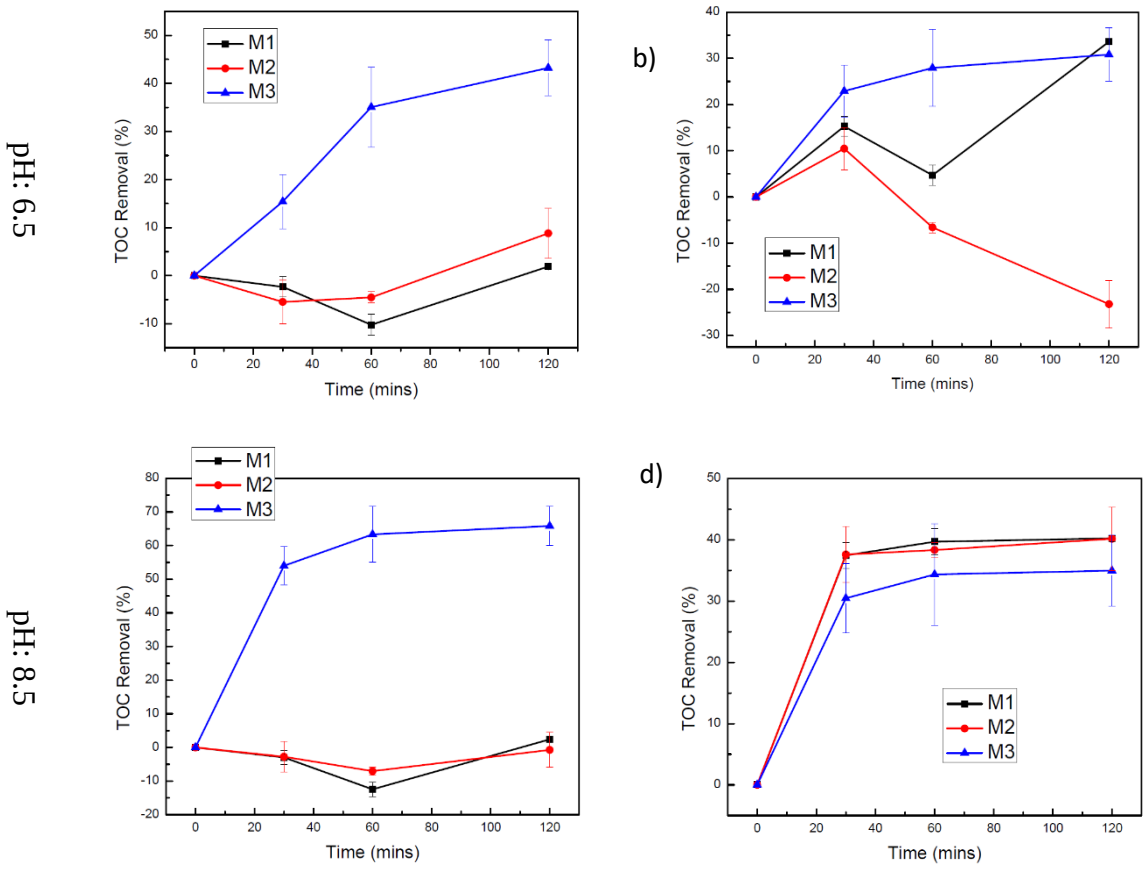

Figure 3-2: Removal of NOM, TOC on M1, M2, and M3 treatments. 3-2a) Conditions: Synthetic NOM electrolyte; pH 6.5; current density: 10 mA cm^{-2}. 3-2b) Conditions: Synthetic NOM electrolyte; pH 6.5; current density: 20 mA cm^{-2}. 3-2c) Conditions: Synthetic NOM electrolyte; pH 8.5; current density: 10 mA cm^{-2}. 3-2d) Conditions: Synthetic NOM electrolyte; pH 8.5; current density: 20 mA cm^{-2}.

3.3.2. COD Efficiency

In theory, COD determines affinity for oxidation by measuring oxygen requirement, as opposed to TOC, which identifies overall carbon content. Consequently, COD efficiency presented unique patterns to TOC efficiency. However, like TOC efficiency, the most prolonged electrolysis duration at 120 mins determined the largest COD efficiency. Furthermore, M1 and M2 anodes

experienced an increase in COD at lower durations. Figure 3-3 maps COD removal as a function of time for M1, M2, and M3.

At 6.5 pH and 10 mA cm^{-2}, M3 exhibited the highest COD removal at 91.6 %., while M1 and M2 had lower COD removals at 11.2 and -22.6 %, respectively. At 8.5 pH and 10 mA cm^{-2}, M3 exceeded M1 and M2 with a COD removal of 54.8 %. However, M1 and M2, although higher than 6.5 pH, still displayed a lower 43.8 and 52.3 % COD removal, respectively. The BDD electrode anode does not indicate any significant advantages for COD removal over MMO electrodes at low current settings. Therefore, at high pH (8.5), all three electrode systems presented similar efficiencies. Although COD efficiency was lower for M1 and M2 at higher pH, it was still more significant than TOC efficiency at the same settings. Once again, the BDD electrodes responded to higher current densities more effectively than the MMO electrodes.

At 6.5 pH and 20 mA cm^{-2}, settings increased the COD removal to 52.7 and 52.2 % for M1 and M2, respectively. Nevertheless, M3 achieved the highest COD efficiency at 90.2 %. On the other hand, at 8.5 pH and 20 mA cm^{-2}, M1 and M2 exhibited COD removals of 57.6 and 75.4 %, respectively. M3 decreased in efficiency at high pH to 68.8 %. M3 exhibited a higher removal at low pH for all current densities; however, M1 and M2 efficiencies improved with increased pH and increased current densities.

Firstly, the widely different conclusions from TOC efficiency are the product of different reaction mechanisms between non-active (BDD) and active (MMO) electrodes. BDD is a ‘non-active’ anode at which the principal reactive species is hydroxyl radicals, whereas MMO is an ‘active’ anode that depends mostly on the ‘higher oxide’ surface mechanisms with chlorides and hypochlorite. In the case of MMO, MOx participates as a mediator in the oxidation of organics on the anodic surface [188]. Although this effect reduced COD (a measurement of the oxygen

required to oxidize soluble and particulate organic matter in water), TOC did not show the same magnitude of removal. The superoxides (MOx) [may] contribute to TOC content, which was not identified by the MANTECH COD analyzer, thus, accounting for the significantly higher COD removal for M3 anodes.

Secondly, low pH favored M3 anodic oxidation through the formation of Cl ions promoted by current density. Cl- mediated oxidation by active chlorine is best around 6 – 6.5 [166].

Lastly, at a higher pH due to the lower concentrations of Cl in the solution, the predominate species (hydroxyls) induced greater TOC efficiencies by BDD anodes. This was coupled with weak adsorption properties of BDD anode and high production of hydroxyl radicals, which benefited TOC removal than COD removal [166].

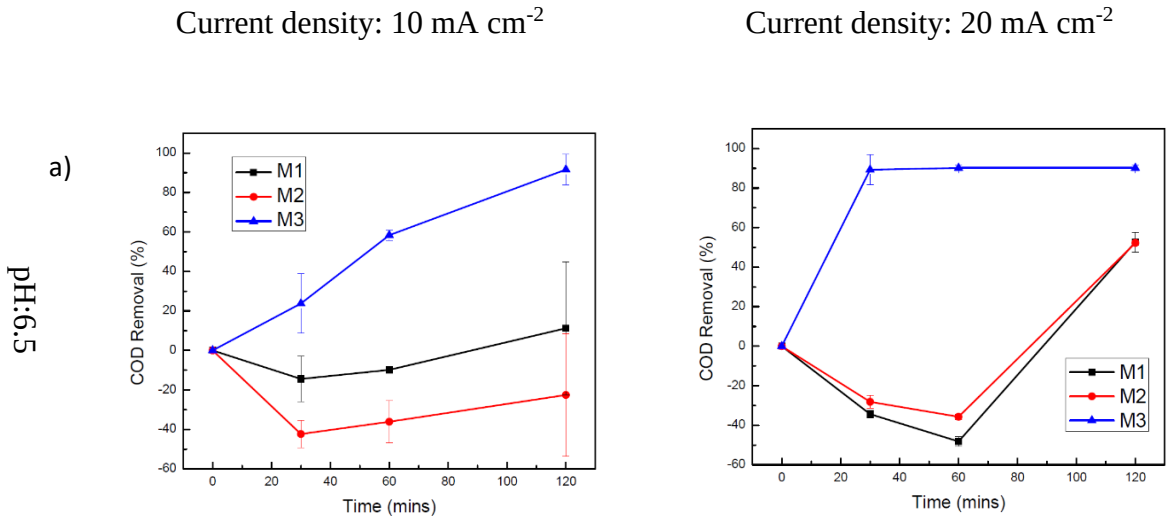

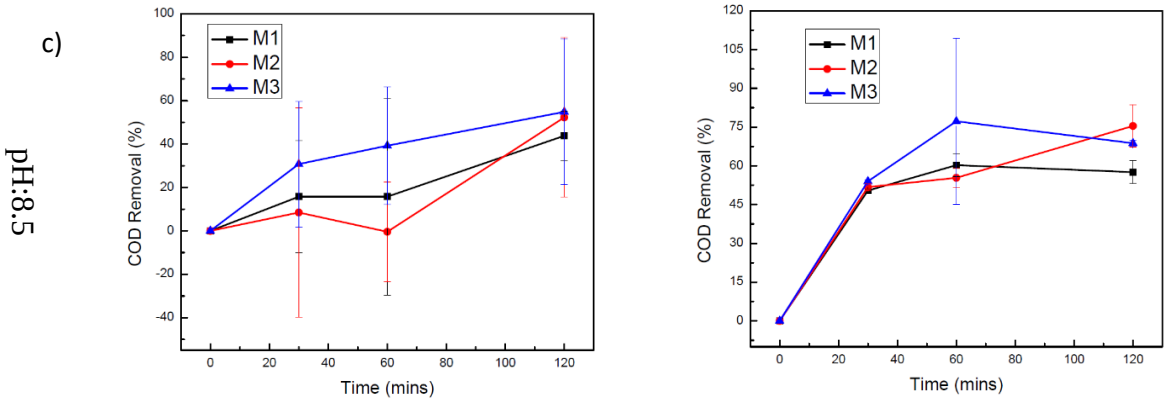

Figure 3-3: Removal of NOM, COD on M1, M2, and M3 treatments. 3-3a) Conditions: Synthetic NOM electrolyte; pH 6.5; current density: 10 mA cm^{-2}. 3-3b) Conditions: Synthetic NOM electrolyte; pH 6.5; current density: 20 mA cm^{-2}. 3-3c) Conditions: Synthetic NOM electrolyte; pH 8.5; current density: 10 mA cm^{-2}. 3-3d) Conditions: Synthetic NOM electrolyte; pH 8.5; current density: 20 mA cm^{-2}.

3.3.3. COD/TOC ratio and COD/TOC efficiency

Individually, the TOC and COD removal analyses presented contradictory and convoluted information. For instance, at a low current density of 10 mA cm^{-2} and high pH 8.5, the TOC content increased in the solution, whereas COD decreased during treatment (from 0 to 60 minutes). Different testing mechanisms and different inherent mechanisms that identify NOM by TOC and COD [may] lead to discrepancies in TOC and COD trends. Furthermore, COD is less sensitive in lower concentrations below (10-20 mg/L) [183]. Additionally, TOC and COD measure different aspects of NOM where TOC is the carbon content of an organic compound (synthetic water), and COD is a measure for the amounts of electrons available in the organic carbon for the reduction of oxygen to water. Therefore, it was possible to have overlapping organic compounds in the synthetic solution, which were unreadable by the TOC or COD tests.

Furthermore, the overall removal (%) at low currents was extremely low and, in most cases, presented an increase in NOM. There were two possibilities for the occurrence: (1) the deionized water leached carbon out of the tubing, and 3D printed experimental setups or more probable (2),

the electrochemical oxidation initially broke the humic acid (NOM) carbon chains into shorter carbon chains such as DBP.

To provide a detailed study of NOM removal, photoelectrochemical oxygen demand (peCOD) was compared to theoretical oxygen demand and total organic compound (TOC). Firstly, theoretical oxygen demand (ThOD) of the NOM solution was calculated according to equation 3-4 formulated by Baker et al. [189]:

Equation 3-4: ThOD stoichiometric calculation

$$C_n H_m O_c X_k N_j S_i P_h + bO_2 \rightarrow nCO_2 + \frac{m-k-3j-2i-3h}{2} H_2O + kHX + jNH_3 + iH_2SO_4$$

In which x is the sum of halogens, and b outlines oxygen demand:

$$b = n + \frac{m-k-3j-2i-3h}{4} - \frac{e}{2} + 2i + 2h$$

ThOD for the synthetic NOM solution was calculated based on acids and Suwannee river NOM components. Through a direct comparison presented in table 3-3, the peCOD was not a good predictor of ThOD for the organic compounds in the synthetic NOM solution. PeCOD estimations were generally lower than theoretical values: over ten iterations, ThOD was, on average, 15% lower than peCOD estimations, whereas SUVA was 33.81% lower.

Table 3-3: Synthetic NOM matrix ThOD comparison to peCOD estimation

	Oxygen Demand [mg L^{-1}]	***SUVA [L mg^{-1} C^{-1} $\cdot m^{-1}$]***
Theoretical Calculation	21.21	3.79

PeCOD Estimation	18	2.51

A more defined metric of NOM quantification was proposed by Stoddart et al. [190], COD/TOC ratio. The ratio is a measure for the degree of reduction of the carbon compounds. The literature identified that the relation between COD and TOC was directly proportional to each other. Increases in COD/TOC ratios over reaction times are attributed to the formation of degradation by-products (DBP)[190], [191]. Previous studies have also shown that TOC was strongly correlated with disinfection by-products.

Additionally, peCOD measurements by Stoddart et al. increased with treatment duration, whereas the TOC/DOC decreased from raw-to-finished water. In summary, Stoddart et al. concluded that the COD/TOC ratio increases demonstrated the extent of treatment effectiveness. Wherein, an increase in the COD/TOC ratio identified successful treatment progression through the production of DBP. Similarly, a higher ratio COD/TOC denoted more DBP production and, therefore, NOM reduction. Lastly, the ratio reduced after an initial rise through treatment duration, as the DBPs and NOM are further oxidized completely to preferred CO_2 and H_2O compounds. Therefore, for [our] experiments, [we should] see an increase in COD/TOC ratio in the earlier stages of electrolysis before reducing to a lower value. The patterns are eminent in Figure 3-4.

At low pH and low current (6.5 pH and 10 mA cm^{-2}) settings, M3 illustrated the most significant COD/TOC ratio peak at 30 mins of 4.5, which suggested a higher degree of breakdown of synthetic NOM solution into DBP. Additionally, M3 had the lowest ratio at the end of the experiment duration (120 minutes), as identified in figure 3-4a. Although the final ratios are not conclusive of electrochemical performance, the COD/TOC ratio data matches TOC and COD removal (%) data. Thus, M3 exhibited the lowest NOM content after electrolysis. In summary,

MMO electrodes performed the best when compared to the BDD electrode setups at low pH and low current standards.

At high pH and low current (8.5 pH and 10 mA cm^{-2}) settings, all treatment setups performed higher than the low pH experiments presented in figure 3-4b. M1 and M2 had the lowest COD/TOC ratio at 1.6 and 1.1, which is far smaller in comparison to all the treatment setups at low pH and low current settings. M3, on the other hand, had a higher COD/TOC ratio of 2.3. These results emphasized lowered electrochemical performance at higher pH.

However, at low pH and high current (6.5 pH and 20 mA cm^{-2}) settings in figure 3-6c, COD/TOC ratios were amplified at M1 and M2 setups, reaching a high value of 6.7 and 5.3 at 60 mins, respectively. In contrast, M3 showed a lower COD/TOC ratio at high current compared to low current. The ratios settled to 1.9, 1.4, and 0.9 for M1, M2, and M3, respectively. Experimentally, M3 setups had yellow particulates in the solution leeching from the titanium surface, which mimic electrocoagulation conditions. At higher currents, the agglomerate concentration increased which presented significant decreases in COD and TOC removal (%) [26], [122], [186], [192]. Despite high TOC and COD removal (%) shown for M3, COD/TOC ratios remained low and decreased linearly through the experiments, thus suggested a lack of DBP presence and thus NOM breakdown.

Lastly, figure 3-6d at high pH and high current (8.5 and 20 mA cm^{-2}) settings, shows that all the electrochemical setups outperformed the previous pH and current settings. M1 and M2 had the highest COD/TOC ratio at 12.65 and 10.85 in a 60-minute duration, whereas M3 performed comparatively poorly at 6.57. The ratios settled to 1.5, 1.1, and 1.2 for M1, M2, and M3, respectively. Therefore, based purely on the COD/TOC ratio peaks, M1 and M2 introduced the most substantial amount of DBP production and, thus, breakdown of synthetic NOM solutions.

In summary, a few conclusions were prominent from the COD/TOC analysis. Firstly, the COD/TOC ratio identified that electrochemical performance was unaffected by pH variation. Secondly, electrochemical duration played a significant role in synthetic NOM reduction, in order to oxidize DBP products into non-harmful organics. Lastly, BDD electrodes, through setups M1 and M2, exhibited a higher linearly positive response to changes in current density.

Furthermore, a one-way ANOVA analysis on the three treatment setups confirmed that differences between them are statistically significant only at 20 mA cm^{-2}. Strictly looking at BDD electrodes versus MMO electrodes, the one-way ANOVA showed a p-value of 0.039 at 20 mA cm^{-2}, however, it also exhibited a p-value of 0.859 at 10 mA cm^{-2}.

Current density: 10 mA cm^{-2} Current density: 20 mA cm^{-2}

pH 5.5

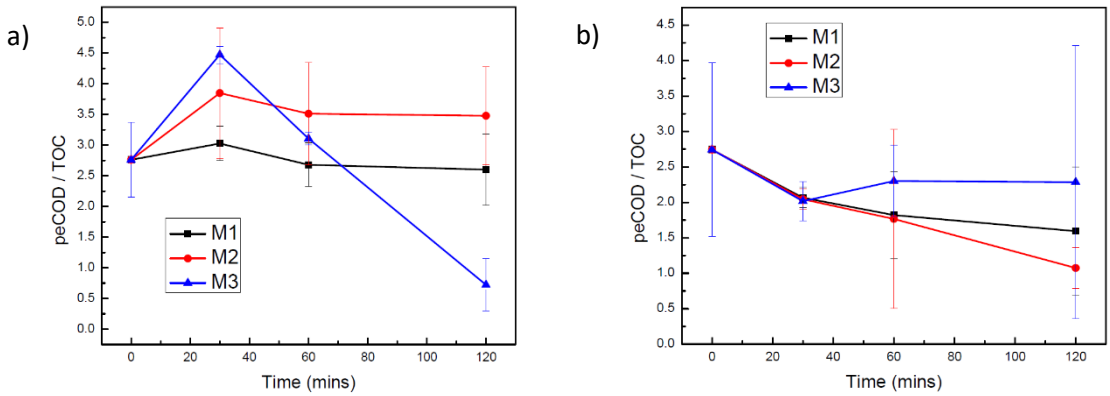

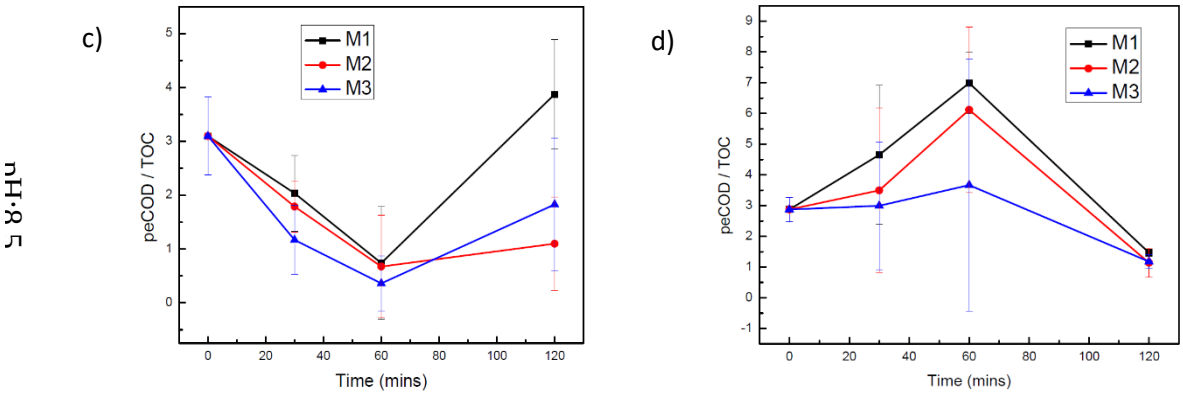

Figure 3-4: COD/TOC on M1, M2, and M3 treatments. 3-4a) Conditions: Synthetic NOM electrolyte; pH 6.5; current density: 10 mA cm^{-2}. 3-4b) Conditions: Synthetic NOM electrolyte; pH 6.5; current density: 20 mA cm^{-2}. 3-4c) Conditions: Synthetic NOM electrolyte; pH 8.5; current density: 10 mA cm^{-2}. 3-4d) Conditions: Synthetic NOM electrolyte; pH 8.5; current density: 20 mA cm^{-2}.

Additionally, figure 3-5 plots COD/TOC removal efficiency as a product of time. Surprisingly, at 6.5 pH and 10 mA cm^{-2} current settings, COD/TOC removal maximized at 73.9 for M3, eclipsing M1 and M2, which reached 5.8 and -26, respectively. Once again, increasing the current density to 20 mA cm^{-2} reduced the efficacy of M3. M3 maximized at 70.6, whereas M1 and M2 peaked at 38.8 and 54.8, respectively.

At 8.5 pH and 10 mA cm^{-2}, all three treatment systems experienced COD/TOC high removal at 41.9, 60.8, and 16.7 for M1, M2, and M3, respectively. M1 and M2 illustrated a more exceptional performance at high pH. Likewise, raising the current density to 20 mA cm^{-2}, increased M3 COD/TOC removal to 59.1. On the other hand, this action increased M1 and M2 COD/TOC removal to 49.1 and 60.3, respectively.

In summary, M3 showed a more significant COD/TOC removal at low pH and low current densities. Furthermore, M1 and M2 exhibited a higher COD/TOC removal at high current densities, wherein M2 outperformed M1.

Current density: 10 mA cm^{-2} Current density: 20 mA cm^{-2}

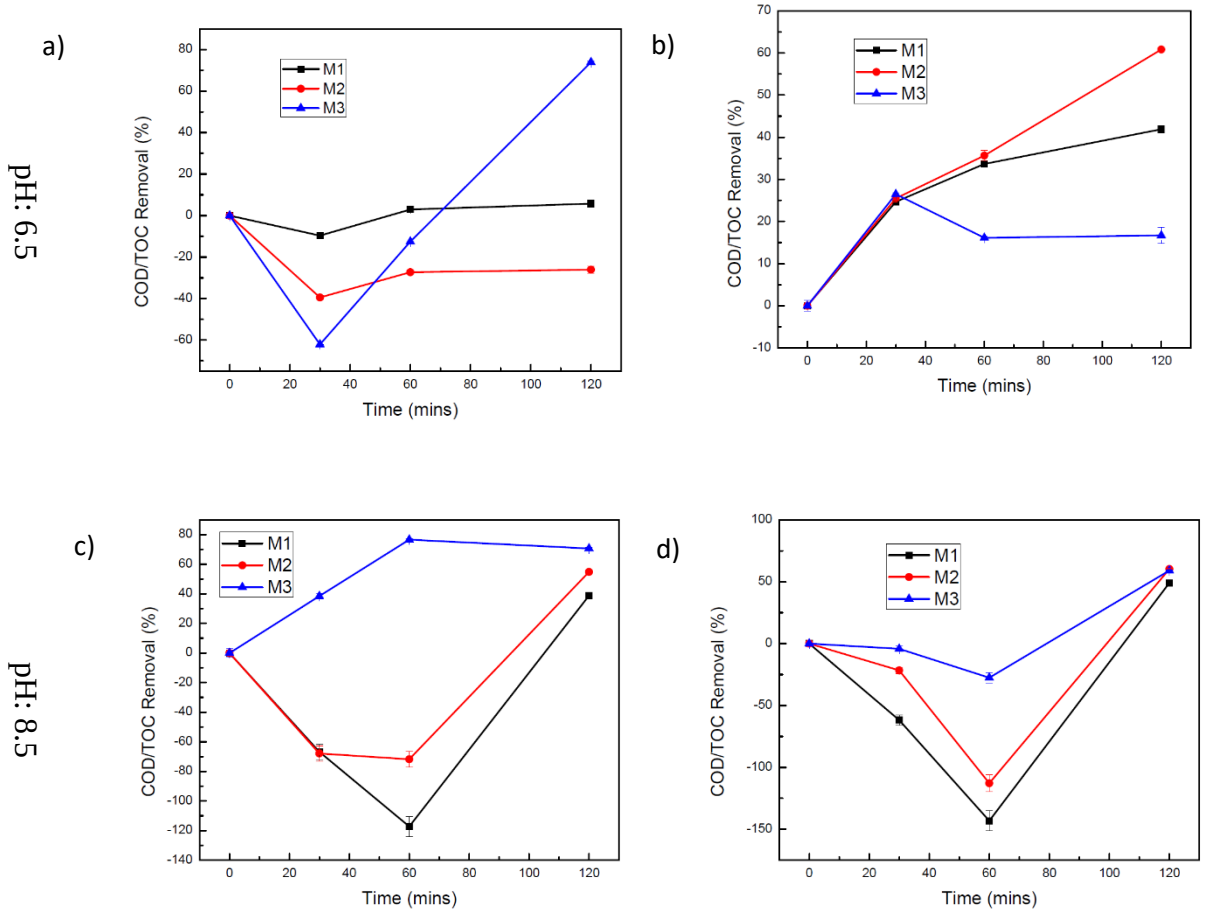

Figure 3-5: COD/TOC removal on M1, M2, and M3 treatments. 3-4a) Conditions: Synthetic NOM electrolyte; pH 6.5; current density: 10 mA cm^{-2}. 3-4b) Conditions: Synthetic NOM electrolyte; pH 6.5; current density: 20 mA cm^{-2}. 3-4c) Conditions: Synthetic NOM electrolyte; pH 8.5; current density: 10 mA cm^{-2}. 3-4d) Conditions: Synthetic NOM electrolyte; pH 8.5; current density: 20 mA cm^{-2}.

3.3.4. SUVA

NOM, a product of decomposition and metabolic reactions, poses a risk to human health through the production of disinfection by-products (DBPs). Specifically, trihalomethanes and haloacetic acids are carcinogenic or genotoxic [193]. Most NOM compounds, notably electronegative and highly reactive structures such as aromatic rings, react to form DBPs. Furthermore, aromatic structures absorb UV light effectively at specific wavelengths, such as 254

nm. Thus, UV_{254} can quantify NOM in water. Likewise, UV_{254} is normalized to DOC to yield SUVA, which acts as a metric to predict the aromaticity and treatability of NOM. Previous research results identified high TOC, color, and SUVA, were found to have higher DBPs such as THMs and HAAs. Although BDD and MMO electrodes are likely to produce OH radicals, the oxidization of chloride ions at the anode to chlorine, which hydrolyze into hypochlorous acids, leads to the electro chlorination of organic matter in the solution[188]. DBP formations are products of electro generation active chlorines. In this study, the electrochemical oxidation efficiency of synthetic NOM was evaluated using SUVA.

SUVA strengthened the conclusions extrapolated by the COD and TOC removal (%). SUVA is an indicator of aromaticity, often attributed to the growth of disinfection by-products (DBP) and synthetic NOM reduction. SUVA was found by the equation 3-3, where UV^{254} is the absorbance at wavelength 254 [cm^{-1}], and DOC is dissolved oxygen content measured in [mg L^{-1}]. DOC is measured by filtering a sample through a 0.45 μm filter, afterward, analyzed by the TOC system.

Synthetic water obtained SUVA values on average of 2.5 L/mg-m. In literature, natural waters with SUVA values less than 4 L/mg-m, generally contain hydrophilic and low molecular weight NOM moieties [194]. In general, SUVA increased for all electrochemical treatment systems, which indicated an increase in UV_{254} absorbing species such as aromatic rings (DBPs). Although SUVA increased as treatment progressed, TOC/DOC decreased as exhibited by the overall TOC removal. Therefore, the organic load of the synthetic water was reduced, but the remaining organic matter had a higher ratio of aromatic character than the initial state. Previous studies concluded aromaticity increase was not correlated with the increase of humic substances. They were merely an indicator of the fraction of aromatic character and general relation to the

formation of DBPs. All SUVA analyses below were performed at 120 mins. Figure 3-6 mapped SUVA as a function of time for M1, M2, and M3.

At 6.5 pH and 10 mA cm^{-2}, SUVA was the greatest for M3 at 14.4. M1 and M2 were significantly lower at 3.4 and 2.7. However, at 8.5 pH, SUVA decreased from M3 to 4.7, while M1 and M2 remained closer to their 6.5 pH values, 3.8 and 3.6 SUVA, respectively. Therefore, M1 and M2 implied a higher resistance to pH changes in the synthetic NOM solution, like the TOC and COD removal. Therefore, MMO electrodes produced less DBP as treatment pH increased.

At 6.5 pH and 20 mA cm^{-2}, SUVA values were 4.6, 3.4, and 6.7 for M1, M2, and M3, respectively. On the other hand, at 8.5 pH and 20 mA cm^{-2}, SUVA increased for all systems to 5, 6.3, and 5.6 for M1, M2, and M3, respectively. M1 and M2 presented an increase in performance at higher current and pH.

The SUVA data collected and portrayed in figure 3-6 shows that the M3 setups (MMO electrodes) were negatively impacted by current and pH increases.

Firstly, at a higher current and pH, more agglomerations were noticeably present in the solution, indicated by a notable discoloration and yellow particulates. The titanium from the MMO electrode surfaces introduced metallic coagulants to the electrochemical treatment, which increased the synthetic NOM floc (size, strength, structure, and recovery ability). The floc deceptively reduced COD and TOC values due to the testing equipment failing to sense larger agglomerates such as salts. However, SUVA information indicated a lower DBP formation as the agglomeration of organics reduced the reactive oxidative species in the solution.

Secondly, due to the lack of agglomeration prominent in BDD electrode systems, increased current density successfully produced a higher rate of DBP production and, therefore, more

significant NOM reduction. Also, increased pH is known to increase the occurrence of oxygen evolution; thus, the more oxidative species in the solution. This exacerbated NOM degradation in M1 and M2; however, reasons for the more reduced M3 performance at higher pH were undetermined and required further experimentation.

In summary, M3 produced more DBPs identified through SUVA. This suggested the presence of more secondary reactions involving chlorine present in MMO anode surfaces. Furthermore, TOC removal data, COD removal data, and COD/TOC ratios confirmed that overall, BDD electrodes reduced NOM to a greater extent than MMO, which concluded that high SUVA is a product of high aromaticity in MMO-SS synthetic water post-treatment.

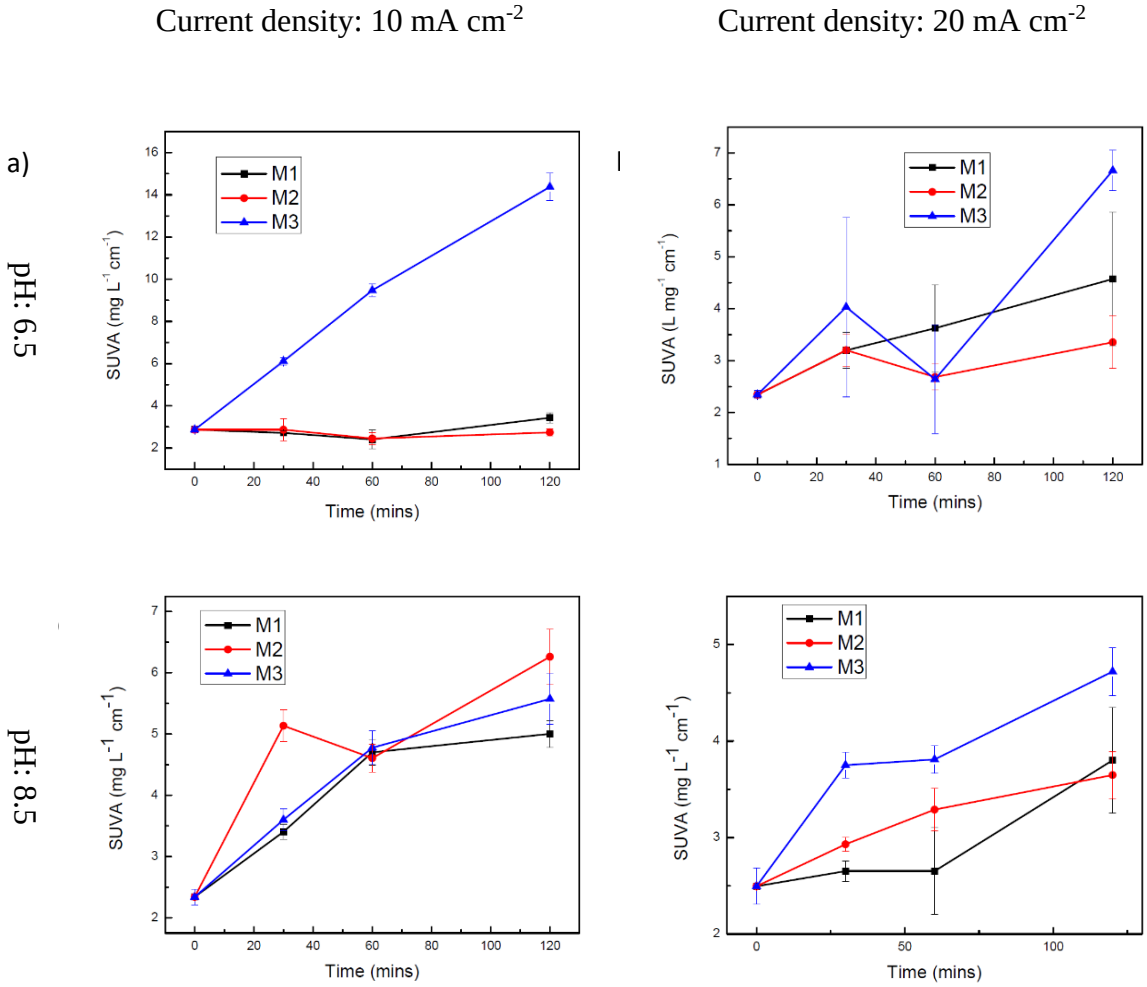

3.3.5. Estimation of Electrochemical Energy Consumption

Figure 3-6: SUVA on M1, M2, and M3 treatments. 3-5a) Conditions: Synthetic NOM electrolyte; pH 6.5; current density: 10 mA cm^{-2}. 3-5b) Conditions: Synthetic NOM electrolyte; pH 6.5; current density: 20 mA cm^{-2}. 3-5c) Conditions: Synthetic NOM electrolyte; pH 8.5; current density: 10 mA cm^{-2}. 3-5d) Conditions: Synthetic NOM electrolyte; pH 8.5; current density: 20 mA cm^{-2}.

Greater extremes, such as higher current densities and duration, increased current density led to an increase of applied potential. Figure 3-7 presents the energy consumption of the systems measured using equation 3-5[166].

Equation 3-5: Specific electrochemical energy consumption in kWh dm^{-3}

$$EC = \frac{\Delta ECIt}{1000V}$$

Here, "t" is the time of electrolysis, "ΔEC" is average cell voltage, "I" is electrolysis current, and "V" is sample volume.

Calculated at a lower applied current density of 10 mA cm^{-2}, M1 was observed to have the highest energy consumption at 0.0014 kWh dm^{-3}, as shown in figure 3-7a. In contrast, M2 and M3 amounted to 0.0004 and 0.0013 kWh dm^{-3}. At 20 mA cm^{-2}, M1, M2, and M3 displayed a consumption of 0.004, 0.0018, and 0.0041 kWh dm^{-3}, respectively. Therefore, BDD electrodes optimize the current input for the electrochemical treatment process at low current densities. Nonetheless, all three treatment setups exhibited a large increase in energy consumption when current density increased from 20 to 30 [mA cm^{-2}]. M1, M2, and M3, finalized at 0.012, 0.0223, and 0.0064 [kWh dm^{-3}] respectively. At higher current densities (>20 mA cm^{-2}), MMO electrodes consumed the least energy. BDD anodes, contrary to the literature, exhibited a greater energy consumption[52][26].

Also, as shown in Figure 3-7b, when the initial pH varied between the range 6.5-8.5, treatment setups generally remained constant in electrical energy consumption. M1 treatment system increased from 0.004 kWh dm^{-3} to 0.0044 kWh dm^{-3}. M2 increased in energy consumption as pH increased from 0.0018 to 0.0027 kWh dm^{-3}. Lastly, M3 decreased slightly from 0.0041 to

0.0036 kWh dm^{-3}. Therefore, the acidic conditions for M1 and M2 systems obtained lower specific energy consumptions.

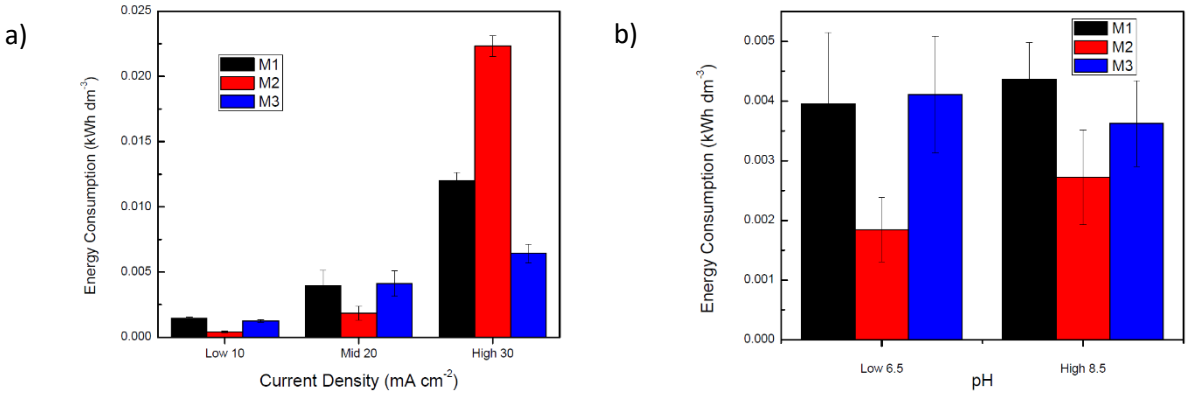

Figure 3-7: Energy Consumption of M1, M2, and M3 treatments. 3-6a) Conditions: Synthetic NOM electrolyte; pH 8.5; time 120 mins. 3-6b) Conditions: Synthetic NOM electrolyte; current density: 10 mA cm^{-2}; time 120 mins.

Figure 3-8 shows the results of electrical energy per order (EEO) as a function time during the NOM removal treatment. Electrical energy per order is listed as a "figure of merit" for the evaluation of advanced oxidation processes by the International Union of Pure of Applied Chemistry (IUPAC) [195]. Here, "P" is the power (kW), "V" is the volume of treatment solution (L), "$C_{i,}$ " and "C_f " are the concentrations of the NOM at initial and final stages respectively represented by TOC, and t is the allotted duration (h). Presented as (kWh $order^{-1}$ m^{-3}), EEO refers to the amount of energy required to reduce the contaminant to one-tenth of its original value in one m^3 of water[196], [197].

Equation 3-6: Electrical energy per order formula

$$EEO = \frac{1000Pt}{Vlog\left(\frac{C_i}{C_f}\right)}$$

At 6.5 pH and 10 mA cm^{-2}, M3 exhibited a stable EEO ranging from 0.9 – 2.7 (kWh $order^{-1}$ m^{-3}). However, M1 and M2 showed negative EEOs, which indicated the ineffective removal of NOM. EEO at 120 mins is not included in the plot as the values are shallow at -1316 and -5183 (kWh $order^{-1}$ m^{-3}) for M1 and M2, respectively. Raising the current density to 20 mA cm^{-2} increased the EEO of M3 to 38.9 (kWh $order^{-1}$ m^{-3}). M2 increased and peaked at 67.2 (kWh $order^{-1}$ m^{-3}), Although M1 increased as well, the EEO remained lower than M2 and M3. M1 reached 22.0 (kWh $order^{-1}$ m^{-3}) respectively.

At 8.5 pH and 10 mA cm^{-2}, once again, M1 and M2 presented negative EEO values at -10.8 and -1.9 (kWh $order^{-1}$ m^{-3}). M3 reached an EEO of 6.5 (kWh $order^{-1}$ m^{-3}). When the current density was increased to 20 mA cm^{-2}, M3 experienced the greatest EEO at 141.1 (kWh $order^{-1}$ m^{-3}). M1 and M2 remained lower compared to 86.7 and 66.4 (kWh $order^{-1}$ m^{-3}), respectively.

In summary, increases in current significantly increased the EEO for all treatment setups meaning lower current systems were more efficient than high current. At low current densities, however, M1 and M2 experienced undefined EEO. Therefore, the BDD electrodes showed low affinity at low current processes. Additionally, further emphasizing removal data, BDD electrodes more efficiently (on average) removed NOM at high current densities, as shown in figure 3-9. BDD electrodes presented an EEO of 36.6 and 31.4 for M1 and M2, whereas M3 remained higher at 44.4 (kWh $order^{-1}$ m^{-3}). Furthermore, 6.5-8.5 pH ranges had minimal effect on EEO.

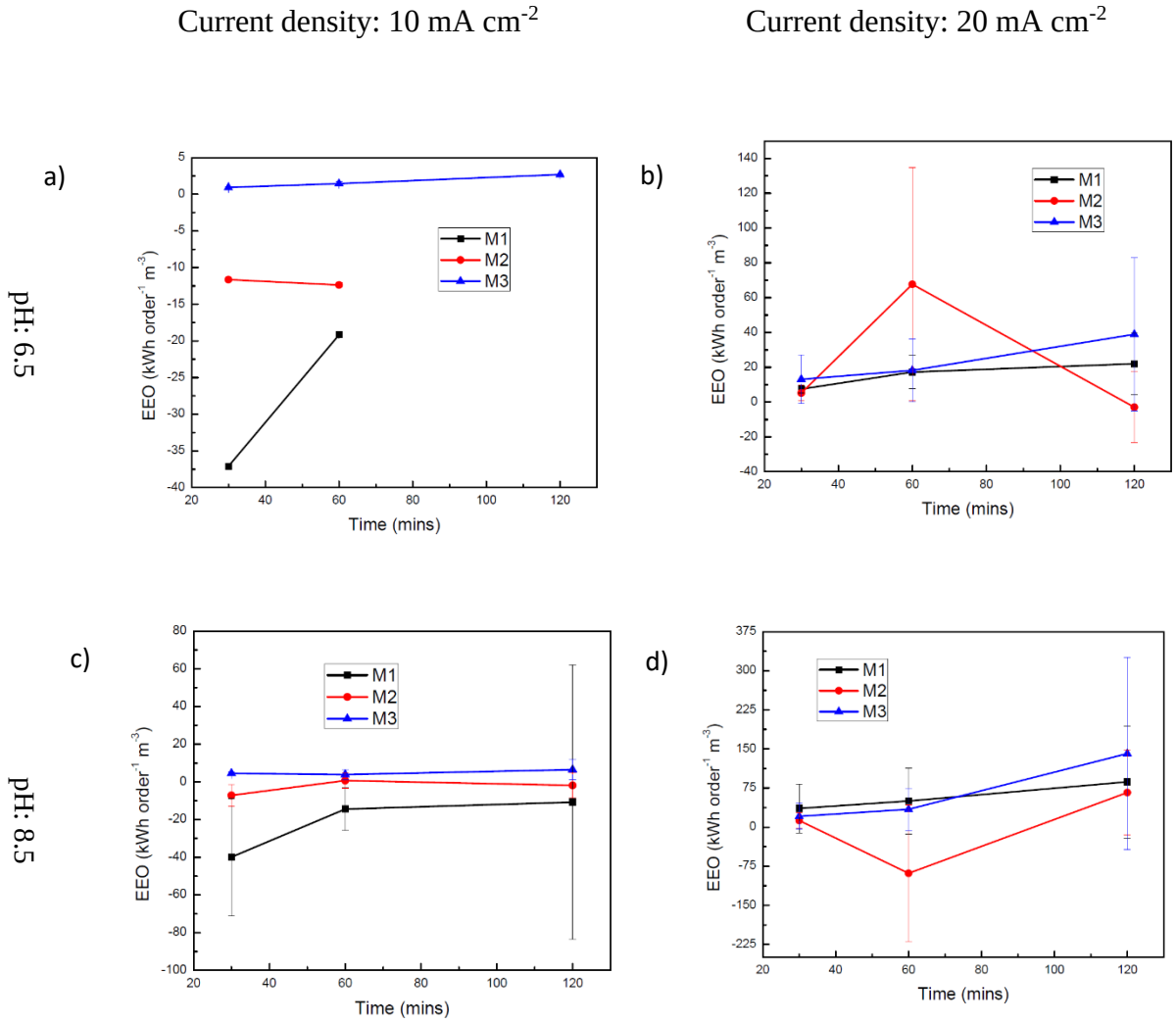

Figure 3-8: EEO on M1, M2, and M3 treatments. 3-5a) Conditions: Synthetic NOM electrolyte; pH 6.5; current density: 10 mA cm^{-2}. 3-5b) Conditions: Synthetic NOM electrolyte; pH 6.5; current density: 20 mA cm^{-2}. 3-5c) Conditions: Synthetic NOM electrolyte; pH 8.5; current density: 10 mA cm^{-2}. 3-5d) Conditions: Synthetic NOM electrolyte; pH 8.5; current density: 20 mA cm^{-}

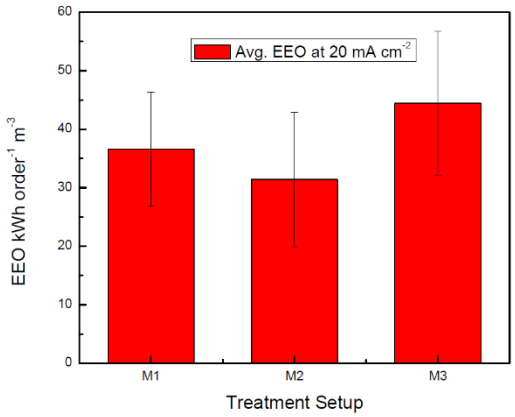

Figure 3-9: Average EEO on M1, M2, and M3 setups at 20 mA cm^{-2}

3.4. Summary

Chapter 3 studies successfully compared removal by electrochemical oxidation using BDD and MMO anodes, as outlined in table 3-4.

Table 3-4: List of conclusions inferred from TOC, COD, SUVA, and specific energy consumption data

Data Analysis Method	***Quantitative Conclusion***	***Supplementary Information***
TOC Removal	Increased with the current for M1 and M2 M1 and M2 increased in TOC initially, suggesting the presence of DBP, not present in M3 M3 produced agglomerates Initial pH did not have a significant effect	Current density is proportional to the number of reactions taking place on the electrode surface: BDD had more active sites compared to MMO Agglomerates produced sulfates and salts, replacing hydroxide ions in the solution
COD Removal	Increased with the current for M1 and M2 Initial pH did not have a profound effect	
Energy Consumption	All setups increased energy consumption with current M3 had the lowest consumption at acidic conditions NOM removal generally increased with current density, however; reduced efficacy at higher extreme current	Higher concentrations of hydroxyls increase undesirable side reactions such as the electrolysis of water which compete with the electrochemical oxidation of the contaminants
PeCOD/TOC Ratio	M3 exhibited the largest COD/TOC ratio peak in low pH and low current conditions COD/TOC ratio was unaffected by pH variation	MMO electrodes produced yellow particulates from the titanium surface They reduced COD and TOC through agglomeration and increased floc size, however; superficially (did not produce DBP)

	M1 and M2 obtained higher COD/TOC ratio at higher current	
	High durations required to oxidize secondary DBP to non-harmful compounds	
SUVA	M1 and M2 produced DBP at higher pH and higher current	MMO agglomerates reduced reactive oxidative species in solution

Although the treatment conditions applied low current densities (compared to existing literature result), it was observed that electrooxidation by BDD and MMO electrodes were heavily reliant on current density. Current density is proportional to the number of reactions taking place on the electrode surface, where BDD has more active sites than MMO, and thus, BDD electrodes showed higher removal with current density increases. On the other hand, initial pH did not have a profound effect on NOM oxidation.

Additionally, the oxidation process suggested that high durations are necessary to oxidize secondary DBP to non-harmful compounds. All removal data showed an increase in NOM at 30- and 60-minutes in duration. Furthermore, MMO electrodes produced a yellow particulate in the solution. They reduced TOC and COD through agglomeration but had minimal effect on SUVA. Lastly, electrooxidation systems were more efficient at low current densities as higher concentrations of hydroxyls increase undesirable side reactions such as the electrolysis of water, which competes with the electrochemical oxidation of the contaminants.

BDD electrodes were determined to be more effective than MMO for NOM removal. Nevertheless, optimization is required for new drinking water processes.

Chapter 4. Process optimization using BBD statistical modeling

4.1. Introduction

The previous chapter highlighted that operating conditions such as initial pH, current density, and electrolysis time have a profound effect on electrooxidation NOM removal processes. Furthermore, BDD and MMO electrode setups reacted uniquely to changes in each operating condition. Similarly, to date, most studies on NOM removal treatment focused on the traditional one-factor-at-a-time approach[159]. Although the approach provided effective numerical results, it does not account for cross effects from the factors. For example, pH changes throughout the electrolysis; however, the interaction effects are ignored when looking at final TOC, COD, and UV_{254}. Therefore, single-factor approaches denote poor optimization results.

Previously, response surface methodology (RSM) was applied to successfully optimize electrochemical treatment processes including, but not limited to, electro Fenton oxidation, electrooxidation, EAOPs, AOPs, and electrocoagulation. This chapter, [we] examined the degradation of NOM through a statistical approach. System variables were proactive chosen to reflect conclusions from chapter 4: initial pH, electrolysis time, and applied current density. Furthermore, besides, to flow rate and supporting electrolyte concentrations, which do not apply to [our] batch system reaction setup, these system variables were established as dependent conditions for electrochemical oxidation of NOM. Moreover, a Box-Behnken response surface design (BBD) coupled with a derringer's desired function methodology was used to monitor the changes of TOC removal, COD removal, and SUVA. Their monitored responses garnered functional relationships with the independent variables. The analysis of variance (ANOVA) was also applied to validate the relationships obtained.

4.2. Materials and Methods

The synthetic water matrix was identical to the solution in chapter 3.

4.2.1. Electrochemical Setup

Identical to the setup in chapter 3.

NOM degradation was carried out in a batch system with three unique electrode setups. All tests for TOC, COD, and SUVA analyses used a two-electrode setup with a volume capacity of 300 mL of the synthetic solutions. The setups include the (M1) BDD anode and BDD cathode electrochemical system, (M2) BDD anode and stainless-steel cathode electrochemical system, and (M3) MMO anode and stainless-steel cathode electrochemical system. These systems were mechanically stirred for the duration of the experiment at 400 rpm. Additionally, the physical properties of the electrodes were machined to have the same surface areas [10 mm x 10 mm x 1 mm]. Furthermore, the distance between electrodes was kept constant at 3 mm in the synthetic NOM water.

Batch tests were run uninterrupted, and the overall TOC, COD, and UV_{254} measurements were taken at the end of the allotted duration(s) at (1) 30 minutes, 60 minutes, and 120 minutes.

4.2.2. Analytical methods

Removal efficiency formula was modified from equation 3-1 and 3-2, where Y_0 and Y represent the initial and final values of TOC and COD.

Equation 4-1 Modified TOC and COD removal efficiency formula for BBD experimental design

$$TOC\ and\ COD\ (\%) = \frac{Y_0 - Y}{Y} * 100$$

SUVA was measured by equation 3-3.

4.2.3. Experimental design of BBD

The response surface design was developed for all three different treatment setups individually: (1) M1, BDD anode and BDD cathode, (2) M2, BDD anode and SS cathode, and (3) M3, MMO anode and SS cathode.

The RSM design optimized three factors at five levels to assess the influence of process variables such as (A) initial pH (6.5 – 8.5), (B) current density (10 – 30), and (C) electrolysis time (30 – 120 min) on (Y1) TOC removal, (Y2) COD removal, and (Y3) SUVA.

A second-order polynomial equation investigated the relationship between independent variables and responses. All statistical analyses were done with Stat-ease Design Expert 8.0.7.1 statistical software.

Experimental data was analyzed and fitted to the second-order polynomial model[153], [162], [198]:

$$Y_{nm} = b_0 + \sum_{i=1}^{4} b_i x_i + b_{12}x_1x_2 + b_{13}x_1x_3 + b_{14}x_1x_4 + b_{23}x_2x_3 + b_{24}x_2x_4 + b_{34}x_3x_4 + \sum_{i=1}^{4} b_{ii}x_i^2$$

Y_{nm} is any of the specified response variables; n denotes experimental setup, and m identifies response factor, b_0 is a constant; b_1, b_2, b_3, and b_4, are regression coefficients for linear effects; b_{11}, b_{22}, b_{33}, and b_{44} are quadratic coefficients, and; b_{12}, b_{13}, b_{23}, b_{24}, and b_{34} are interaction effects. The models are subjected to change and reduction; in the event, specific factors and interaction effects are not determined significantly by p-value analysis.

4.3. Results and Discussion

Electrooxidation processes were used to treat synthetic NOM water. A total number of 17 batch experiments were required to analyze the data. Appendix A presents the data used for the experimental design, for all treatment setups and response factors.

4.3.1. Mathematical model selection

As highlighted in the literature review of previous applications of BBD designs for electrochemical processes, second-order quadratic models best represent the pseudo-first-order EO reaction mechanisms. Additionally, the experimental data were analyzed by Stat-ease's model summary statistics to obtain regression models to represent the EO process. Table 4-1 outlines the results below. The highest p-values and lower coefficient of determinations were found for quadratic models for all treatment setups and responses. On the other hand, the cubic model was aliased, suggesting more data terms unnecessarily were required than unique points in the design. Therefore, the quadratic model was chosen to gauge the effects of initial pH, current density, and electrolysis time.

Table 4-1: Model summary statistics tested for the responses

Source	*Sequential p-value*	*Lack of Fit p-value*	*Adjusted R^2*	*Predicted R^2*	*Remarks*
					M1: TOC Efficiency
Linear	0.0455		0.3220	0.1133	
2FI	0.7604		0.2117	-0.5747	
Quadratic	**0.0002**		**0.9188**	**0.3500**	**Suggested**
Cubic			1.0000		Aliased
					M1: COD Efficiency
Linear	0.1803	< 0.0001	0.1437	-0.0187	
2FI	0.8842	< 0.0001	-0.0459	-0.4802	
Quadratic	**< 0.0001**	**0.0027**	**0.9804**	**0.8565**	**Suggested**

Cubic	0.0027		0.9987		Aliased
					M1: SUVA
Linear	**0.0148**		**0.4360**	**0.0101**	**Suggested**
2FI	0.2988		0.4839	-1.2573	
Quadratic	**0.0106**		**0.8375**	**-0.3247**	**Suggested**
Cubic			1.0000		Aliased
					M2: TOC Efficiency
Linear	0.0625		0.2853	-0.0095	
2FI	0.8571		0.1365	-1.2150	
Quadratic	**< 0.0001**		**0.9766**	**0.8196**	**Suggested**
Cubic			1.0000		Aliased
					M2: COD Efficiency
Linear	0.0608	< 0.0001	0.2884	-0.0109	
2FI	0.4264	< 0.0001	0.2909	-0.5084	
Quadratic	**0.0068**	**< 0.0001**	**0.8041**	**-0.3464**	**Suggested**
Cubic	< 0.0001		0.9997		Aliased
					M2: SUVA
Linear	0.0478		0.3165	-0.0574	
2FI	0.6495		0.2405	-1.3081	
Quadratic	**< 0.0001**		**0.9907**	**0.9249**	**Suggested**
Cubic			1.0000		Aliased
					M3: TOC Efficiency
Linear	0.5226		-0.0417	-0.7253	
2FI	0.5104		-0.0860	-2.8472	
Quadratic	**0.0002**		**0.8960**	**0.2850**	**Suggested**
Cubic			1.0000		Aliased
					M3: COD Efficiency
Linear	0.4089	< 0.0001	0.0068	-0.5252	

2FI	0.1882	< 0.0001	0.1828	-0.7591	
Quadratic	**0.1545**	**< 0.0001**	**0.4232**	**-3.8520**	**Suggested**
Cubic	< 0.0001		0.9988		Aliased
					M3: SUVA
Linear	0.3667		0.0270	-0.5504	
2FI	0.1448		0.2451	-1.2693	
Quadratic	**0.0012**		**0.8748**	**-0.0303**	**Suggested**
Cubic			1.0000		Aliased

Moreover, the analysis of variance confirmed the adequacy of the models. Operating factors and their interactions that had p-values greater than 0.1 were removed from the model to increase fit. ANOVA tables are presented for each treatment setup and response variable in appendix D to 4-14. All models for COD efficiency with setups M1, M2, and M3 had a significant lack-of-fit.

4.3.2. Mathematical model fitting

The results from the BBD experimental design were evaluated by multiple regression analyses proposed for EO processes in literature. An empirical relationship for TOC removal, COD removal, and SUVA, was determined by a second-order polynomial equation with interaction terms. Therefore, the concrete influence of independent variables was assessed. Models were broken down into treatment setups.

M1 TOC efficiency

$$TOC\ Efficiency\ (\%) = 1903.7659 - 481.16\ (A) - 0.5688\ (B) - 14.7328\ (C) - 0.0504\ (B * C) + 31.5812\ (A^2) + 0.0138\ (B^2) + 0.5602\ (C^2)$$

M1 COD efficiency

$$COD\ Efficiency\ (\%)$$

$$= 1847.0338 - 482.957\ (A) - 0.2287\ (B) - 16.8466\ (C) - 0.4246\ (A * B)$$

$$- 0.02184(B * C) + 35.27\ (A^2) + 0.02849\ (B^2) + 0.52\ (C^2)$$

M1 SUVA

$$SUVA\ \left(\frac{L}{mg\ M}\right) = 33.38 - 0.2035\ (B) - 3.48668\ (C) + 0.01476\ (B * C) + 0.084\ (C^2)$$

M2 TOC efficiency

$$TOC\ Efficiency\ (\%)$$

$$= 344.6132 - 14.892\ (A) - 4.3311\ (B) - 20.9551\ (C) + 0.2718\ (A * B)$$

$$+ 0.02595\ (B * C) + 0.01065\ (B^2) + 0.5794\ (C^2)$$

M2 COD efficiency

$$COD\ Efficiency\ (\%)$$

$$= 2179.9154 - 693.591\ (A) - 1.7114\ (B) + 31.3578\ (C) - 3.7437\ (A * C)$$

$$+ 52.9673\ (A^2) + 0.014649\ (B^2)$$

M2 SUVA

$$SUVA\ \left(\frac{L}{mg\ M}\right)$$

$$= -2.25485 + 3.1056\ (A) - 0.06992\ (B) - 0.8935\ (C) - 0.1447\ (A * C)$$

$$+ 0.00368\ (B * C) + 0.05255\ (C^2)$$

M3 TOC Efficiency

$$TOC\ Efficiency\ (\%)$$

$$= -1332.3612 + 426.0882\ (A) + 0.4951\ (B) - 19.7912\ (C)$$
$$+ 1.5411\ (A * C) + 0.0263\ (B * C) - 31.2231\ (A^2) - 0.00663\ (B^2)$$
$$+ 0.1783\ (C^2)$$

M3 COD efficiency

$$COD\ Efficiency\ (\%)$$

$$= -846.4401 + 243.1878\ (A) + 0.6228\ (B) - 2.6127\ (C) + 0.06408\ (B * C)$$
$$- 16.078\ (A^2) - 0.01275\ (B^2)$$

M3 SUVA

$$SUVA\ \left(\frac{L}{mg\ M}\right)$$

$$= +178.6326 - 35.7319\ (A) + 0.1224\ (B) - 4.2555\ (C) + 0.3645\ (A * C)$$
$$- 0.0046\ (B * C) + 1.816\ (A^2) + 0.042\ (C^2)$$

A, B, and C are initial pH, the time elapsed, and current density, respectively. The obtained models had high values of the coefficient of determination (R^2).

The evaluation of the models, in addition to ANOVA tables, was performed by constructing diagnostic plots to illustrate the predicted and actual values for the experimental data, as shown in Appendix C. Good agreements were found between experimental and predicted values for TOC removal, COD removal, and SUVA, for all three experimental setups. Coupled with AVOVA, the results from the Derringer's fitting demonstrated that BBD RSM was suitable to describe the electrochemical oxidation process.

The lack-of-fit with COD efficiency models determined a failure of the model to describe the functional relationship between factors and response variables adequately. Furthermore, since the Stat-Ease model summary analysis aliased the cubic regression model and therefore, the model

does not overlook interactions and cubic terms, the lack-of-fit [may be] a product of (1) peCOD ineffectively measuring NOM, and (2) inadequate amount of iterations. Nevertheless, the chapter continues with the analysis of COD efficiency.

4.3.3. ANOVA interpretation

ANOVA tables are presented in appendix D. ANOVA tables, and consequently generated p-values can provide essential insight on significant factors affecting the response variables.

4.3.3.1. Effect of initial pH

4.3.3.1.1. M1

Initial pH effects were analyzed through M1 ANOVA tables for TOC efficiency, COD efficiency, and SUVA. For TOC efficiency and SUVA, the initial pH was not significant. The effect of pH on the electrochemical oxidation of organics was previously investigated; nonetheless, the results indicated that the initial pH effects on oxidation efficiency were mixed. According to literature and direct oxidation reaction processes, the effect of pH strongly depends on the nature of investigated organics and in [our] case, synthetic water matrix. Additionally, the selected range for pH is 6.5 – 8.5, which reflects natural water pH ranges, but the degradation of organics between 2 – 9 is generally stable in BDD anodes. A broader pH range [may] present different results if inspected.

On the other hand, COD efficiency was influenced by initial pH. Initial pH value affected the presence of active chlorine in the solution. At acidic pH, the preferred chlorine product is HClO, and above pH 8, it is ClO- [192], [199]. Therefore, an additional oxidation side reaction occurs. Overall, the total organic content paralleled (TOC) equally; however, the additional reaction increased the amount of oxygen consumed and, thus, COD.

4.3.3.1.2. M2

ANOVA tables determined the effect of initial pH on M2 TOC efficiency, COD efficiency, and SUVA. Similar to M1, the initial pH had a profound effect only on COD efficiency, whereas TOC efficiency and SUVA were mostly unaffected by changes in initial pH.

Although the effects were similar, ANOVA p-values for initial pH for M2 were closer to the null hypothesis than M1. The presence of stainless-steel cathodes may make the electrochemical system more susceptible to initial pH fluctuations. Therefore, BDD electrodes are more stable in electrochemical processes.

4.3.3.1.3. M3

Initial pH influence on M3 TOC efficiency, COD efficiency, and SUVA was investigated through ANOVA tables. Unlike M1 and M2, initial pH had a significant effect on TOC efficiency, COD efficiency, and SUVA. MMO electrodes promoted indirect oxidation and involved hypochlorite mediated chemistry. Since pH directly altered the preferred chlorine product, organic oxidation was influenced by initial pH. Furthermore, the reaction mechanism with an MMO electrode was different from BDD highlighted by the presence of yellow particulates in the synthetic solution. Initially, pitting and corrosion were suspected to occur, but further research highlighted, the visible yellow hue was a product of the agglomerate formation of M(O)x species from indirect electro-oxidation methods with MMO (Ti)[200]. Thus, BDD electrodes performed well in wider pH ranges and could provide advantages over MMO in practical applications.

4.3.3.2. Effect of Current Density

4.3.3.2.1. M1

Initial current significance was determined through ANOVA tables for M1 TOC efficiency, COD efficiency, and SUVA. As predicted in literature, current density was indicated

to be significant in determining all response factors. Current density rapidly increases the productions of hydroxyl radicals for BDD direct oxidation, which in turn increases oxidation of NOM.

4.3.3.2.2. M2

From M2 ANOVA tables for TOC efficiency, COD efficiency, and SUVA, initial current density played a significant role in response factor determination. The results were identical to M1 ANOVA.

4.3.3.2.3. M3

Extrapolated from M3 ANOVA tables for TOC efficiency, COD efficiency, and SUVA, initial current density was a significant factor. An increase in current density resulted in an increased role for halogen salts in the synthetic water to generate active chlorine species. Although both electrodes founded a significant relation to current density, throughout all response factors, M3 had the highest p-value.

4.3.3.3. Effect of Electrolysis Time

4.3.3.3.1. M1

The effect of electrolysis time was analyzed from ANOVA tables for M1 TOC efficiency, COD efficiency, and SUVA. Time was a significant factor for NOM oxidation. Increased electrolysis time upsurged the concentration of oxidant species, such as hydroxyl radicals.

4.3.3.3.2. M2

Similar to M1, ANOVA tables for M2 TOC efficiency, COD efficiency, and SUVA presented electrolysis time was a significant factor for the response factors.

4.3.3.3.3. M3

Surprisingly, from the M3 ANOVA tables, electrolysis time was determined to be not significant in determining TOC efficiency and COD efficiency. Although indirect oxidation mechanisms introduce hydroxyl radicals and hypochlorite in the presence of chlorine, electrolysis time does not affect agglomerates and MOx species production.

Furthermore, M3 SUVA showed that electrolysis time was a significant factor. This suggested that the increase of agglomerates raised the aromaticity of the synthetic matrix (as time progressed), but it failed to decrease overall TOC and COD content.

4.3.4. Effect of process variables; Contour interaction plots

ANOVA tables merely reflect the significance of process variables. 3-D contour plots provided an in-depth look at the trends and interaction effects of process variables. The plots provided individual and interactive effects among the process variables to determine the optimal condition of each factor for TOC efficiency, COD efficiency, and SUVA. Figure(s) 4-1 to 4-9 present contour plots for M1, M2, and M3. Multi-factor analyses, presented in appendix E, were performed to supplement contour plot data.

4.3.4.1. M1 TOC Efficiency

Figure 4-1 illustrates 3D contour plots for M1 TOC efficiency.

From the literature and ANOVA tables, initial pH had a minimal effect on TOC efficiency[64], [201], [202]. Nonetheless, the contour plots affirmed that within the span of the experimental range 6.5 – 8.5, TOC efficiency is not affected by initial pH. The plots also showed lowered efficiency at 7.5 pH. Additionally, higher electrolysis time and applied current densities reduced the lowered performance at 7.5 pH.

Furthermore, electrolysis time showed a linear trend for TOC efficiency. In BDD anodes, increased electrolysis time allotted more time for surface reactions to produce hydroxyl radicals [21]. However, at large applied current density (<25 mA cm^2), the effect of time is minimized, which suggests there is a maximum concentration of oxidative species in the synthetic matrix.

Lastly, applied current density had a positive effect on TOC efficiency. Generally, an increase in applied current density increased the positive effect of initial pH and electrolysis time.

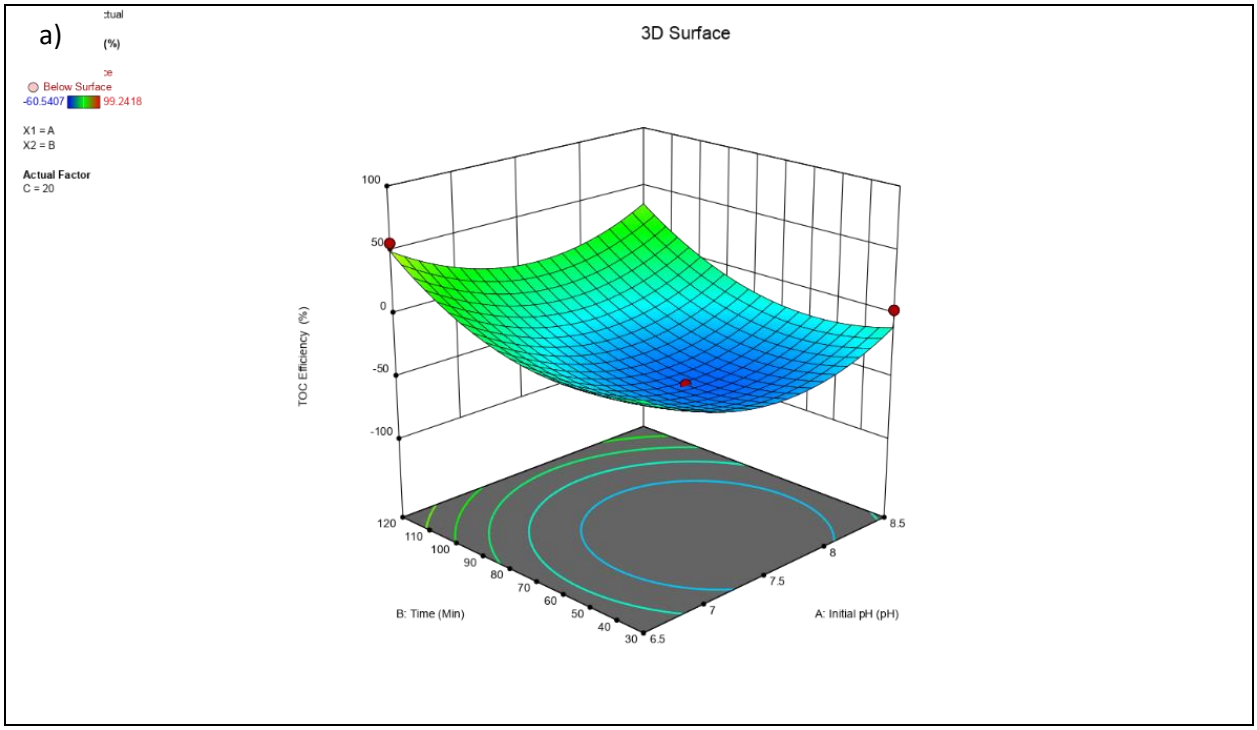

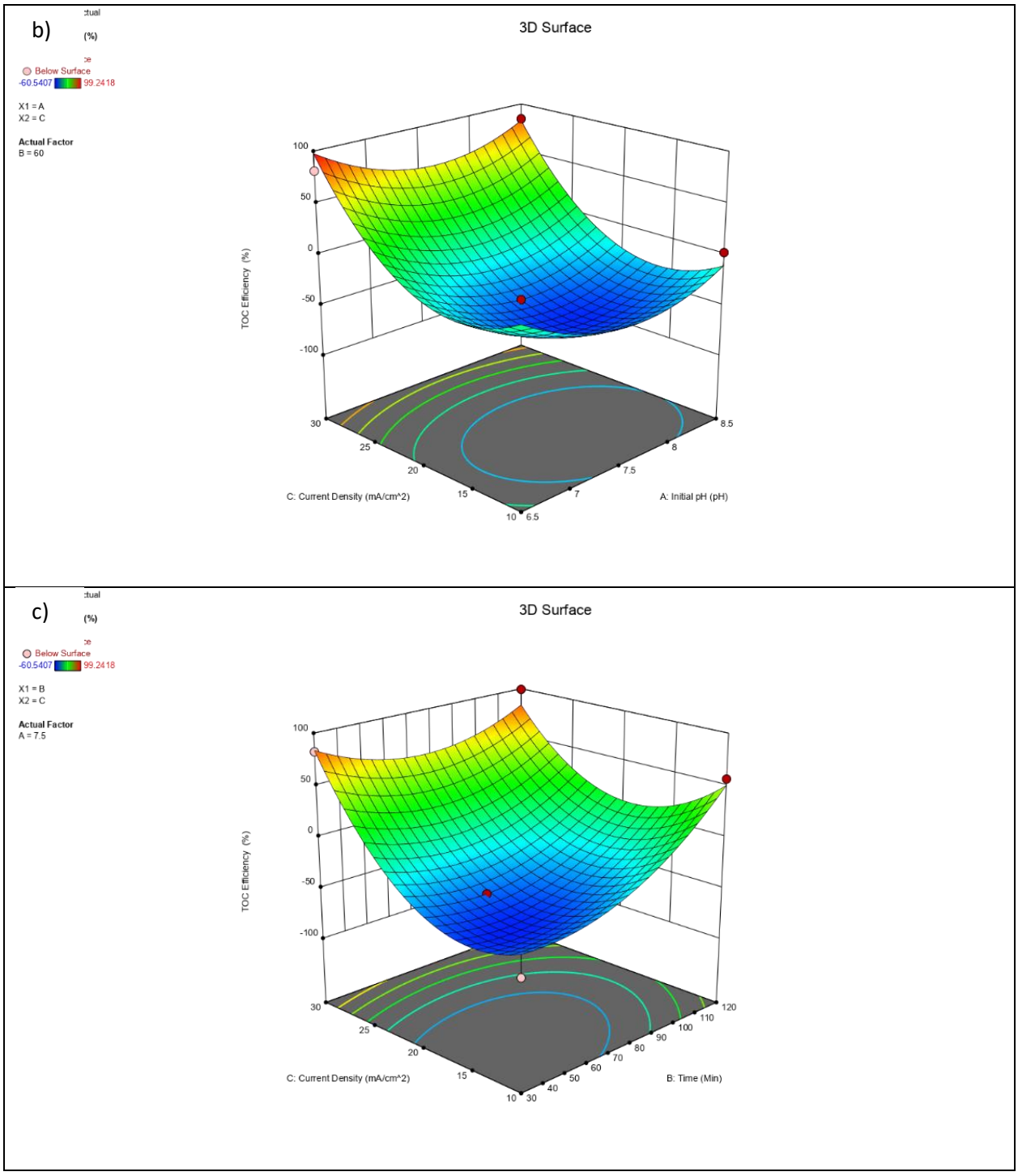

Figure 4-1 Response surface plots (3D) for the effects of variables on M1 TOC efficiency. 4-10a) Initial pH and electrolysis time, 4-10b) Initial pH and current density, 4-10c) electrolysis time and current density

4.3.4.2. M1 COD Efficiency

Figure 4-2 presents 3D contour plots for M1 COD efficiency. They presented identical trends to TOC efficiency. However, TOC efficiency was higher than COD efficiency for M1 electrode setups.

Surprisingly, COD efficiency was maximized at higher pH. From COD efficiency contour parts, although there is an increase in efficiency as time progresses, it takes a longer time to reach a high efficiency at lower current density. Additionally, at high current density, electrolysis time played a minimal role in determining COD efficiency.

Lastly, current density positively influenced COD efficiency, including interactions with other process variables. Nonetheless, similar to TOC efficiency, changes in current density were less effective at higher electrolysis time.

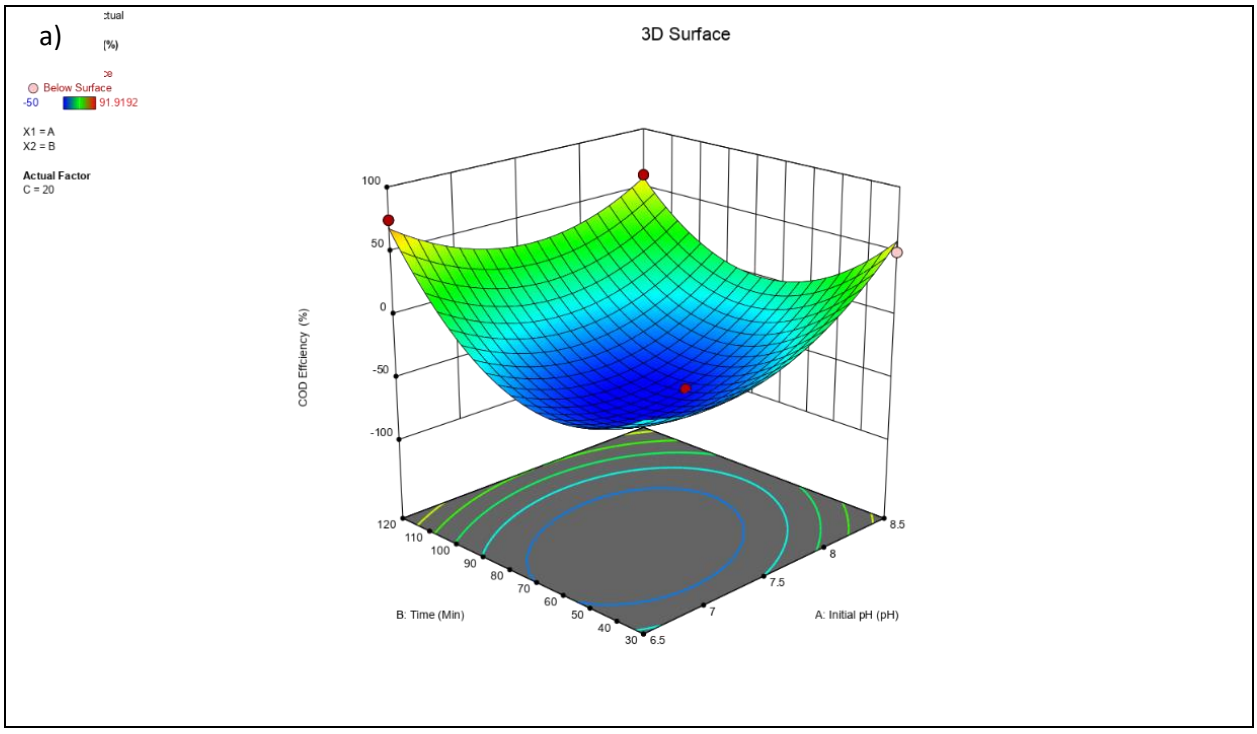

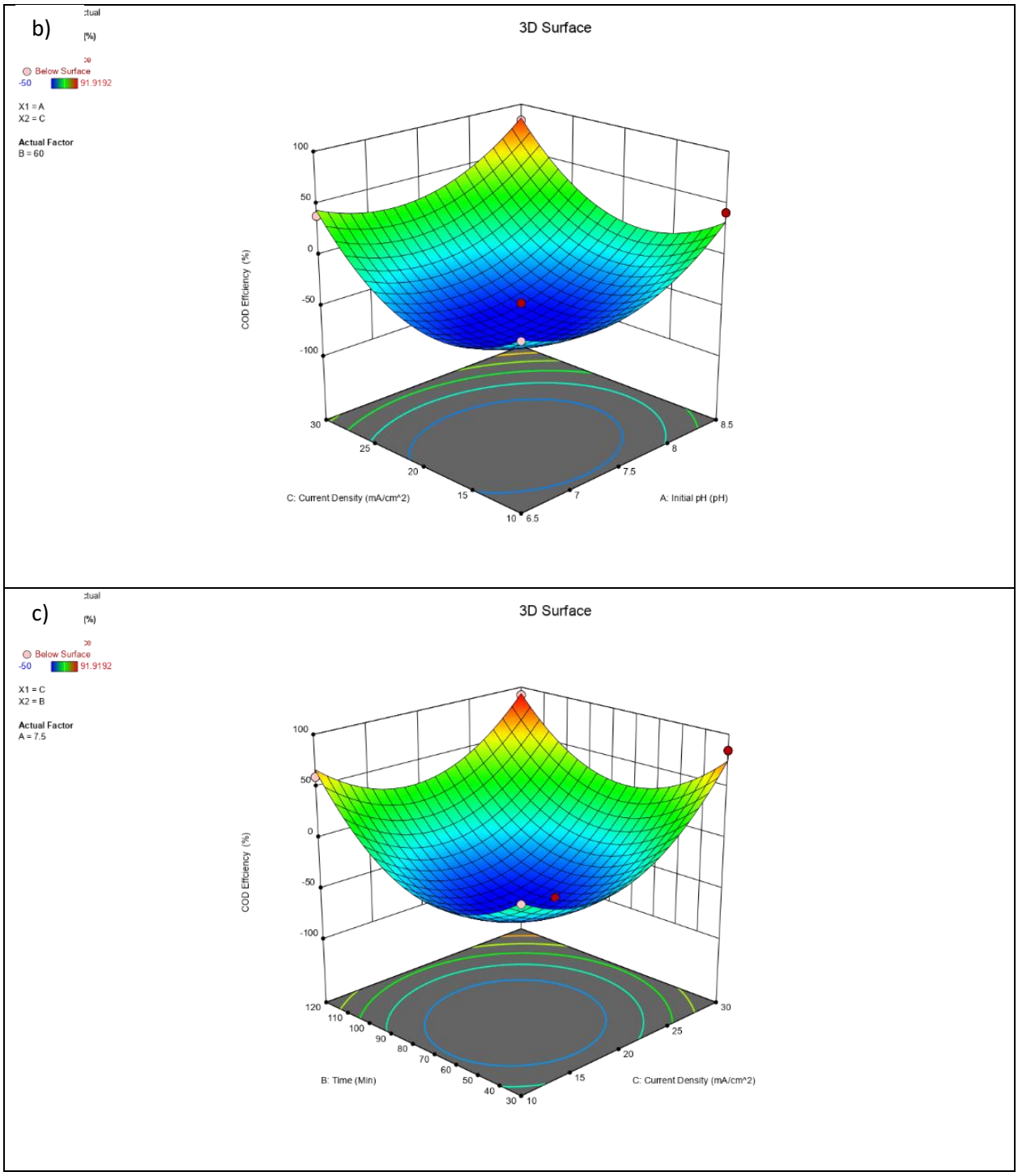

Figure 4-2 Response surface plots (3D) for the effects of variables on M1 COD efficiency. 4-11a) Initial pH and electrolysis time, 4-11b) Initial pH and current density, 4-11c) electrolysis time and current density

4.3.4.3. M1 SUVA

Figure 4-3 presents contour plots for M1 SUVA; the identified initial pH had no effect on SUVA for dual BDD anode and cathode systems. There was no interaction effect of initial pH with electrolysis time and applied current density. BDD anodes have a high overpotential for oxidation, wherein their active species generation is affected by initial pH; however, breakdown of functional groups into DBPs and thus, aromaticity was unaffected by pH [21], [203].

On the other hand, electrolysis time and current exhibited a positive effect on SUVA. Although the increases facilitated by electrolysis time were minimal, significant positive feedback was shown with the current.

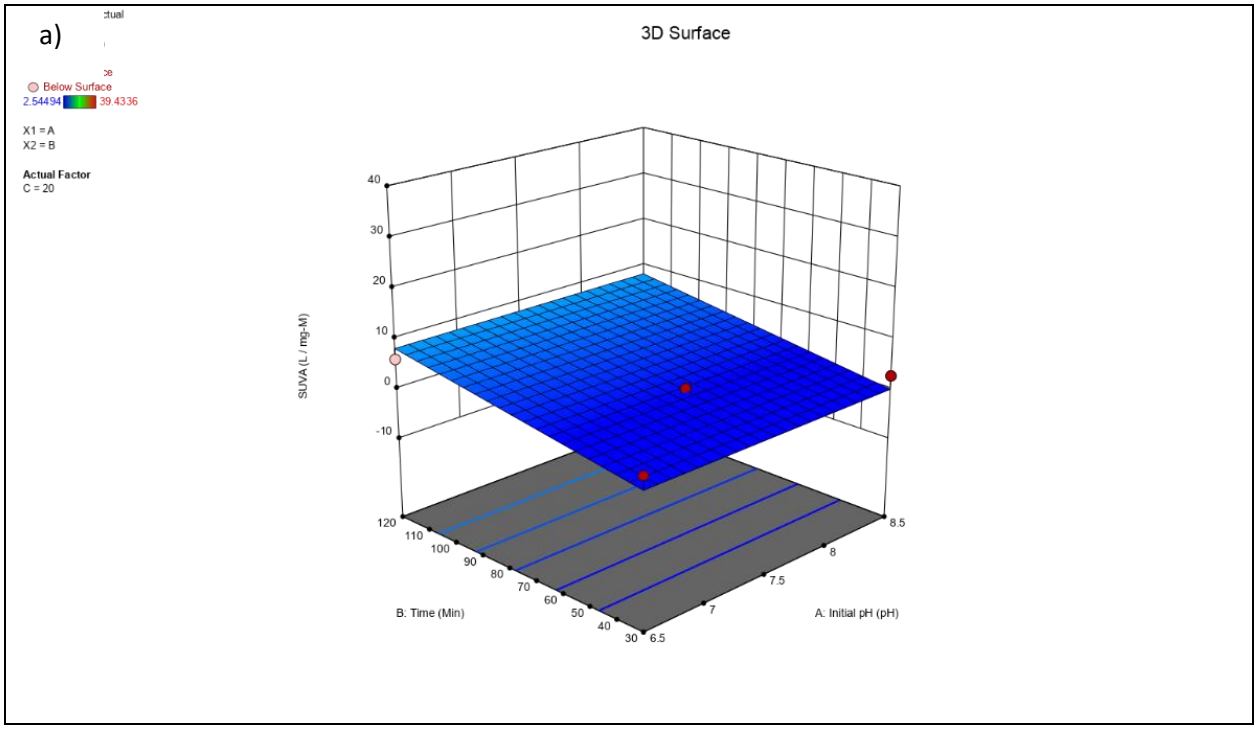

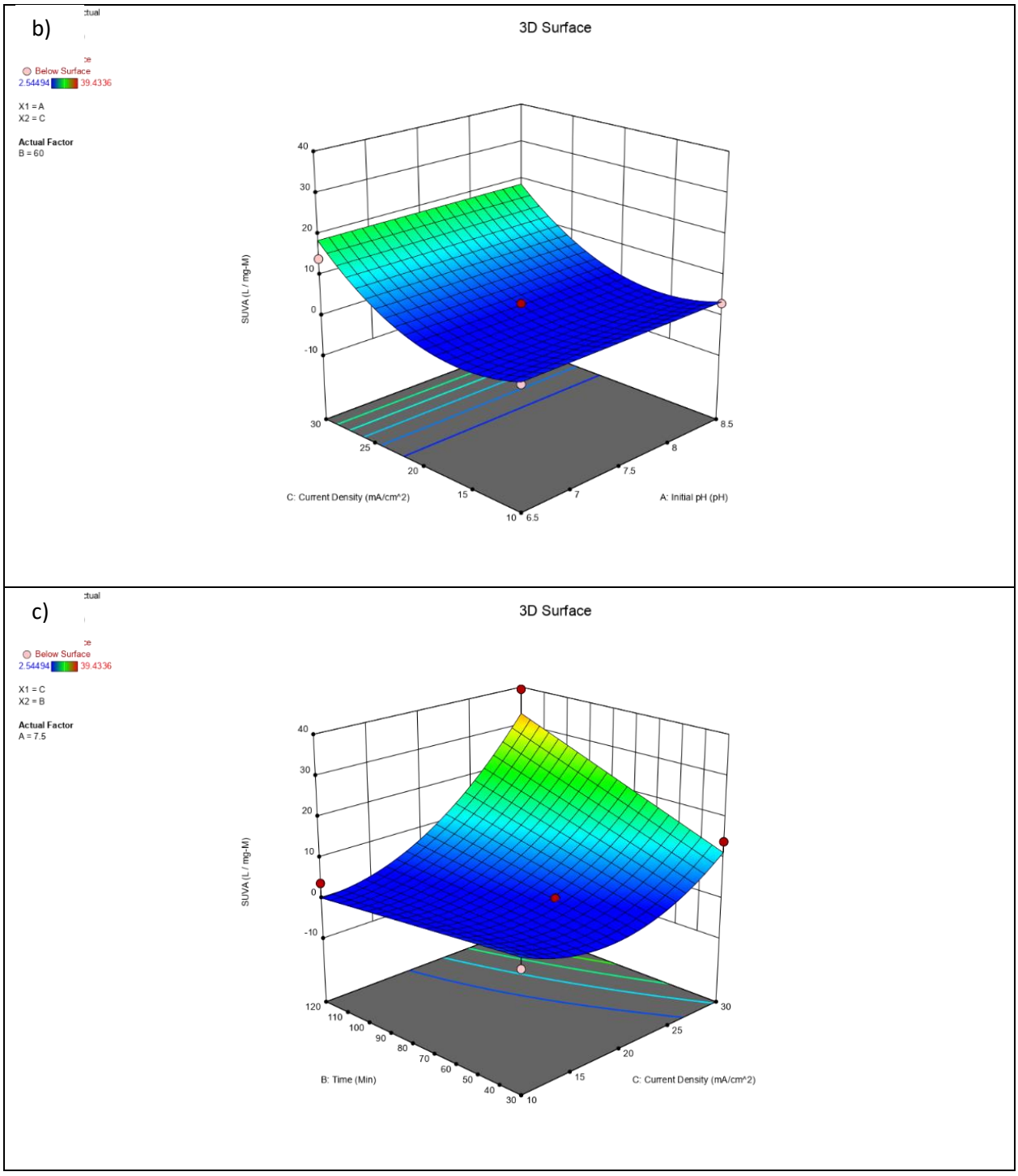

Figure 4-3 Response surface plots (3D) for the effects of variables on M1 SUVA. 4-12a) Initial pH and electrolysis time, 4-12b) Initial pH and current density, 4-12c) electrolysis time and current density

4.3.4.4. M2 TOC efficiency

Contour plots for M2 TOC efficiency are presented in figure 4-4. M2 showed a lower overall TOC efficiency than M1 electrochemical systems at the controlled process condition ranges.

Additionally, initial pH had little to no interaction effect with current, unlike M1. Therefore, dual BDD systems are more likely to be influenced by solution pH than BDD-SS. Furthermore, electrolysis time played a minimal role in M2 TOC efficiency. At lower applied current densities, TOC efficiency was higher at 30 minutes.

Lastly, applied current density had a positive linear effect on M2 TOC efficiency. However, at low current density, increasing electrolysis time reduced TOC efficiency. This suggested that the concentration of active species stagnated at lower current. This [may] breakdown organic matter to secondary DBPs, however, not fully oxidized to CO2 and H2O from lack of active species [187].

a)

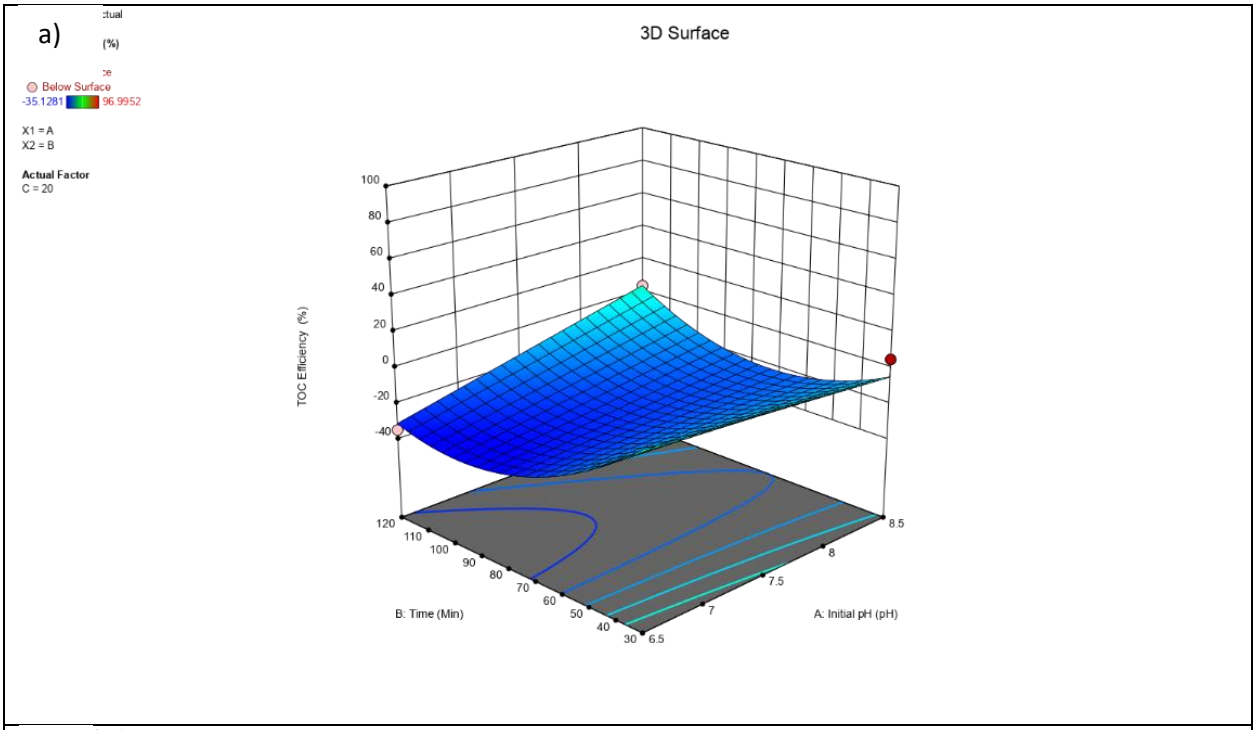
Below Surface
-35.1281
96.9952
X1 = A
X2 = B
Actual Factor
C = 20
3D Surface
TOC Efficiency (%)
100
80
60
40
20
0
-20
-40
120
110
100
90
80
70
60
50
40
30
B: Time (Min)
6.5
7
7.5
8
8.5
A: Initial pH (pH)

b)

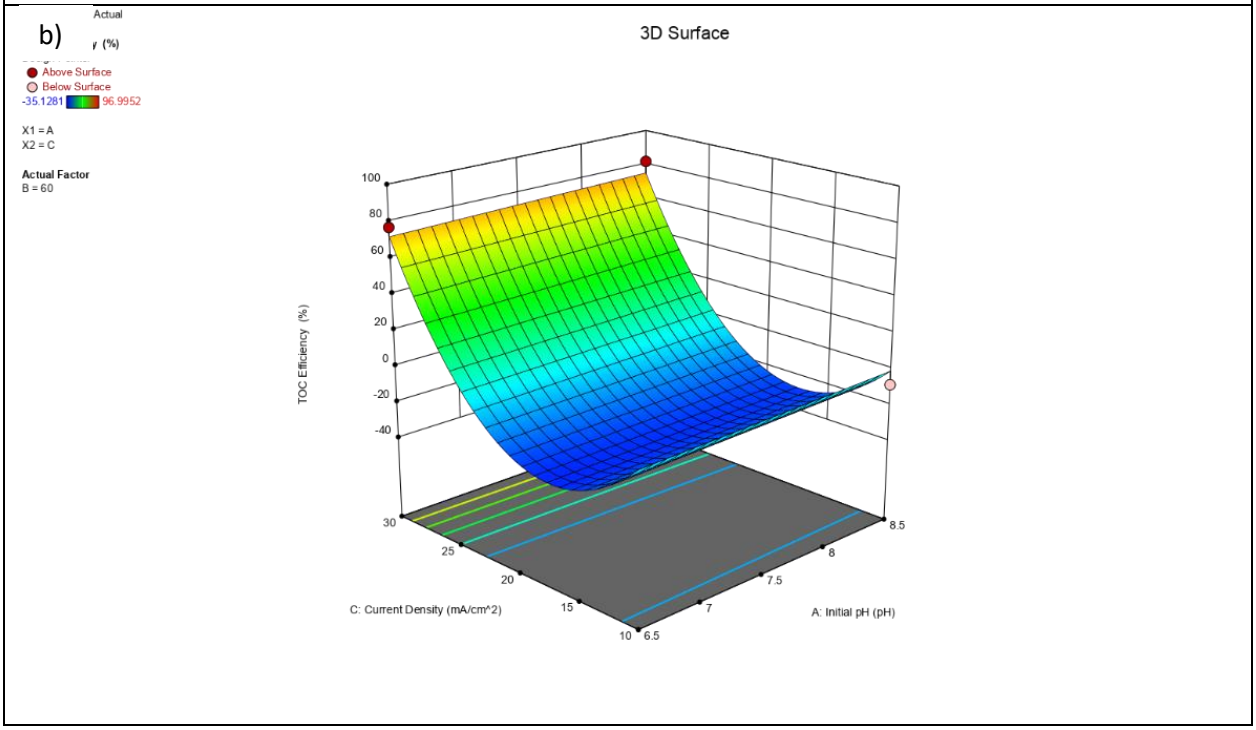
Above Surface
Below Surface
-35.1281
96.9952
X1 = A
X2 = C
Actual Factor
B = 60
3D Surface
TOC Efficiency (%)
100
80
60
40
20
0
-20
-40
30
25
20
15
10
C: Current Density (mA/cm^2)
6.5
7
7.5
8
8.5
A: Initial pH (pH)

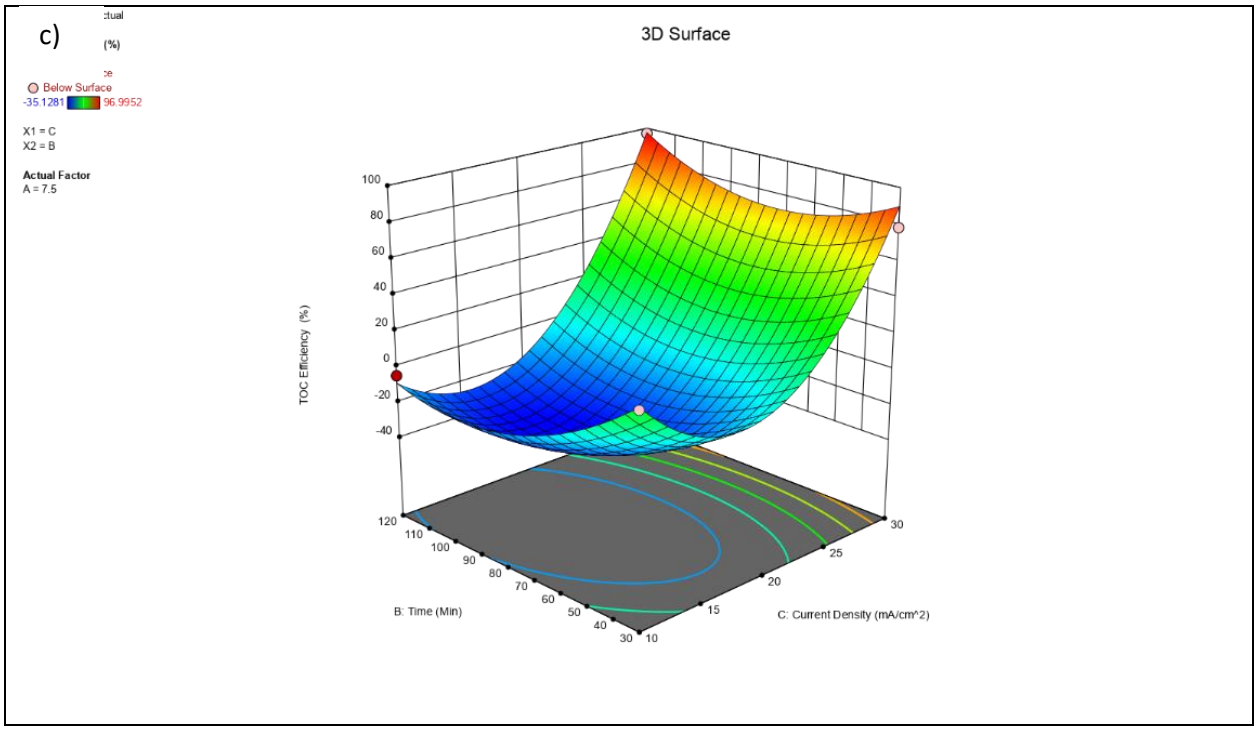

Figure 4-4 Response surface plots (3D) for the effects of variables on M2 TOC efficiency. 4-13a) Initial pH and electrolysis time, 4-13b) Initial pH and current density, 4-13c) electrolysis time and current density

4.3.4.5. M2 COD Efficiency

Contour plots are presented for M2 COD efficiency in figure 4-5. Overall, M2 COD efficiency was greater than M1 COD efficiency. Stainless-steel cathodes had a greater effect on COD than TOC.

M2 COD efficiency was reliant on initial pH, unlike TOC efficiency. Therefore, initial pH has a lower effect on total carbon in a system; however, the number of electrons available in organic carbon reduction (COD) is higher at basic pH. Hydroxyl production was better at non-neutral pH. Additionally, at high current, the initial pH had minimal effect on COD efficiency.

Electrolysis time provided a positive effect on COD efficiency. Raising the time increased COD efficiency; however, at higher pH, the increase was minimized.

a)

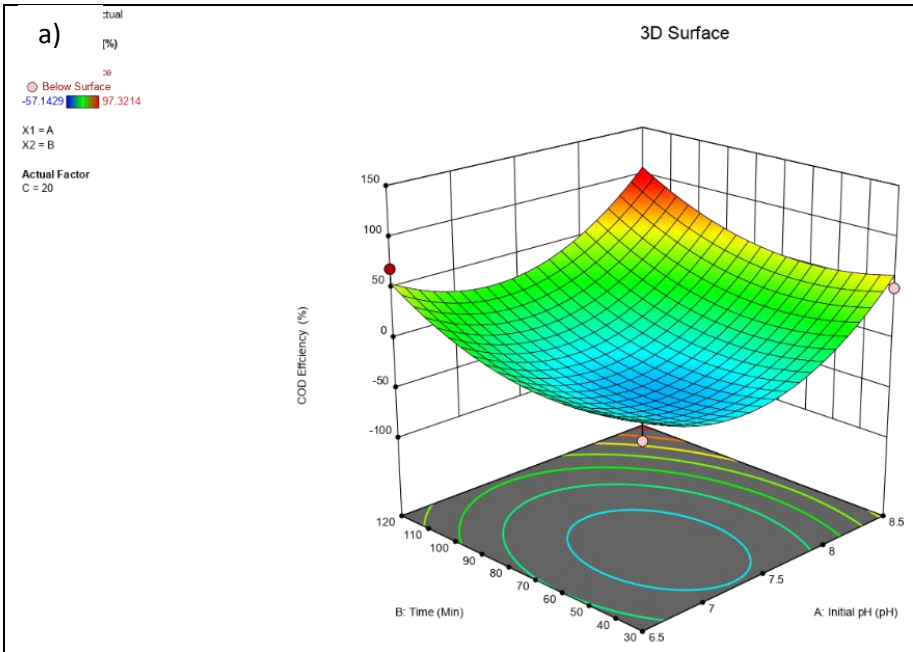
Below Surface
-57.1429
97.3214
X1 = A
X2 = B
Actual Factor
C = 20
3D Surface
COD Efficiency (%)
150
100
50
0
-50
-100
120
110
100
90
80
70
60
50
40
30
B: Time (Min)
6.5
7
7.5
8
8.5
A: Initial pH (pH)

b)

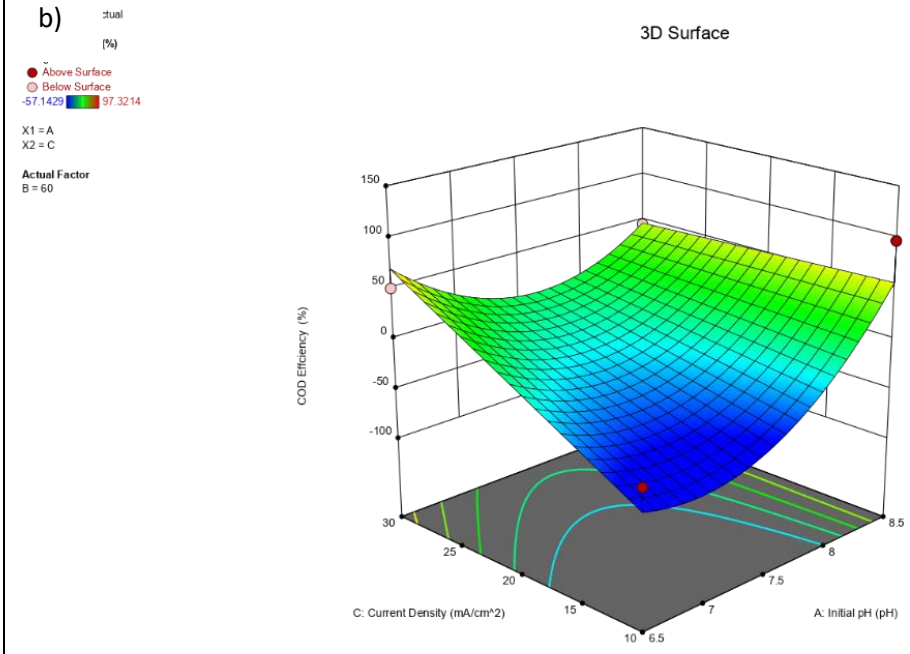
Above Surface
Below Surface
-57.1429
97.3214
X1 = A
X2 = C
Actual Factor
B = 60
3D Surface
COD Efficiency (%)
150
100
50
0
-50
-100
30
25
20
15
10
C: Current Density (mA/cm^2)
6.5
7
7.5
8
8.5
A: Initial pH (pH)

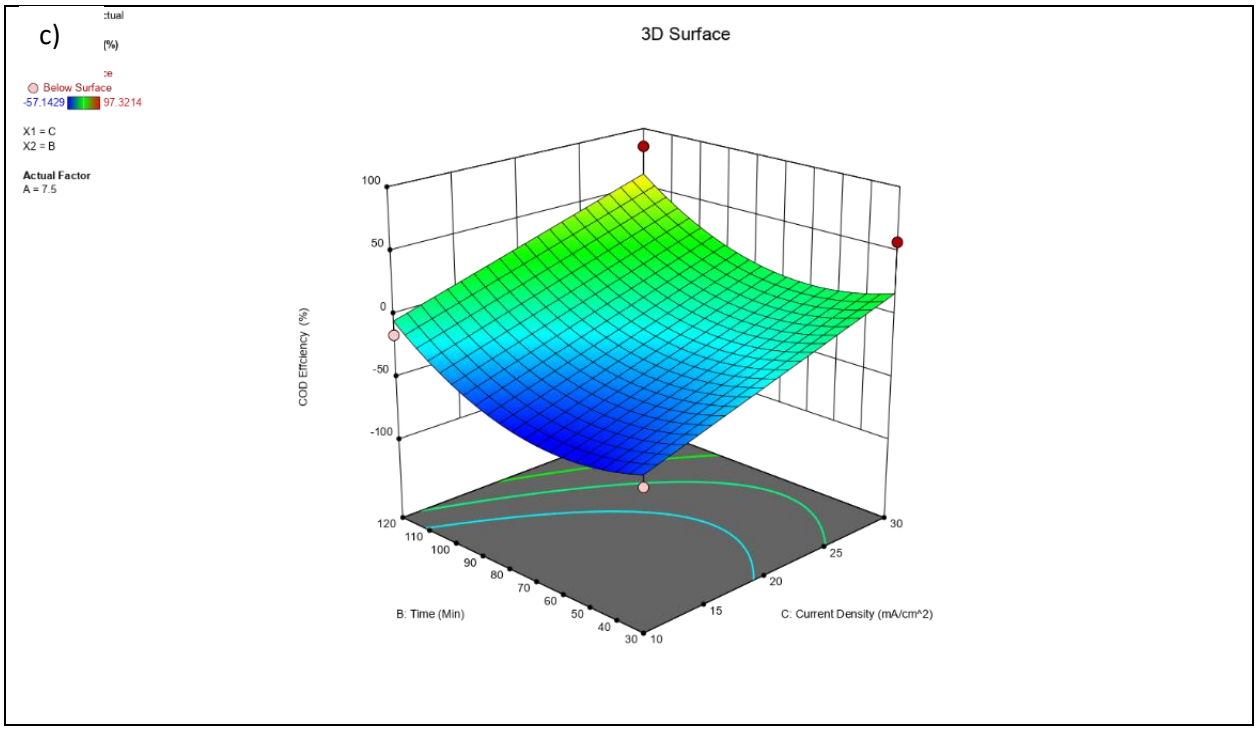

Figure 4-5 Response surface plots (3D) for the effects of variables on M2 COD efficiency. 4-14a) Initial pH and electrolysis time, 4-14b) Initial pH and current density, 4-14c) electrolysis time and current density

4.3.4.6. M2 SUVA

Contour plots for M2 SUVA are presented in figure 4-6. Similar to M1 SUVA trends, initial pH had little to no effect on SUVA. Time also had a minimal effect on SUVA.

Lastly, the applied current was the only metric shown to have a positive effect on SUVA. Reflected by M1 SUVA, DBP production and aromaticity were only a product of applied current.

a)

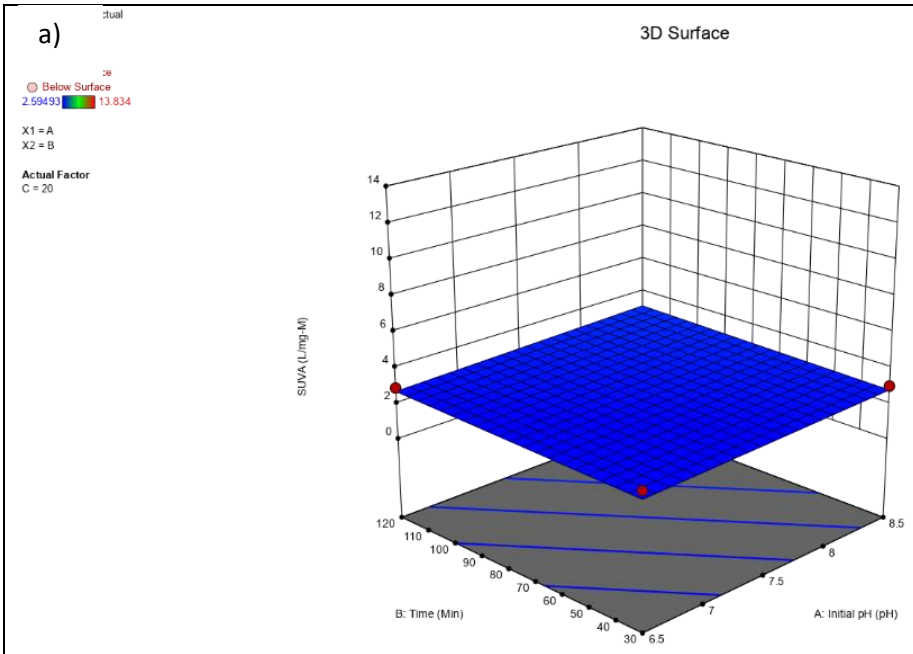
3D Surface
Below Surface
2.59493
13.834
X1 = A
X2 = B
Actual Factor
C = 20
SUVA (L/mg-M)
14
12
10
8
6
4
2
0
120
110
100
90
80
70
60
50
40
30
B: Time (Min)
6.5
7
7.5
8
8.5
A: Initial pH (pH)

b)

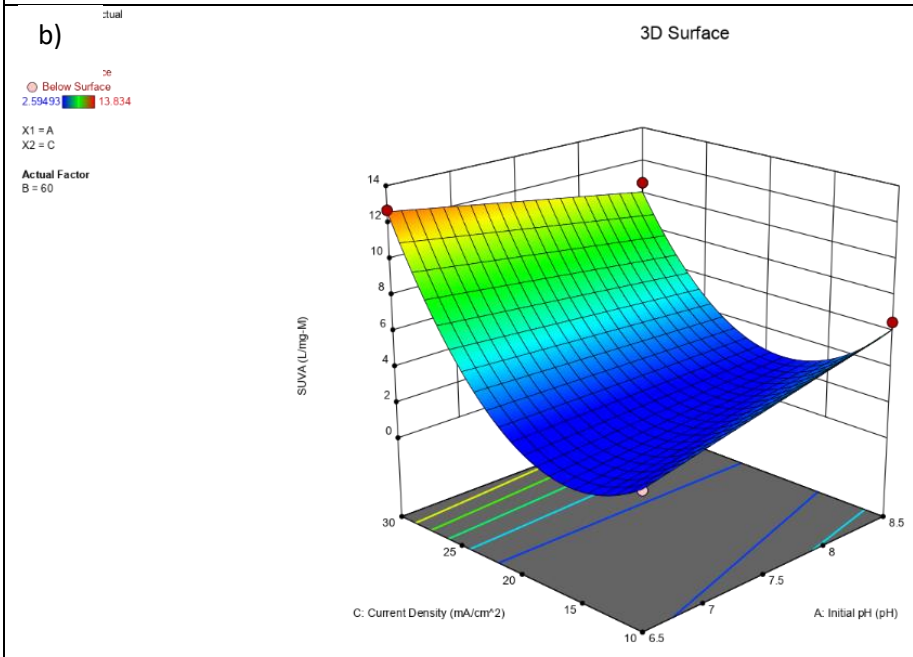
3D Surface
Below Surface
2.59493
13.834
X1 = A
X2 = C
Actual Factor
B = 60
SUVA (L/mg-M)
14
12
10
8
6
4
2
0
30
25
20
15
10
C: Current Density (mA/cm^2)
6.5
7
7.5
8
8.5
A: Initial pH (pH)

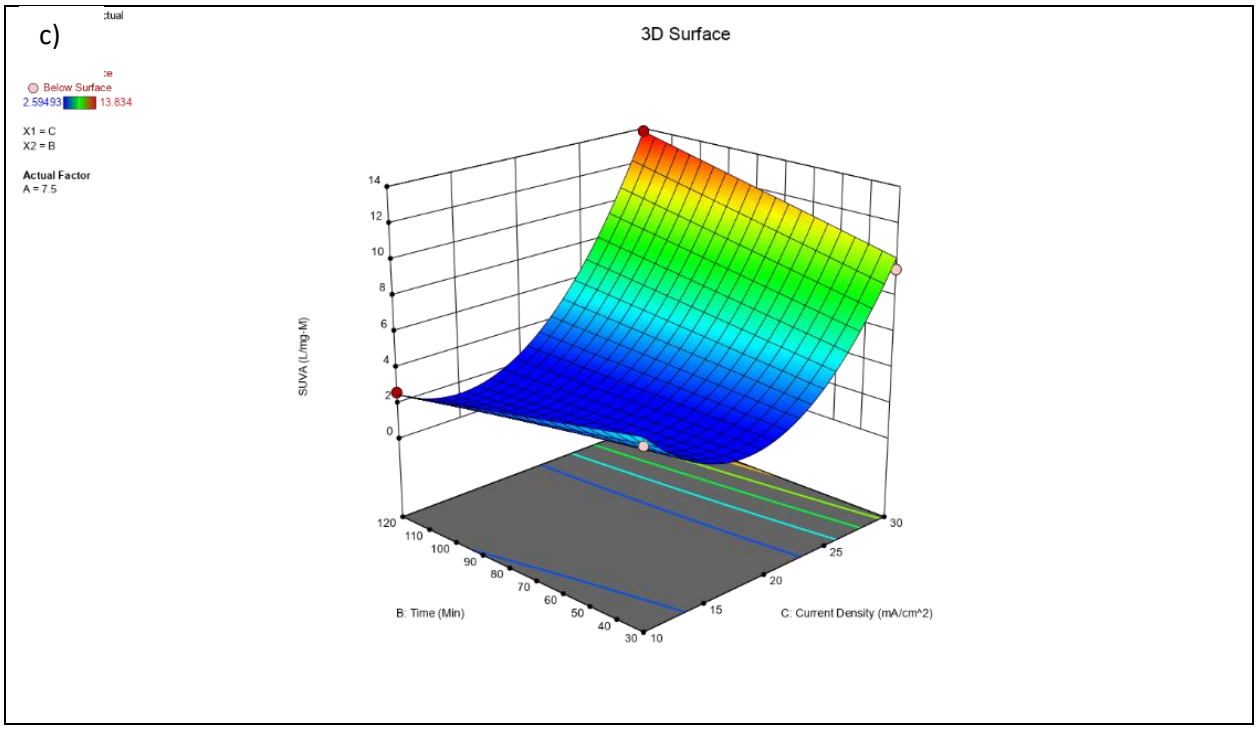

Figure 4-6 Response surface plots (3D) for the effects of variables on M2 SUVA. 4-12a) Initial pH and electrolysis time, 4-12b) Initial pH and current density, 4-12c) electrolysis time and current density

4.3.4.7. M3 TOC Efficiency

Contour plots for M3 TOC efficiency are shown in figure 4-7. Contour plots of MMO anode systems suggest that MMO anodes induce a different reaction pathway for organic reduction. Additionally, flocs were formed in the M3 system, which [may] encapsulate coagulant properties. Overall, TOC efficiency was higher in M1 and M2 setups.

Consequent to M1 and M2, initial pH had a polarizing effect on TOC efficiency for MMO anode systems. The highest efficiencies were outlined at a neutral pH. Also, unlike BDD systems, initial pH influenced how the current affected TOC efficiency. Instead of linearly increasing the efficiency with current density, the highest efficiencies were only recorded at 20.

Electrolysis time also played a different role from M1 and M2 TOC efficiency. Increasing the time did not have a significant effect on TOC efficiency. Applied current generally had a positive correlation with TOC efficiency, with the exception at low pH and low time durations.

Indirect oxidation was more reliant on pH with more hypochlorous formed at neutral pH. Therefore, increasing current at lower pH was not impactful at reducing TOC content[204] [205].

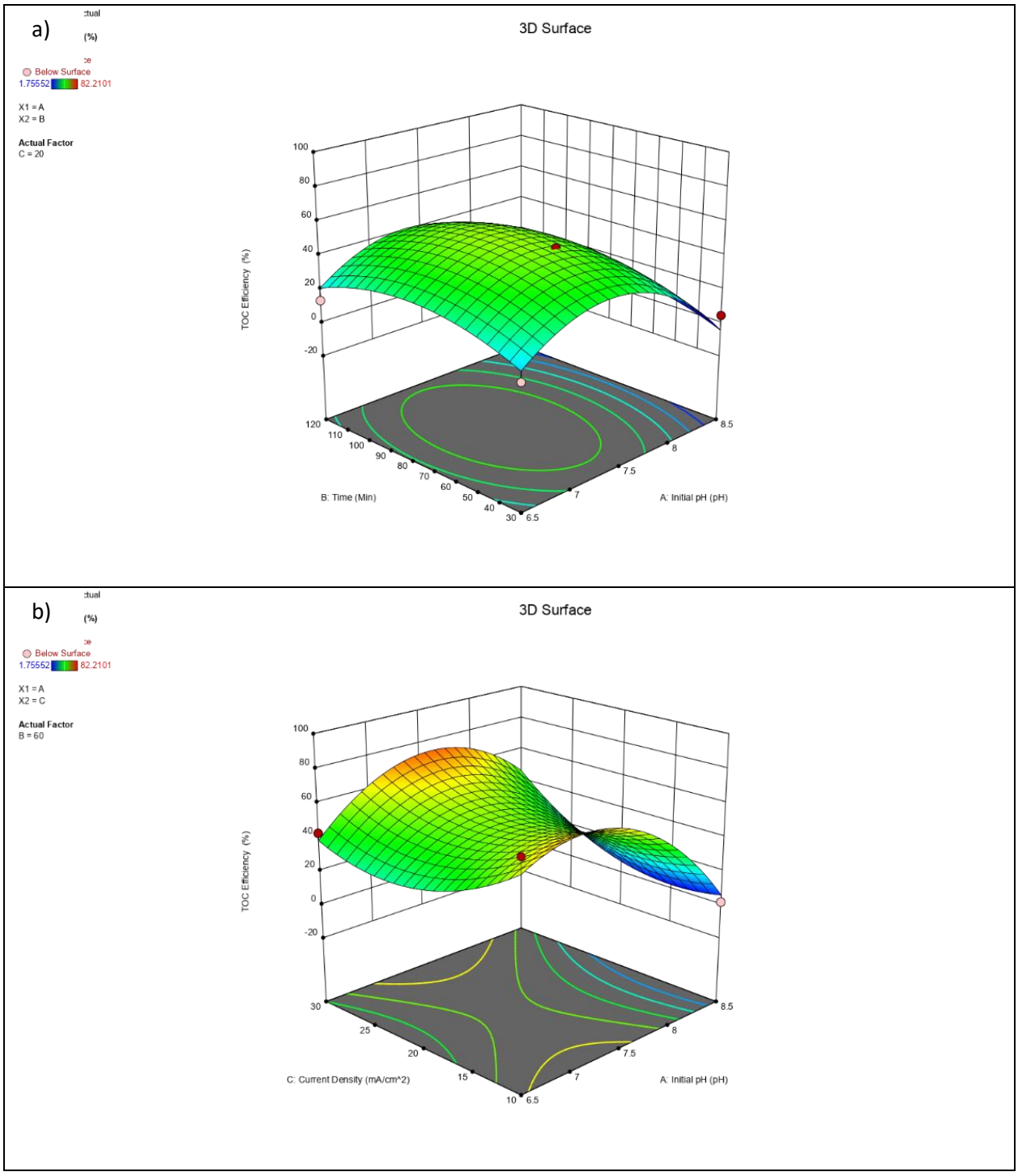

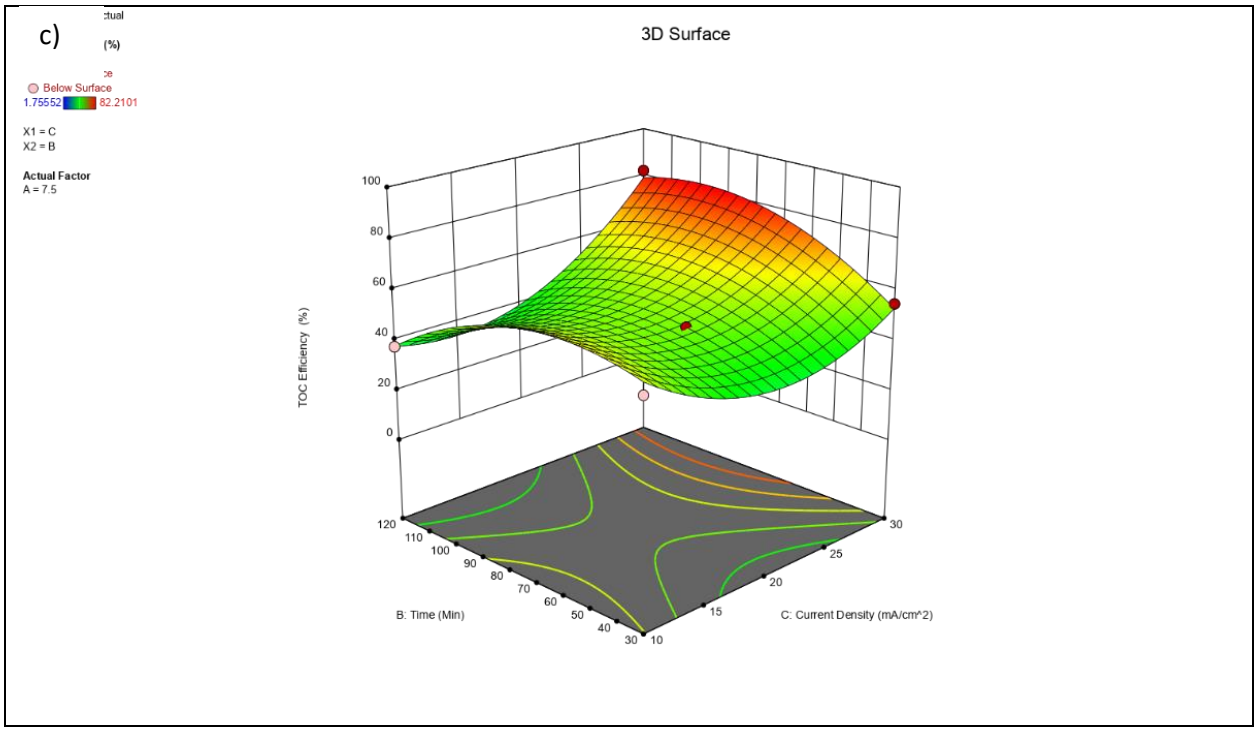

Figure 4-7 Response surface plots (3D) for the effects of variables on M3 TOC efficiency. 4-16a) Initial pH and electrolysis time, 4-16b) Initial pH and current density, 4-16c) electrolysis time and current density

4.3.4.8. M3 COD Efficiency

Contour plots of M3 COD efficiency are presented in figure 4-8. Overall, COD efficiency was higher than TOC efficiency in M3. Additionally, M3 performed better at COD removal than M1 and M2.

Similar to M3 TOC efficiency, M3 systems were better performers in reducing COD at neutral pH. Therefore, DSA electrodes, which are heavily reliant on chloride indirect oxidation mechanisms in addition to hydroxyl production, have the best efficiency production at neutral pH. up to 90%.

Furthermore, COD efficiency decreased as elapsed time is increased over 60 mins at low current density applied. After (60 mins), toxic matters are removed by flocs; however, floc concentration continues to increase and [may] deviate COD evaluation and lower efficiency.

Increasing applied current had a positive effect on COD efficiency. However, at a low duration, the effect was minimized.

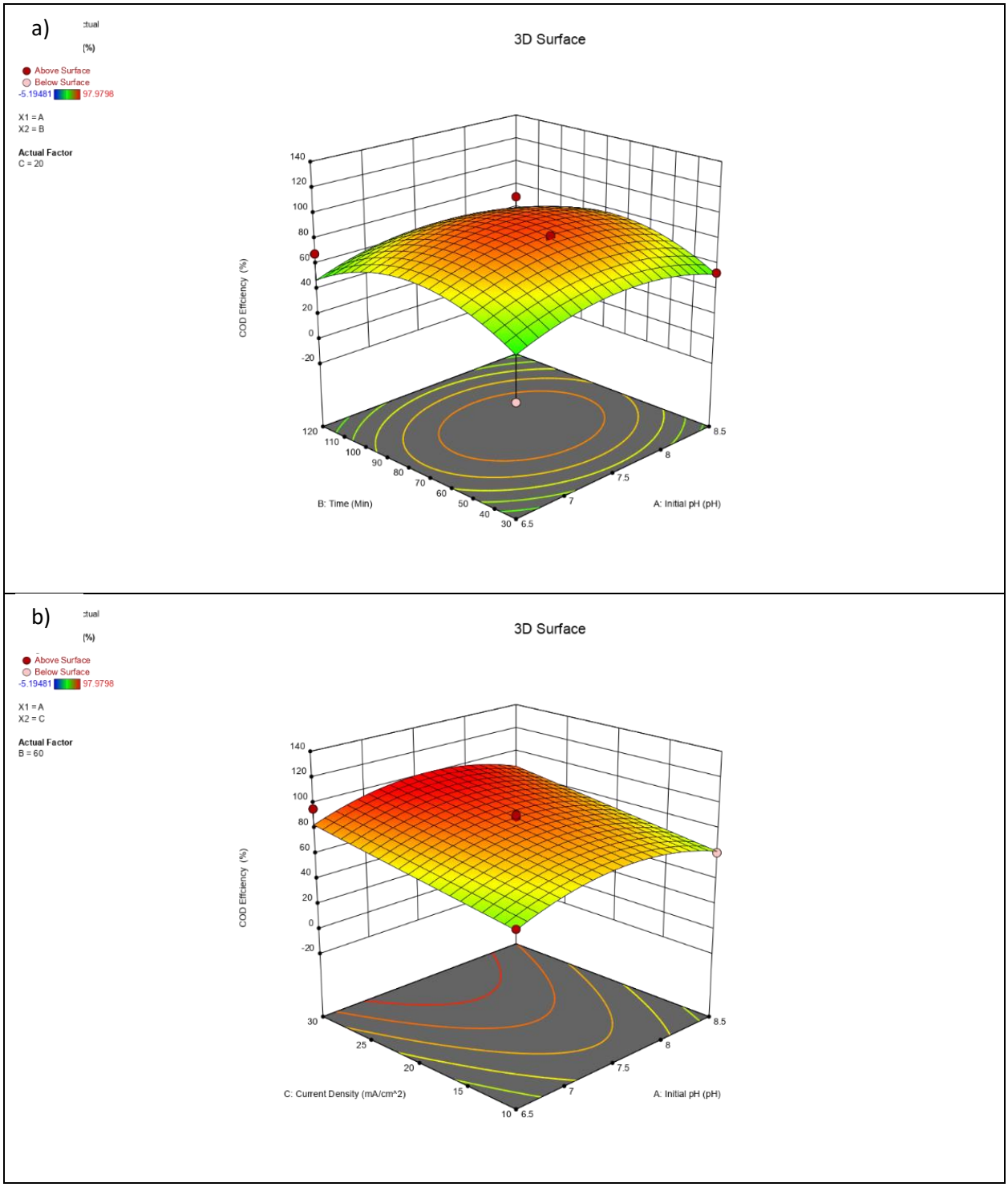

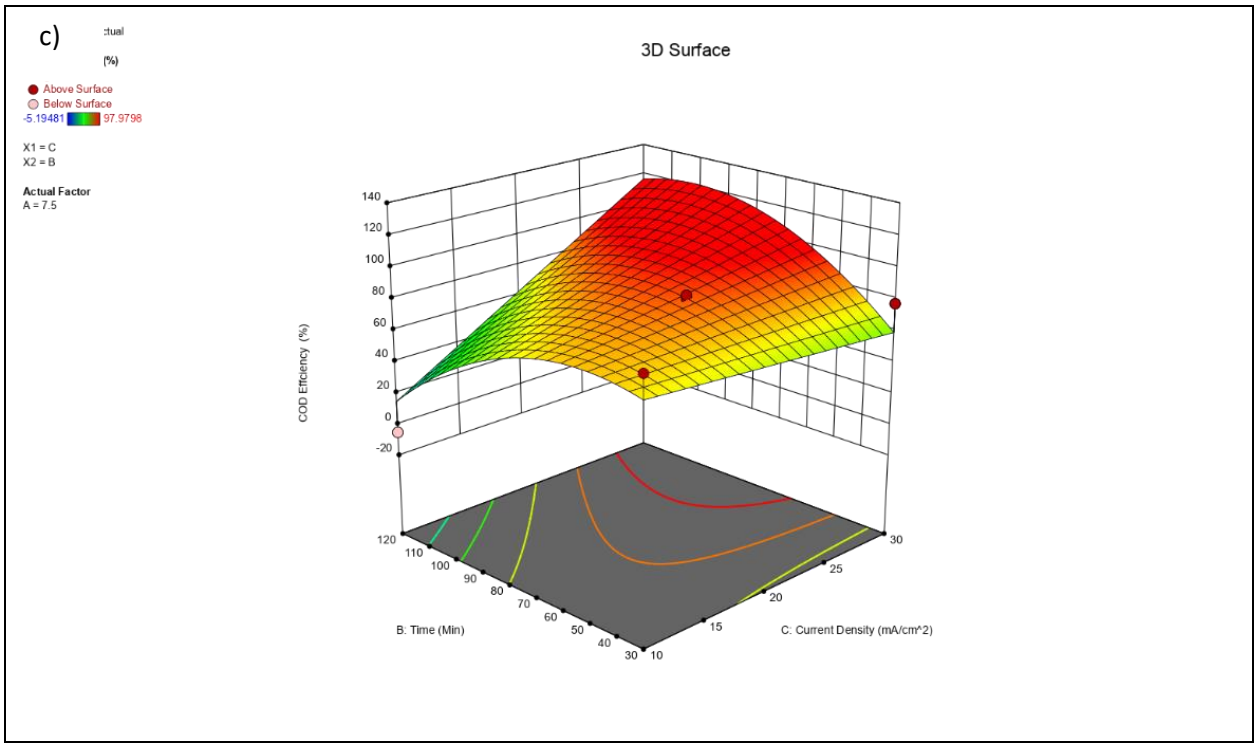

Figure 4-8 Response surface plots (3D) for the effects of variables on M3 COD efficiency. 4-17a) Initial pH and electrolysis time, 4-17b) Initial pH and current density, 4-17c) electrolysis time and current density

4.3.4.9. M3 SUVA

Contour plots of M3 SUVA are observed in figure 4-9. Furthermore, SUVA contour plots indicated the presence of unique reaction mechanisms for MMO systems, as SUVA is affected by initial pH, unlike M1 and M2 SUVA. Also, the greatest SUVA values are at lower pH, lower current, and high treatment durations.

Initial pH from 6.5 to 8.5 generally decreased SUVA. Therefore, acidic conditions were best for DBP production in MMO electrodes. Increasing time generally increased SUVA. Applied current density had a dissimilar effect on SUVA than M1 and M2. MMO anodes had a higher SUVA at lower currents.

a)

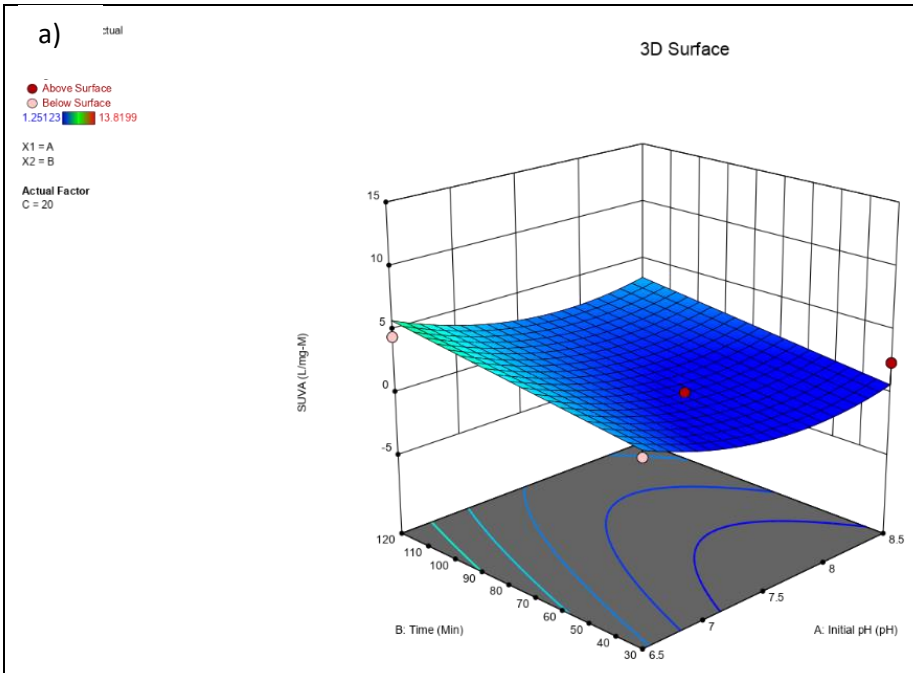
ctual
Above Surface
Below Surface
1.25123
13.8199
X1 = A
X2 = B
Actual Factor
C = 20
3D Surface
SUVA (L/mg-M)
15
10
5
0
-5
120
110
100
90
80
70
60
50
40
30
B: Time (Min)
6.5
7
7.5
8
8.5
A: Initial pH (pH)

b)

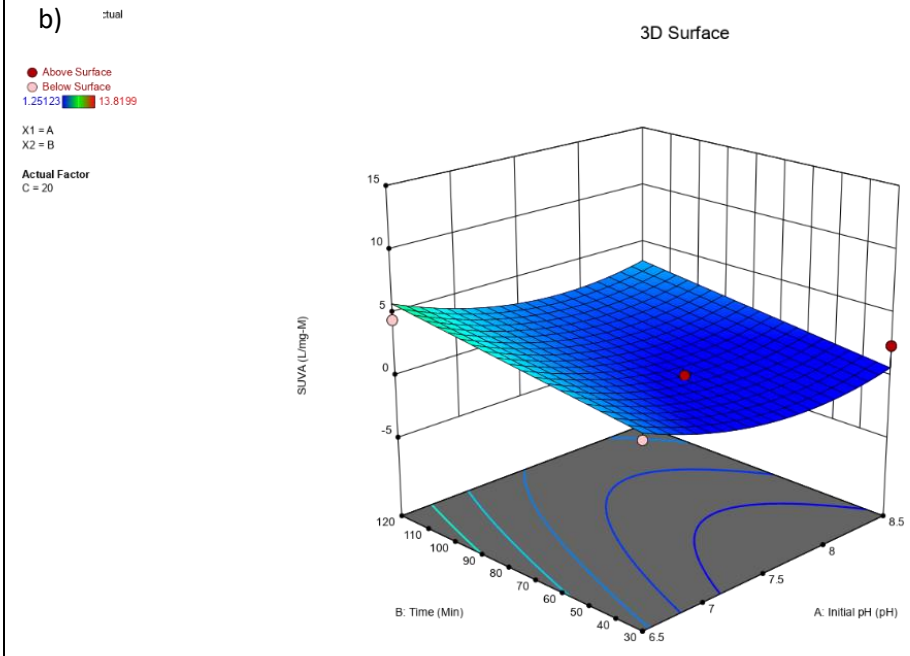
ctual
Above Surface
Below Surface
1.25123
13.8199
X1 = A
X2 = B
Actual Factor
C = 20
3D Surface
SUVA (L/mg-M)
15
10
5
0
-5
120
110
100
90
80
70
60
50
40
30
B: Time (Min)
6.5
7
7.5
8
8.5
A: Initial pH (pH)

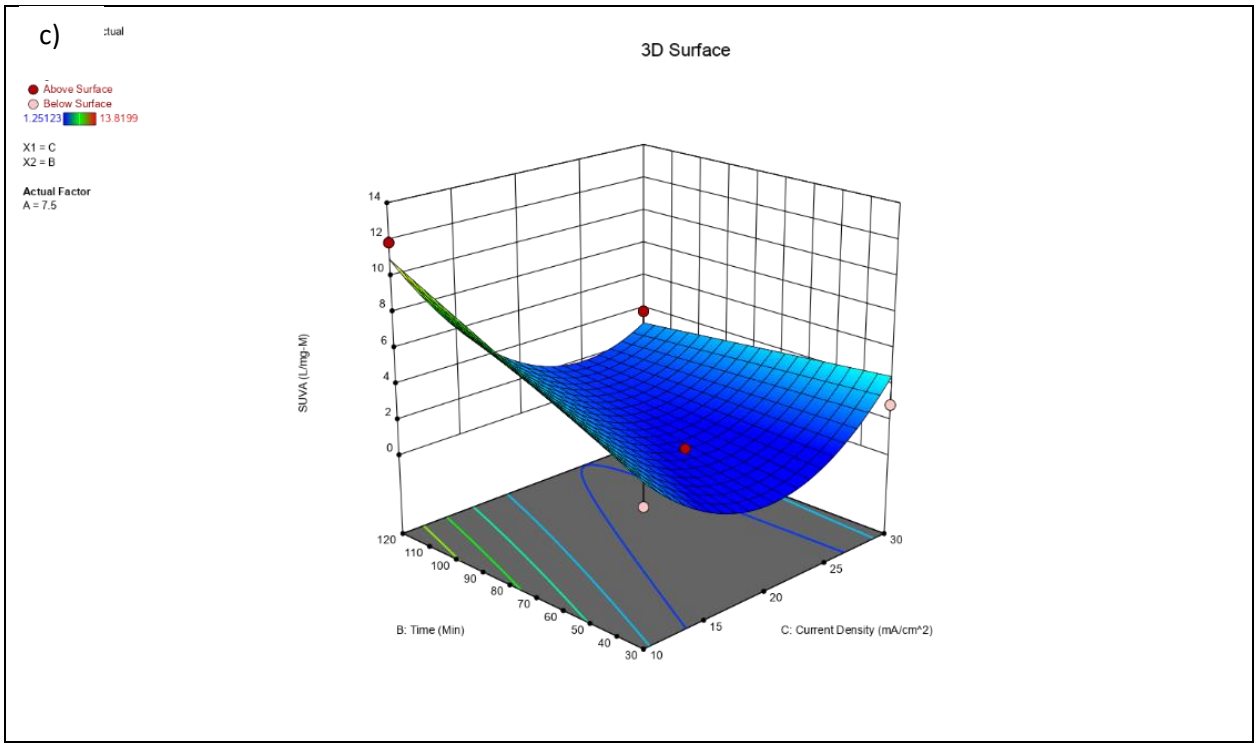

Figure 4-9 Response surface plots (3D) for the effects of variables on M3 SUVA. 4-12a) Initial pH and electrolysis time, 4-12b) Initial pH and current density, 4-12c) electrolysis time and current density

4.3.5. Optimization

Derringer's desired function was applied to maximize TOC removal, COD removal, and SUVA. The optimization technique evaluates points at the designated limits: (1) TOC removal at 100 %, (2) COD removal at 100 %, and (3) SUVA maximized, all process variables limited within operating conditions.

For M1, optimal conditions were determined to be an initial pH of 7.5, electrolysis time of 120, and a current density of 30. Under the conditions, predicted responses were: TOC efficiency 83.2 %, COD efficiency 93.4 %, and SUVA 33.1.

For M2, optimal conditions were an initial pH of 6.5, electrolysis time of 120, and a current density of 30. Under the conditions, predicted responses were: TOC efficiency 84.24 %, COD efficiency 99.9 %, and SUVA 14.7.

For M3, optimal conditions were predicted to be an initial pH of 6.5, electrolysis time of 60, and a current density of 10. Under the conditions, projected responses were: TOC efficiency 65.9 %, COD efficiency 64.2 %, and SUVA 11.5.

Table 4-2 optimal operating conditions for the maximum removal

		M1	***M2***	***M3***
Optimal Conditions	Initial pH	7.5	6.5	6.5
	Electrolysis Time	120	120	60
	Current Density	30	30	10
Response Values	TOC Efficiency	83.2	84.2	65.9
	COD Efficiency	93.4	99.9	64.2
	SUVA	33.1	14.7	11.5

Results summary

Table 4-3 Operating variables and their effects on NOM removal for M1, M2, and M3 systems

Treatment setup		*ANOVA Analysis*		*Contour Plots*	*Derringers Optimization*	
M1	TOC	• *Initial pH was not a significant factor* • *Electrolysis time and current density were significant*	TOC	• Initial pH had little-to-no effect on TOC removal • Electrolysis time had a positive effect on TOC efficiency • Current density linearly proportional to TOC efficiency	TOC	83.2
	COD	• *Initial pH, electrolysis time, and current were all significant factors*	COD	• COD efficiency Increased with higher pH • increase in COD efficiency as time progressed • Current density positively influenced COD efficiency	COD	93.4
	SUVA	• *Initial pH was not a significant factor* • *Electrolysis time and current density were significant*	SUVA	• Initial pH did not affect SUVA • Positive correlation for electrolysis time and SUVA • SUVA increased with higher current density	SUVA	33.1
M2	TOC	• *Initial pH was not a significant factor*	TOC	• Initial pH did not affect incl. interactions	TOC	84.2

		• *Electrolysis time and current density were significant*		• Electrolysis time did not have a positive effect on TOC removal • TOC removal increased with higher current density		
	COD	• *Initial pH, electrolysis time, and current were all significant factors*	COD	• COD efficiency Increased with higher pH • increase in COD efficiency as time progressed • Current density positively influenced COD efficiency	COD	99.9
	SUVA	• *Initial pH was not a significant factor* • *Electrolysis time and current density were significant*	SUVA	• Initial pH did not affect SUVA • Electrolysis time did not affect SUVA • SUVA increased with higher current density	SUVA	14.7
M3	TOC	• *Initial pH and current density were significant factors* • *Electrolysis time was not a significant factor*	TOC	• Initial pH affected TOC removal, highest around seven pH • Electrolysis time did not have a positive effect on TOC removal • TOC removal increased with higher current density	TOC	65.9
	COD	• *Initial pH and current density were significant factors* • *Electrolysis time was not a significant factor*	COD	• COD efficiency was highest at neutral pH • COD efficiency decreased with time elapsed after 60 mins • Current density positively influenced COD efficiency	COD	64.2
	SUVA	• *Initial pH, electrolysis time, and current density were significant factors*	SUVA	• Initial pH had a great effect on SUVA, maximized at low pH • Electrolysis time had a positive effect on SUVA • SUVA decreased with higher current density	SUVA	11.5

4.4. Summary

This chapter employed BBD RSM to study and optimize the process variables under different operating conditions such as initial pH, electrolysis time, and current density to treat NOM by electrochemical oxidation. From the results, it was observed that operating variables have a significant effect on TOC removal, COD removal, and SUVA.

The optimal conditions were found to be neutral pH., high electrolysis time, and high current densities for M1 and M2. Additionally, M1 and M2, on average, presented more excellent TOC removal, COD removal, and SUVA. On the other hand, M3 performed better at acidic pH, low-to-mid electrolysis duration, and low current densities.

Chapter 5. Conclusions and Recommendations

5.1. Conclusion

The objective of this thesis was to explore the use of BDD electrodes for NOM removal in water and wastewater purification. Although innate research has been conducted on electrochemical processes, BDD remains commercially inviable. Functional application of a BDD facilitated electrochemical process was assessed adequately in a batch setting to determine the following: if BDD anodes warrant application potential over MMO electrodes (chapter 3), and whether or not BDD and MMO anodic oxidation can be optimized for NOM removal (chapter 4). Although through the experimental process collected precise results, the synthetic NOM solution posed challenges for NOM characterization. Quantifying all aspects of NOM was virtually impossible, and thus, surrogate measures were utilized, such as TOC, COD, and SUVA. Mixed-results were obtained from the characterization methods, which was undeniably a product of (1) a high degree of variability of chemical and physical properties of organics used for the synthetic mixture, and to a lesser extent, (2) different reactions mechanisms of electrode setups. However, studies have concluded that TOC is the best NOM characterization tool, and those results take precedence over other metrics [206].

Experimentally, the effect of electrode material on NOM removal was assessed through three electrochemical setups in batch mode; M1 - BDD anode and BDD cathode; M2 - BDD anode and SS cathode; and M3 - MMO anode and SS cathode.

Before proceeding to the data results, the setups illustrated BDD electrodes incurred a different pollutant oxidation reaction mechanism from MMO electrodes. The contrast was visually present by yellow agglomerates in the solution of MMO treated systems. Furthermore, the agglomerates may be a product of (1) metal leachates from an anodic surface such as titanium, (2)

hypochlorite induced oxidation by-products, or (3) coagulants formed by electrocoagulation. Additionally, BDD anodes exhibited an increase in NOM at lower electrolysis durations as shown by negative TOC and COD removal efficiencies at 30 minutes with low applied current densities. This phenom was not present in MMO systems, which further highlighted the presence of unique electrochemical oxidation pathways between BDD and MMO anodes.

5.1.1. Conclusions from comparative study

Noticeably, the low experimental current densities (<30 mA cm^{-2}) exhibited low NOM removal. Studies that used BDD anodes for NOM reduction exhibited greater NOM removal (>50 mA cm^{-2}) than the experimental results.

Firstly, the TOC data determined M1 and M2 were more (1) electrochemically stable over a broader range of pH and (2) competent at NOM at higher applied current densities and higher electrolysis durations. TOC removal, on average, remained constant between 6.5 and 8.5 pH, with a variation of 14 % for M1 and 18 % for M2. M3, on the other hand, exhibited a decrease in electrochemical performance at higher pH, with an average variation of 30 %. Additionally, M1 and M2 exhibited a greater TOC removal at high current density with 40.2 % TOC removal.

Secondly, COD data identified M3 as the most effective electrochemical system for NOM removal. Although the effects of pH, electrolysis time, and current density were similar to TOC results, M3 eclipsed M1 and M2 at low current density with a 40 % higher COD removal on average. This further strengthened the hypothesis of a different reaction mechanism. The agglomerate species (MOx) participated as mediators of oxidation in M3, which could contribute to TOC, however, not identified by the MANTECH COD analyzer.

Thirdly, the degree of reduction of the carbon compounds was measured through the COD/TOC metric, which illustrates the amount of DBP in the system. Similar to TOC and COD

efficiency, there was no variation with pH for M1 and M2. Additionally, M1 and M2 obtained higher COD/TOC at higher applied current. Lastly, the metric confirmed the presence of secondary oxidants and by-products in the oxidation mechanisms for all three treatment setups. Therefore, high durations are required to oxidize DBPs to non-harmful compounds completely. Furthermore, the M3 pseudo electrocoagulation/electrooxidation reaction mechanism illustrated a high TOC and COD removal, but low COD/TOC ratios. This suggested that the TOC and COD removal was superficial in M3, and the organic content was not broken down into DBPs (and further reduced to non-harmful compounds), and merely only forming flocs (from agglomeration) of organic clumps unidentifiable by TOC and COD analyzers.

Fourthly, SUVA, an indicator of aromaticity attributed to the growth of DBPs, surmised synthetic NOM reduction. Furthermore, M1 and M2 produced more DBP at higher pH and higher applied current.

Lastly, all electrode setups increased in energy consumption as a product of increased applied current. Surprisingly, M1 and M2 exhibited higher energy consumption than M3, at 0.012, 0.0223, and 0.0064 [kWh dm^{-3}] respectively. However, M3 still exhibited the lowest TOC and COD removal at that energy consumption. TOC removal as a function of energy consumption showed a sharp increase in consumption after 50 % NOM removal. Whereas COD removal was not as reliant on applied current density, and high removal rates can be reached at lower energy consumption.

Overall, M1 and M2 outperformed M3. However, high applied current and lengthy durations are required for 90%+ NOM removal, which can foreshadow high operating costs for effluent treatments.

5.1.2. Conclusions from statistical modeling and optimization

A BBD response surface methodology was applied to examine the effects of initial pH, electrolysis time, and applied current density on NOM removal to optimize M1, M2, and M3 processes.

Firstly, through a Pareto analysis of variance, COD has deemed an ineffective measure of NOM as it displayed high degrees of lack-of-fit for a 2^{nd} order regression model. Although COD data was optimized and analyzed, conclusions from TOC and SUVA data should be prioritized. Secondly, 3D contour plots determined that operating variables have a significant effect on TOC removal, COD removal, and SUVA. For M1 and M2, initial pH had minimal effect on NOM removal, and showed electrolysis time and applied current density were proportional to NOM removal. On the other hand, M3 showed the influence of pH on NOM removal. Additionally, NOM removal stagnated after (1) 60 minutes of electrolysis and at (2) 10 mA cm^{-2} for M3. Therefore, the floc and agglomerate formation had a maximum concentration for the synthetic NOM solution, as the addition of more flocs through higher durations and higher applied current did not affect NOM removal.

Lastly, optimized parameters confirmed BDD as better NOM removal anodes. Under optimal conditions, M1 and M2 showed a TOC removal of 83.2 % and 84.2 % respectively, whereas M3 paled in comparison at 65.9 %.

5.2. Recommendations

Future research should focus on specific NOM compounds when comparing BDD and MMO anodes. A considerable complication for the experimental setup was the mixed results for TOC, COD, and SUVA because the synthetic NOM solution contained a wide variety of

compounds; however, that was necessary to emulate real source water NOM conditions. Likewise, small molecular sizes suggested MANTECH COD analyzer was not a good indicator for NOM.

Additionally, to ascertain the commercialization of BDD anodes for NOM removal, more studies with higher applied current densities are required. Although our lower current settings showed lower unattractive removal rates, we saw noticeable oxidation patterns as a result, such as increases in NOM through the presence of DBPs.

5.2.1. Fundamentals of EAOPs

Although, there is a large body of knowledge on the effectiveness of BDD anodes for NOM oxidation, which this paper further strengthens, fewer studies that dwell in the understanding of the mechanisms of compound transformation at the electrode surface. Thus, a large portion of the thesis which showed differences between BDD and MMO anode reaction pathways are potential areas of study. Methods such as in-situ spectroscopic techniques and DFT simulations can be applied. Furthermore, a better understanding of the reaction mechanism can allow a better design of the electrochemical reactors and operating conditions.

5.2.2. EAOP application studies

In addition to innate organic removal, EAOPs form DBPs, which hinder it from comprehensive implementation for water treatment. Cl- and HOC by-products are typical in oxidations.

Additionally, low-active surface areas of electrodes limit treatment durations for large scale water utilities. Therefore, a larger number of cells are required for effective NOM removal, which translates to high capital costs and prevents the adoption of the relatively new EAOP technology. More studies are needed to provide a full cost analysis of EAOPs for specific water treatment

scenarios. Electrodes exhibit wear and tear from regular use. Therefore, future work should focus on a life cycle analysis model to gauge the sustainability for long term EAOPs.

References

[1] Y. Hu, X. Liu, J. Bai, K. Shih, E. Y. Zeng, and H. Cheng, "Assessing heavy metal pollution in the surface soils of a region that had undergone three decades of intense industrialization and urbanization," *Environ. Sci. Pollut. Res.*, 2013, doi: 10.1007/s11356-013-1668-z.

[2] Salameh Azimi and M. Sadeghi Moghaddam, "Effect of Mercury Pollution on the Urban Environment and Human Health," *Environ. Ecol. Res.*, 2013, doi: 10.13189/eer.2013.010102.

[3] P. Rajasulochana and V. Preethy, "Comparison on efficiency of various techniques in treatment of waste and sewage water – A comprehensive review," *Resour. Technol.*, 2016, doi: 10.1016/j.reffit.2016.09.004.

[4] Y. Wu, T. Li, and L. Yang, "Mechanisms of removing pollutants from aqueous solutions by microorganisms and their aggregates: A review," *Bioresource Technology*. 2012, doi: 10.1016/j.biortech.2011.12.088.

[5] M. S. Mauter and M. Elimelech, "Environmental applications of carbon-based nanomaterials," *Environmental Science and Technology*. 2008, doi: 10.1021/es8006904.

[6] J. T. Nurmi and P. G. Tratnyek, "Electrochemical properties of natural organic matter (NOM), fractions of NOM, and model biogeochemical electron shuttles," *Environ. Sci. Technol.*, 2002, doi: 10.1021/es0110731.

[7] E. H. Goslan *et al.*, "Seasonal variations in the disinfection by-product precursor profile of a reservoir water," *J. Water Supply Res. Technol. - AQUA*, 2002, doi: 10.2166/aqua.2002.0041.

[8] D. J. Barker, S. M. L. Salvi, A. A. M. Langenhoff, and D. C. Stuckey, "Soluble microbial products in ABR treating low-strength wastewater," *J. Environ. Eng.*, 2000, doi: 10.1061/(ASCE)0733-9372(2000)126:3(239).

[9] C. Jarusutthirak, G. Amy, and J. P. Croué, "Fouling characteristics of wastewater effluent organic matter (EfOM) isolates on NF and UF membranes," *Desalination*, 2002, doi: 10.1016/S0011-9164(02)00419-8.

[10] S. Chowdhury, P. Champagne, and P. J. McLellan, "Models for predicting disinfection byproduct (DBP) formation in drinking waters: A chronological review," *Science of the Total Environment*. 2009, doi: 10.1016/j.scitotenv.2009.04.006.

[11] G. Wang, L. Zhang, and J. Zhang, "A review of electrode materials for electrochemical supercapacitors," *Chemical Society Reviews*. 2012, doi: 10.1039/c1cs15060j.

[12] H. C. Kim and M. J. Yu, "Characterization of natural organic matter in conventional water treatment processes for selection of treatment processes focused on DBPs control," *Water Res.*, 2005, doi: 10.1016/j.watres.2005.09.021.

[13] *Natural Organic Matter in Water*. 2015.

[14] D. LI and J. QU, "The progress of catalytic technologies in water purification: A review," *J. Environ. Sci.*, 2009, doi: 10.1016/S1001-0742(08)62329-3.

[15] H. Särkkä, A. Bhatnagar, and M. Sillanpää, "Recent developments of electro-oxidation in water treatment - A review," *Journal of Electroanalytical Chemistry*. 2015, doi: 10.1016/j.jelechem.2015.06.016.

[16] D. M. Drennan, R. E. Koshy, D. B. Gent, and C. E. Schaefer, "Electrochemical treatment for greywater reuse: Effects of cell configuration on COD reduction and disinfection byproduct formation and removal," *Water Sci. Technol. Water Supply*, 2019, doi: 10.2166/ws.2018.138.

[17] S. O. Ganiyu, E. D. Van Hullebusch, M. Cretin, G. Esposito, and M. A. Oturan, "Coupling of membrane filtration and advanced

oxidation processes for removal of pharmaceutical residues: A critical review," *Sep. Purif. Technol.*, 2015, doi: 10.1016/j.seppur.2015.09.059.

[18] G. Chen, "Electrochemical technologies in wastewater treatment," *Sep. Purif. Technol.*, 2004, doi: 10.1016/j.seppur.2003.10.006.

[19] M. Sillanpää, H. Särkkä, and M. Vepsäläinen, "NOM Removal by Electrochemical Methods," in *Natural Organic Matter in Water: Characterization and Treatment Methods*, 2015.

[20] H. Särkkä, M. Vepsäläinen, and M. Sillanpää, "Natural organic matter (NOM) removal by electrochemical methods - A review," *Journal of Electroanalytical Chemistry*. 2015, doi: 10.1016/j.jelechem.2015.07.029.

[21] B. P. Chaplin, "Critical review of electrochemical advanced oxidation processes for water treatment applications," *Environmental Sciences: Processes and Impacts*. 2014, doi: 10.1039/c3em00679d.

[22] H. B. Suffredini, S. A. S. Machado, and L. A. Avaca, "The water decomposition reactions on boron-doped diamond electrodes," *J. Braz. Chem. Soc.*, 2004, doi: 10.1590/S0103-50532004000100004.

[23] Y. Harada *et al.*, "High-speed synthesis of heavily boron-doped diamond films by in-liquid microwave plasma CVD," *Diam. Relat. Mater.*, vol. 92, no. October 2018, pp. 41–46, 2019, doi: 10.1016/j.diamond.2018.12.013.

[24] E. Brillas and C. A. Martínez-Huitle, *Synthetic Diamond Films: Preparation, Electrochemistry, Characterization, and Applications*. 2011.

[25] M. Zhou, L. Liu, Y. Jiao, Q. Wang, and Q. Tan, "Treatment of high-salinity reverse osmosis concentrate by electrochemical oxidation on BDD and DSA electrodes," *Desalination*, 2011, doi: 10.1016/j.desal.2011.04.030.

[26] M. Zhou, H. Särkkä, and M. Sillanpää, "A comparative experimental study on methyl orange degradation by electrochemical oxidation on BDD and MMO electrodes," *Sep. Purif. Technol.*, 2011, doi: 10.1016/j.seppur.2011.02.013.

[27] B. D. Soni, U. D. Patel, A. Agrawal, and J. P. Ruparelia, "Application of BDD and DSA electrodes for the removal of RB 5 in batch and continuous operation," *J. Water Process Eng.*, 2017, doi: 10.1016/j.jwpe.2017.01.009.

[28] N. Bektaş, H. Akbulut, H. Inan, and A. Dimoglo, "Removal of phosphate from aqueous solutions by electro-coagulation," *J. Hazard. Mater.*, 2004, doi: 10.1016/j.jhazmat.2003.10.002.

[29] N. Adhoum, L. Monser, N. Bellakhal, and J. E. Belgaied, "Treatment of electroplating wastewater containing Cu2+, Zn 2+ and Cr(VI) by electrocoagulation," *J. Hazard. Mater.*, 2004, doi: 10.1016/j.jhazmat.2004.04.018.

[30] R. Sridhar, V. Sivakumar, V. Prince Immanuel, and J. Prakash Maran, "Treatment of pulp and paper industry bleaching effluent by electrocoagulant process," *J. Hazard. Mater.*, 2011, doi: 10.1016/j.jhazmat.2010.12.028.

[31] C. L. Lai and S. H. Lin, "Treatment of chemical mechanical polishing wastewater by electrocoagulation: System performances and sludge settling characteristics," *Chemosphere*, 2004, doi: 10.1016/j.chemosphere.2003.08.014.

[32] S. A. Huber, A. Balz, M. Abert, and W. Pronk, "Characterisation of aquatic humic and non-humic matter with size-exclusion chromatography - organic carbon detection - organic nitrogen detection (LC-OCD-OND)," *Water Res.*, 2011, doi: 10.1016/j.watres.2010.09.023.

[33] D. M. Owen, G. L. Amy, Z. K. Chowdhury, R. Paode, G. McCoy, and K. Viscosil, "NOM characterization and treatability," *J. / Am. Water Work. Assoc.*, 1995, doi: 10.1002/j.1551-8833.1995.tb06301.x.

[34] D. A. Reckhow, P. C. Singer, and R. L. Malcolm, "Chlorination of Humic Materials: Byproduct Formation and Chemical

Interpretations," *Environ. Sci. Technol.*, 1990, doi: 10.1021/es00081a005.

[35] R. E. Miller, S. J. Randtke, L. R. Hathaway, and J. E. Denne, "Organic carbon and THM formation potential in Kansas groundwaters," *J. / Am. Water Work. Assoc.*, 1990, doi: 10.1002/j.1551-8833.1990.tb06936.x.

[36] S. W. Krasner, M. J. McGuire, J. G. Jacangelo, N. L. Patania, K. M. Reagan, and E. Marco Aieta, "Occurrence of disinfection by-products in US drinking water," *J. / Am. Water Work. Assoc.*, 1989, doi: 10.1002/j.1551-8833.1989.tb03258.x.

[37] P. C. Singer, "Humic substances as precursors for potentially harmful disinfection by- products," *Water Sci. Technol.*, 1999, doi: 10.1016/S0273-1223(99)00636-8.

[38] A. Kraft, M. Wuensche, M. Stadelmann, and M. Blaschke, "Electrochemical water disinfection," *Recent Res. Dev. Electrochem.*, 2003.

[39] G. Aiken and J. Leenheer, "Isolation and chemical characterization of dissolved and colloidal organic matter," *Chem. Ecol.*, 1993, doi: 10.1080/02757549308035305.

[40] M. R. Collins, G. L. Amy, and C. Steelink, "Molecular Weight Distribution, Carboxylic Acidity, and Humic Substances Content of Aquatic Organic Matter: Implications for Removal during Water Treatment," *Environ. Sci. Technol.*, 1986, doi: 10.1021/es00152a011.

[41] A. Matilainen, E. T. Gjessing, T. Lahtinen, L. Hed, A. Bhatnagar, and M. Sillanpää, "An overview of the methods used in the characterisation of natural organic matter (NOM) in relation to drinking water treatment," *Chemosphere*. 2011, doi: 10.1016/j.chemosphere.2011.01.018.

[42] J. Świetlik, A. Dąbrowska, U. Raczyk-Stanisławiak, and J. Nawrocki, "Reactivity of natural organic matter fractions with chlorine dioxide and ozone," *Water Res.*, 2004, doi: 10.1016/j.watres.2003.10.034.

[43] K. Mopper, "Organic geochemistry of natural waters," *Org. Geochem.*, 1987, doi: 10.1016/0146-6380(87)90051-9.

[44] J. Hur, M. A. Williams, and M. A. Schlautman, "Evaluating spectroscopic and chromatographic techniques to resolve dissolved organic matter via end member mixing analysis," *Chemosphere*, 2006, doi: 10.1016/j.chemosphere.2005.08.069.

[45] L. G. Danielsson, "On the use of filters for distinguishing between dissolved and particulate fractions in natural waters," *Water Res.*, 1982, doi: 10.1016/0043-1354(82)90108-7.

[46] J. K. Edzwald and J. E. Tobiason, "Enhanced coagulation: US requirements and a broader view," *Water Sci. Technol.*, 1999, doi: 10.1016/S0273-1223(99)00641-1.

[47] C. M. PRESTON, "Humus Chemistry, Genesis, Composition and Reactions," *Soil Sci.*, 1995, doi: 10.1097/00010694-199505000-00012.

[48] J. A. Leenheer, "Comprehensive Approach to Preparative Isolation and Fractionation of Dissolved Organic Carbon from Natural Waters and Wastewaters," *Environ. Sci. Technol.*, 1981, doi: 10.1021/es00087a010.

[49] R. Toor and M. Mohseni, "UV-H2O2 based AOP and its integration with biological activated carbon treatment for DBP reduction in drinking water," *Chemosphere*, 2007, doi: 10.1016/j.chemosphere.2006.09.043.

[50] Y. Bichsel and U. Von Gunten, "Formation of iodo-trihalomethanes during disinfection and oxidation of iodide-containing waters," *Environ. Sci. Technol.*, 2000, doi: 10.1021/es9914590.

[51] H. Ødegaard, S. Østerhus, E. Melin, and B. Eikebrokk, "NOM removal technologies - Norwegian experiences," *Drinking Water Engineering and Science*. 2010, doi: 10.5194/dwes-3-1-2010.

[52] B. Eikebrokk, R. D. Vogt, and H. Liltved, "NOM increase in Northern European source waters: Discussion of possible causes and

impacts on coagulation/contact filtration processes," in *Water Science and Technology: Water Supply*, 2004, doi: 10.2166/ws.2004.0060.

[53] R. Fabris, C. W. K. Chow, M. Drikas, and B. Eikebrokk, "Comparison of NOM character in selected Australian and Norwegian drinking waters," *Water Res.*, 2008, doi: 10.1016/j.watres.2008.06.023.

[54] H. Ødegaard, S. Østerhus, E. Melin, and B. Eikebrokk, "NOM removal technologies – Norwegian experiences," *Drink. Water Eng. Sci. Discuss.*, 2009, doi: 10.5194/dwesd-2-161-2009.

[55] I. Machenbach and H. Ødegaard, "Drinking Water Production by Coagulation and Membrane Filtration," 2007.

[56] E. Melin, B. Eikebrokk, M. Brugger, and H. Ødegaard, "Treatment of humic surface water at cold temperatures by ozonation and biofiltration," in *Water Science and Technology: Water Supply*, 2002, doi: 10.2166/ws.2002.0203.

[57] E. S. Melin and H. Ødegaard, "Biofiltration of ozonated humic water in expanded clay aggregate filters," *Water Sci. Technol.*, 1999, doi: 10.1016/S0273-1223(99)00653-8.

[58] C. Comninellis and C. Pulgarin, "Electrochemical oxidation of phenol for wastewater treatment using SnO2, anodes," *J. Appl. Electrochem.*, 1993, doi: 10.1007/BF00246946.

[59] C. Borrás, C. Berzoy, J. Mostany, and B. R. Scharifker, "Oxidation of p-methoxyphenol on SnO2-Sb2O5 electrodes: Effects of electrode potential and concentration on the mineralization efficiency," *J. Appl. Electrochem.*, 2006, doi: 10.1007/s10800-005-9088-5.

[60] Y. He, H. Lin, Z. Guo, W. Zhang, H. Li, and W. Huang, "Recent developments and advances in boron-doped diamond electrodes for electrochemical oxidation of organic pollutants," *Separation and Purification Technology*. 2019, doi: 10.1016/j.seppur.2018.11.056.

[61] F. García-Lugo *et al.*, "Mediated electrochemical oxidation of pollutants in crude oil desalter effluent," *Int. J. Electrochem. Sci.*, 2018, doi: 10.20964/2018.01.03.

[62] A. Kraft, "Electrochemical Water Disinfection: A Short Review ELECTRODES USING PLATINUM GROUP METAL OXIDES," *Platin. Met. Rev.*, 2008, doi: Doi 10.1595/147106708x329273.

[63] S. Stucki, R. Kötz, B. Carcer, and W. Suter, "Electrochemical waste water treatment using high overvoltage anodes Part II: Anode performance and applications," *J. Appl. Electrochem.*, 1991, doi: 10.1007/BF01464288.

[64] G. M. Swain, "Chapter 4 Electroanalytical applications of diamond electrodes," *Semicond. Semimetals*, 2004, doi: 10.1016/S0080-8784(04)80016-4.

[65] G. M. Swain, "The use of CVD diamond thin films in electrochemical systems," *Adv. Mater.*, 1994, doi: 10.1002/adma.19940060511.

[66] M. Panizza and G. Cerisola, "Application of diamond electrodes to electrochemical processes," *Electrochimica Acta*. 2005, doi: 10.1016/j.electacta.2005.04.023.

[67] Y. V. Pleskov, A. Y. Sakharova, E. V. Kasatkin, and V. A. Shepelin, "The synthetic semiconducting diamond electrode: A photoelectrochemical estimation of the diffusion length," *J. Electroanal. Chem.*, 1993, doi: 10.1016/0022-0728(93)80073-Q.

[68] B. P. Chaplin, I. Wyle, H. Zeng, J. A. Carlisle, and J. Farrell, "Characterization of the performance and failure mechanisms of boron-doped ultrananocrystalline diamond electrodes," *J. Appl. Electrochem.*, 2011, doi: 10.1007/s10800-011-0351-7.

[69] P. Bartlett, *Electrochemistry of Carbon Electrodes*. 2015.

[70] A. Perret *et al.*, "Electrochemical behavior of synthetic diamond thin film electrodes," *Diam. Relat. Mater.*, 1999, doi: 10.1016/s0925-9635(98)00280-5.

[71] N. Yang, S. R. Waldvogel, and X. Jiang, “Electrochemistry of Carbon Dioxide on Carbon Electrodes,” *ACS Applied Materials and Interfaces*. 2016, doi: 10.1021/acsami.5b09825.

[72] M. H. P. Santana, L. A. D. Faria, and J. F. C. Boodts, “Electrochemical characterisation and oxygen evolution at a heavily boron doped diamond electrode,” *Electrochim. Acta*, 2005, doi: 10.1016/j.electacta.2004.08.050.

[73] S. Ayadi *et al.*, “Elaboration and characterization of new conductive porous graphite membranes for electrochemical advanced oxidation processes,” *J. Memb. Sci.*, 2013, doi: 10.1016/j.memsci.2013.06.005.

[74] G. Gao, M. Pan, and C. D. Vecitis, “Effect of the oxidation approach on carbon nanotube surface functional groups and electrooxidative filtration performance,” *J. Mater. Chem. A*, 2015, doi: 10.1039/c4ta07191c.

[75] G. Ren, M. Zhou, M. Liu, L. Ma, and H. Yang, “A novel vertical-flow electro-Fenton reactor for organic wastewater treatment,” *Chem. Eng. J.*, 2016, doi: 10.1016/j.cej.2016.04.011.

[76] F. Zhao, L. Liu, F. Yang, and N. Ren, “E-Fenton degradation of MB during filtration with Gr/PPy modified membrane cathode,” *Chem. Eng. J.*, 2013, doi: 10.1016/j.cej.2013.06.117.

[77] S. Klamklang, H. Vergnes, F. Senocq, K. Pruksathorn, P. Duverneuil, and S. Damronglerd, “Deposition of tin oxide, iridium and iridium oxide films by metal-organic chemical vapor deposition for electrochemical wastewater treatment,” in *Journal of Applied Electrochemistry*, 2010, doi: 10.1007/s10800-009-9968-1.

[78] C. R. Costa, C. M. R. Botta, E. L. G. Espindola, and P. Olivi, “Electrochemical treatment of tannery wastewater using DSA® electrodes,” *J. Hazard. Mater.*, 2008, doi: 10.1016/j.jhazmat.2007.09.005.

[79] D. Gandini, E. Mahé, P. A. Michaud, W. Haenni, A. Perret, and C. Comninellis, “Oxidation of carboxylic acids at boron-doped diamond electrodes for wastewater treatment,” *J. Appl. Electrochem.*, 2000, doi: 10.1023/A:1026526729357.

[80] P. Cañizares, J. García-Gómez, J. Lobato, and M. A. Rodrigo, “Electrochemical oxidation of aqueous carboxylic acid wastes using diamond thin-film electrodes,” *Ind. Eng. Chem. Res.*, 2003, doi: 10.1021/ie020594+.

[81] B. Marselli, J. Garcia-Gomez, P.-A. Michaud, M. A. Rodrigo, and C. Comninellis, “Electrogeneration of Hydroxyl Radicals on Boron-Doped Diamond Electrodes,” *J. Electrochem. Soc.*, 2003, doi: 10.1149/1.1553790.

[82] R. Bellagamba, P. A. Michaud, C. Comninellis, and N. Vatistas, “Electro-combustion of polyacrylates with boron-doped diamond anodes,” *Electrochem. commun.*, 2002, doi: 10.1016/S1388-2481(01)00302-2.

[83] A. Kraft *et al.*, “Electrochemical water disinfection. Part I: Hypochlorite production from very dilute chloride solutions,” *J. Appl. Electrochem.*, 1999, doi: 10.1023/A:1003650220511.

[84] D. Clematis *et al.*, “Application of electro-fenton process for the treatment of methylene blue,” *Bulg. Chem. Commun.*, 2018.

[85] M. Panizza, M. Delucchi, and G. Cerisola, “Electrochemical degradation of anionic surfactants,” in *Journal of Applied Electrochemistry*, 2005, doi: 10.1007/s10800-005-0793-x.

[86] I. Tröster *et al.*, “Electrochemical advanced oxidation process for water treatment using DiaChem® electrodes,” *Diam. Relat. Mater.*, 2002, doi: 10.1016/S0925-9635(01)00706-3.

[87] M. A. Rodrigo, P. A. Michaud, I. Duo, M. Panizza, G. Cerisola, and C. Comninellis, “Oxidation of 4-Chlorophenol at Boron-Doped Diamond Electrode for Wastewater Treatment,” *J. Electrochem. Soc.*, 2001, doi: 10.1149/1.1362545.

[88] M. Panizza, P. A. Michaud, G. Cerisola, and C. H. Comninellis, “Anodic oxidation of 2-naphthol at boron-doped diamond electrodes,”

J. Electroanal. Chem., 2001, doi: 10.1016/S0022-0728(01)00398-9.

[89] P. Cañizares, J. Lobato, J. García-Gómez, and M. A. Rodrigo, "Combined adsorption and electrochemical processes for the treatment of acidic aqueous phenol wastes," *J. Appl. Electrochem.*, 2004, doi: 10.1023/B:JACH.0000005607.37738.71.

[90] P. Cañizares, M. Díaz, J. A. Domínguez, J. García-Gómez, and M. A. Rodrigo, "Electrochemical oxidation of aqueous phenol wastes on synthetic diamond thin-film electrodes," *Ind. Eng. Chem. Res.*, 2002, doi: 10.1021/ie0105526.

[91] P. Cañizares, J. García-Gómez, C. Sáez, and M. A. Rodrigo, "Electrochemical oxidation of several chlorophenols on diamond electrodes: Part II. Influence of waste characteristics and operating conditions," *J. Appl. Electrochem.*, 2004, doi: 10.1023/B:JACH.0000005587.52946.66.

[92] F. Shen, X. Chen, P. Gao, and G. Chen, "Electrochemical removal of fluoride ions from industrial wastewater," *Chem. Eng. Sci.*, 2003, doi: 10.1016/S0009-2509(02)00639-5.

[93] E. Bazrafshan, L. Mohammadi, A. Ansari-Moghaddam, and A. H. Mahvi, "Heavy metals removal from aqueous environments by electrocoagulation process - A systematic review," *Journal of Environmental Health Science and Engineering*. 2015, doi: 10.1186/s40201-015-0233-8.

[94] V. K. Kovatcheva and M. D. Parlapanski, "Sono-electrocoagulation of iron hydroxides," in *Colloids and Surfaces A: Physicochemical and Engineering Aspects*, 1999, doi: 10.1016/S0927-7757(98)00414-2.

[95] Q. Fang, C. Shang, and G. Chen, "MS2 inactivation by chloride-assisted electrochemical disinfection," *J. Environ. Eng.*, 2006, doi: 10.1061/(ASCE)0733-9372(2006)132:1(13).

[96] J. Jeong, J. Y. Kim, and J. Yoon, "The role of reactive oxygen species in the electrochemical inactivation of microorganisms," *Environ. Sci. Technol.*, 2006, doi: 10.1021/es0604313.

[97] V. Schmalz, T. Dittmar, D. Haaken, and E. Worch, "Electrochemical disinfection of biologically treated wastewater from small treatment systems by using boron-doped diamond (BDD) electrodes - Contribution for direct reuse of domestic wastewater," *Water Res.*, 2009, doi: 10.1016/j.watres.2009.08.036.

[98] R. Mallikarjunan and S. Venkatachalam, "ELECTROFLOTATION - A REVIEW.," in *Proceedings - The Electrochemical Society*, 1984.

[99] G. B. Raju and P. R. Khangaonkar, "ELECTROFLOTATION - A CRITICAL REVIEW.," *Trans. Indian Inst. Met.*, 1984.

[100] Y. Fukui and S. Yuu, "Removal of colloidal particles in electroflotation," *AIChE J.*, 1985, doi: 10.1002/aic.690310205.

[101] A. G. Vlyssides and C. J. Israilides, "Detoxification of tannery waste liquors with an electrolysis system," *Environ. Pollut.*, 1997, doi: 10.1016/S0269-7491(97)00062-6.

[102] L. Szpyrkowicz, F. Zilio-Grandi, and J. Naumczyk, "Application of electrochemical processes for tannery wastewater treatment," *Toxicol. Environ. Chem.*, 1994, doi: 10.1080/02772249409358057.

[103] S. J. Allen, K. Y. H. Khader, and M. Bino, "Electrooxidation of dyestuffs in waste waters," *J. Chem. Technol. Biotechnol.*, 1995, doi: 10.1002/jctb.280620202.

[104] J. C. Farmer, F. T. Wang, P. R. Lewis, and L. J. Summers, "Electrochemical treatment of mixed and hazardous wastes: oxidation of ethylene glycol by cobalt(III) and iron(III)," in *Institution of Chemical Engineers Symposium Series*, 1992.

[105] J. C. Farmer, "Electrochemical Treatment of Mixed and Hazardous Wastes: Oxidation of Ethylene Glycol and Benzene by Silver (II),"

J. Electrochem. Soc., 1992, doi: 10.1149/1.2069280.

[106] J. Bringmann, K. Ebert, U. Galla, and H. Schmieder, "Electrochemical mediators for total oxidation of chlorinated hydrocarbons: formation kinetics of Ag(II), Co(III), and Ce(IV)," *J. Appl. Electrochem.*, 1995, doi: 10.1007/BF00233903.

[107] C. Comninellis, "Electrocatalysis in the electrochemical conversion/combustion of organic pollutants for waste water treatment," *Electrochim. Acta*, 1994, doi: 10.1016/0013-4686(94)85175-1.

[108] J. Naumczyk, L. Szpyrkowicz, and F. Zilio-Grandi, "Electrochemical treatment of textile wastewater," in *Water Science and Technology*, 1996, doi: 10.1016/S0273-1223(96)00816-5.

[109] G. M. Swain, A. B. Anderson, and J. C. Angus, "Applications of diamond thin films in electrochemistry," *MRS Bull.*, 1998, doi: 10.1557/S0883769400029389.

[110] R. Mráz and J. Krýsa, "Long service life IrO2/Ta2O5 electrodes for electroflotation," *J. Appl. Electrochem.*, 1994, doi: 10.1007/BF00249891.

[111] J. Feng, "Electrocatalysis of Anodic Oxygen-Transfer Reactions: Titanium Substrates for Pure and Doped Lead Dioxide Films," *J. Electrochem. Soc.*, 1991, doi: 10.1149/1.2085410.

[112] B. Correa-Lozano, C. Comninellis, and A. De Battisti, "Preparation of SnO2-Sb2O5 films by the spray pyrolysis technique," *J. Appl. Electrochem.*, 1996, doi: 10.1007/BF00248192.

[113] I. Tröster, L. Schäfer, and M. Fryda, "Recent developments in production and application of DiaChem®-Electrodes for wastewater treatment," in *New Diamond and Frontier Carbon Technology*, 2002.

[114] J. R. Smith, F. C. Walsh, and R. L. Clarke, "Electrodes based on Magnéli phase titanium oxides: The properties and applications of Ebonex® materials," *Journal of Applied Electrochemistry*. 1998, doi: 10.1023/A:1003469427858.

[115] J. H. T. Luong, K. B. Male, and J. D. Glennon, "Boron-doped diamond electrode: Synthesis, characterization, functionalization and analytical applications," *Analyst*. 2009, doi: 10.1039/b910206j.

[116] H. B. Martin, "Hydrogen and Oxygen Evolution on Boron-Doped Diamond Electrodes," *J. Electrochem. Soc.*, 1996, doi: 10.1149/1.1836901.

[117] X. Chen, G. Chen, F. Gao, and P. L. Yue, "High-Performance Ti/BDD Electrodes for Pollutant Oxidation," *Environ. Sci. Technol.*, 2003, doi: 10.1021/es026443f.

[118] V. S. Vavilov, "Handbook of industrial diamonds and diamond films," *Uspekhi Fiz. Nauk*, 1998, doi: 10.3367/ufnr.0168.199810h.1149.

[119] X. Chen, G. Chen, and P. L. Yue, "Anodic oxidation of dyes at novel Ti/B-diamond electrodes," *Chem. Eng. Sci.*, 2003, doi: 10.1016/S0009-2509(02)00640-1.

[120] J. Iniesta, P. A. Michaud, M. Panizza, and C. H. Comninellis, "Electrochemical oxidation of 3-methylpyridine at a boron-doped diamond electrode: Application to electroorganic synthesis and wastewater treatment," *Electrochem. commun.*, 2001, doi: 10.1016/S1388-2481(01)00174-6.

[121] R. Tenne, K. Patel, K. Hashimoto, and A. Fujishima, "Efficient electrochemical reduction of nitrate to ammonia using conductive diamond film electrodes," *J. Electroanal. Chem.*, 1993, doi: 10.1016/0022-0728(93)80105-Q.

[122] S. K. Trabelsi, N. B. Tahar, B. Trabelsi, and R. Abdelhedi, "Electrochemical oxidation of ferulic acid in aqueous solutions at gold oxide and lead dioxide electrodes," *J. Appl. Electrochem.*, 2005, doi: 10.1007/s10800-005-6723-0.

[123] N. Belhadj Tahar and A. Savall, “Electrochemical degradation of phenol in aqueous solution on bismuth doped lead dioxide: a comparison of the activities of various electrode formulations,” *J. Appl. Electrochem.*, 1999, doi: 10.1023/A:1003433519200.

[124] N. Belhadj Tahar, R. Abdelhédi, and A. Savall, “Electrochemical polymerisation of phenol in aqueous solution on a Ta/PbO2 anode,” *J. Appl. Electrochem.*, 2009, doi: 10.1007/s10800-008-9706-0.

[125] N. Belhadj Tahar and A. Savall, “Electropolymerization of phenol on a vitreous carbon electrode in acidic aqueous solution at different temperatures,” *J. Appl. Electrochem.*, 2011, doi: 10.1007/s10800-011-0327-7.

[126] M. Panizza and G. Cerisola, “Electrochemical degradation of methyl red using BDD and PbO2 anodes,” *Ind. Eng. Chem. Res.*, 2008, doi: 10.1021/ie8001292.

[127] F. Xu *et al.*, “Microstructure and tribological properties of cubic boron nitride films on Si3N4 inserts via boron-doped diamond buffer layers,” *Diam. Relat. Mater.*, 2014, doi: 10.1016/j.diamond.2014.07.014.

[128] E. A. McGaw and G. M. Swain, “A comparison of boron-doped diamond thin-film and Hg-coated glassy carbon electrodes for anodic stripping voltammetric determination of heavy metal ions in aqueous media,” *Anal. Chim. Acta*, 2006, doi: 10.1016/j.aca.2006.05.094.

[129] H. Dong, S. Wang, J. J. Galligan, and G. M. Swain, “Boron-doped diamond nano/microelectrodes for biosensing and in vitro measurements,” *Front. Biosci. - Sch.*, 2011, doi: 10.2741/s169.

[130] M. Gattrell and D. W. Kirk, “The electrochemical oxidation of aqueous phenol at a glassy carbon electrode,” *Can. J. Chem. Eng.*, 1990, doi: 10.1002/cjce.5450680615.

[131] J. Iniesta, P. A. Michaud, M. Panizza, G. Cerisola, A. Aldaz, and C. H. Comninellis, “Electrochemical oxidation of phenol at boron-doped diamond electrode,” *Electrochim. Acta*, 2001, doi: 10.1016/S0013-4686(01)00630-2.

[132] G. Busca, S. Berardinelli, C. Resini, and L. Arrighi, “Technologies for the removal of phenol from fluid streams: A short review of recent developments,” *Journal of Hazardous Materials*. 2008, doi: 10.1016/j.jhazmat.2008.03.045.

[133] S. Esplugas, J. Giménez, S. Contreras, E. Pascual, and M. Rodríguez, “Comparison of different advanced oxidation processes for phenol degradation,” *Water Res.*, 2002, doi: 10.1016/S0043-1354(01)00301-3.

[134] E. R. V. Dickenson, R. S. Summers, J. P. Croué, and H. Gallard, “Haloacetic acid and trihalomethane formation from the chlorination and bromination of aliphatic β-Dicarbonyl acid model compounds,” *Environ. Sci. Technol.*, 2008, doi: 10.1021/es0711866.

[135] S. E. Feller and A. D. MacKerell, “An improved empirical potential energy function for molecular simulations of phospholipids,” *J. Phys. Chem. B*, 2000, doi: 10.1021/jp0007843.

[136] S. Garcia-Segura and E. Brillas, “Advances in solar photoelectro-Fenton: Decolorization and mineralization of the Direct Yellow 4 diazo dye using an autonomous solar pre-pilot plant,” *Electrochim. Acta*, 2014, doi: 10.1016/j.electacta.2014.04.009.

[137] A. F. Sousa, A. Gandini, A. J. D. Silvestre, and C. P. Neto, “Determination of the hydroxy and carboxylic acid groups in natural complex mixtures of hydroxy fatty acids by 1H nuclear magnetic resonance spectroscopy,” *Appl. Spectrosc.*, 2009, doi: 10.1366/000370209788964557.

[138] N. Hanari *et al.*, “Polychlorinated naphthalenes and polychlorinated biphenyls in benthic organisms of a Great Lakes food chain,” *Arch. Environ. Contam. Toxicol.*, 2004, doi: 10.1007/s00244-003-3106-6.

[139] N. Yamashita, S. Taniyasu, N. Hanari, Y. Horii, and J. Falandysz, “Polychlorinated naphthalene contamination of some recently manufactured industrial products and commercial goods in Japan,” *J. Environ. Sci. Heal. - Part A Toxic/Hazardous Subst. Environ.*

Eng., 2003, doi: 10.1081/ESE-120022876.

[140] N. Zulfareen, K. Kannan, T. Venugopal, and S. Gnanavel, "Synthesis, characterization and corrosion inhibition efficiency of N-(4-(Morpholinomethyl Carbamoyl Phenyl) Furan-2-Carboxamide for brass in HCl medium," *Arab. J. Chem.*, 2016, doi: 10.1016/j.arabjc.2015.08.023.

[141] R. Kannan, R. Sandhya, V. Ganesan, M. Valsan, and K. Bhanu Sankara Rao, "Effect of sodium environment on the low cycle fatigue properties of modified 9Cr-1Mo ferritic martensitic steel," *J. Nucl. Mater.*, 2009, doi: 10.1016/j.jnucmat.2008.11.036.

[142] P. Kannan and S. A. John, "Highly sensitive determination of hydroxylamine using fused gold nanoparticles immobilized on sol-gel film modified gold electrode," *Anal. Chim. Acta*, 2010, doi: 10.1016/j.aca.2010.01.045.

[143] I. K. *et al.*, "Perfluorooctane sulfonate (PFOS) and related perfluorinated compounds in human maternal and cord blood samples: Assessment of PFOS exposure in a susceptible population during pregnancy," *Environ. Health Perspect.*, 2004.

[144] A. Y. Bagastyo, D. J. Batstone, I. Kristiana, B. I. Escher, C. Joll, and J. Radjenovic, "Electrochemical treatment of reverse osmosis concentrate on boron-doped electrodes in undivided and divided cell configurations," *J. Hazard. Mater.*, 2014, doi: 10.1016/j.jhazmat.2014.06.060.

[145] A. Y. Bagastyo, J. Keller, Y. Poussade, and D. J. Batstone, "Characterisation and removal of recalcitrants in reverse osmosis concentrates from water reclamation plants," *Water Res.*, 2011, doi: 10.1016/j.watres.2011.01.024.

[146] A. Y. Bagastyo, D. J. Batstone, K. Rabaey, and J. Radjenovic, "Electrochemical oxidation of electrodialysed reverse osmosis concentrate on Ti/Pt-IrO2, Ti/SnO2-Sb and boron-doped diamond electrodes," *Water Res.*, 2013, doi: 10.1016/j.watres.2012.10.001.

[147] D. C. Montgomery, *Design and Analysis of Experiments Eighth Edition*. 2012.

[148] E. GilPavas, J. Medina, I. Dobrosz-Gómez, and M. A. Gómez-García, "Statistical optimization of industrial textile wastewater treatment by electrochemical methods," *J. Appl. Electrochem.*, 2014, doi: 10.1007/s10800-014-0767-y.

[149] L. Vera Candioti, M. M. De Zan, M. S. Cámara, and H. C. Goicoechea, "Experimental design and multiple response optimization. Using the desirability function in analytical methods development," *Talanta*. 2014, doi: 10.1016/j.talanta.2014.01.034.

[150] "5." .

[151] M. A. Bezerra, R. E. Santelli, E. P. Oliveira, L. S. Villar, and L. A. Escaleira, "Response surface methodology (RSM) as a tool for optimization in analytical chemistry," *Talanta*. 2008, doi: 10.1016/j.talanta.2008.05.019.

[152] P. Sengottuvel, S. Satishkumar, and D. Dinakaran, "Optimization of multiple characteristics of EDM parameters based on desirability approach and fuzzy modeling," in *Procedia Engineering*, 2013, doi: 10.1016/j.proeng.2013.09.185.

[153] "Hierarchical Model_ Definition - Statistics How To." .

[154] T. Karichappan, S. Venkatachalam, and P. M. Jeganathan, "Optimization of electrocoagulation process to treat grey wastewater in batch mode using response surface methodology," *J. Environ. Heal. Sci. Eng.*, 2014, doi: 10.1186/2052-336X-12-29.

[155] C. T. Benatti, C. R. G. Tavares, and T. A. Guedes, "Optimization of Fenton's oxidation of chemical laboratory wastewaters using the response surface methodology," *J. Environ. Manage.*, 2006, doi: 10.1016/j.jenvman.2005.08.014.

[156] X. Zhu, J. Tian, R. Liu, and L. Chen, "Optimization of fenton and electro-fenton oxidation of biologically treated coking wastewater using response surface methodology," *Sep. Purif. Technol.*, 2011, doi: 10.1016/j.seppur.2011.08.023.

[157] A. I. Khuri and S. Mukhopadhyay, "Response surface methodology," *Wiley Interdisciplinary Reviews: Computational Statistics*. 2010,

doi: 10.1002/wics.73.

[158] J. Wu, H. Zhang, N. Oturan, Y. Wang, L. Chen, and M. A. Oturan, “Application of response surface methodology to the removal of the antibiotic tetracycline by electrochemical process using carbon-felt cathode and DSA (Ti/RuO2-IrO2) anode,” *Chemosphere*, 2012, doi: 10.1016/j.chemosphere.2012.01.036.

[159] R. M. G. de Lima, G. R. da Silva Wildhagen, J. W. S. D. da Cunha, and J. C. Afonso, “Removal of ammonium ion from produced waters in petroleum offshore exploitation by a batch single-stage electrolytic process,” *J. Hazard. Mater.*, 2009, doi: 10.1016/j.jhazmat.2008.04.058.

[160] C. J. Hwang, M. J. Sclimenti, and S. W. Krasner, “Disinfection by-product formation reactivities of natural organic matter fractions of a low-humic water,” *ACS Symp. Ser.*, 2000.

[161] A. J. C. da Silva, E. V. dos Santos, C. C. de Oliveira Morais, C. A. Martínez-Huitle, and S. S. L. Castro, “Electrochemical treatment of fresh, brine and saline produced water generated by petrochemical industry using Ti/IrO2-Ta2O5 and BDD in flow reactor,” *Chem. Eng. J.*, 2013, doi: 10.1016/j.cej.2013.08.023.

[162] M. Ben-Sasson, Y. Zidon, R. Calvo, and A. Adin, “Enhanced removal of natural organic matter by hybrid process of electrocoagulation and dead-end microfiltration,” *Chem. Eng. J.*, 2013, doi: 10.1016/j.cej.2013.07.101.

[163] A. Bagga, S. Chellam, and D. A. Clifford, “Evaluation of iron chemical coagulation and electrocoagulation pretreatment for surface water microfiltration,” *J. Memb. Sci.*, 2008, doi: 10.1016/j.memsci.2007.10.009.

[164] N. P. Gamage and S. Chellam, “Mechanisms of physically irreversible fouling during surface water microfiltration and mitigation by aluminum electroflotation pretreatment,” *Environ. Sci. Technol.*, 2014, doi: 10.1021/es405080g.

[165] S. Chellam and M. A. Sari, “Aluminum electrocoagulation as pretreatment during microfiltration of surface water containing NOM: A review of fouling, NOM, DBP, and virus control,” *Journal of Hazardous Materials*. 2016, doi: 10.1016/j.jhazmat.2015.10.054.

[166] M. Panizza, I. Sirés, and G. Cerisola, “Anodic oxidation of mecoprop herbicide at lead dioxide,” *J. Appl. Electrochem.*, 2008, doi: 10.1007/s10800-008-9497-3.

[167] M. Panizza and G. Cerisola, “Electrocatalytic materials for the electrochemical oxidation of synthetic dyes,” *Appl. Catal. B Environ.*, 2007, doi: 10.1016/j.apcatb.2007.04.001.

[168] Y. Kitazono, I. Ihara, G. Yoshida, K. Toyoda, and K. Umetsu, “Selective degradation of tetracycline antibiotics present in raw milk by electrochemical method,” *J. Hazard. Mater.*, 2012, doi: 10.1016/j.jhazmat.2012.10.009.

[169] F. Fu and Q. Wang, “Removal of heavy metal ions from wastewaters: A review,” *Journal of Environmental Management*. 2011, doi: 10.1016/j.jenvman.2010.11.011.

[170] B. B. Potter and J. C. Wimsatt, “USEPA method 415.3: Quantifying TOC, DOC, and SUVA,” *Journal - American Water Works Association*. 2012, doi: 10.5942/jawwa.2012.104.0086.

[171] A. D. Archer and P. C. Singer, “An evaluation of the relationship between SUVA and NOM coagulation using the ICR database,” *Journal / American Water Works Association*. 2006, doi: 10.1002/j.1551-8833.2006.tb07715.x.

[172] N. W. Green, D. McInnis, N. Hertkorn, P. A. Maurice, and E. M. Perdue, “Suwannee River natural organic matter: Isolation of the 2R101N reference sample by reverse osmosis,” *Environ. Eng. Sci.*, 2015, doi: 10.1089/ees.2014.0284.

[173] E. J. Rosenfeldt and K. G. Linden, “Degradation of endocrine disrupting chemicals bisphenol A, ethinyl estradiol, and estradiol during

UV photolysis and advanced oxidation processes," *Environ. Sci. Technol.*, 2004, doi: 10.1021/es035413p.

[174] E. J. Rosenfeldt, P. J. Chen, S. Kullman, and K. G. Linden, "Destruction of estrogenic activity in water using UV advanced oxidation," *Sci. Total Environ.*, 2007, doi: 10.1016/j.scitotenv.2007.01.096.

[175] F. Manea, A. Jakab, M. Ardelean, A. Pop, and I. Vlaicu, "Boron-doped diamond electrode-based advanced treatment methods for drinking water," *Environ. Eng. Manag. J.*, vol. 13, no. 9, pp. 2167–2172, 2014, doi: 10.30638/eemj.2014.240.

[176] M. Drikas, M. Dixon, and J. Morran, "Long term case study of MIEX pre-treatment in drinking water; understanding NOM removal," *Water Res.*, 2011, doi: 10.1016/j.watres.2010.11.024.

[177] Shimadzu, "TOC Application Handbook," *Www.Shimadzu.Com/an/Toc*, 2017, doi: 10.1016/0257-8972(95)08283-2.

[178] "MANTECH," in *Encyclopedia of Production and Manufacturing Management*, 2006.

[179] "SpectraMax M Series Microplate Readers, Cuvette Port, IQ OQ Validation _ Molecular Devices." .

[180] E. Lacasa, J. Llanos, P. Cañizares, and M. A. Rodrigo, "Electrochemical denitrificacion with chlorides using DSA and BDD anodes," *Chem. Eng. J.*, 2012, doi: 10.1016/j.cej.2011.12.090.

[181] S. Zhou, L. Bu, Y. Yu, X. Zou, and Y. Zhang, "A comparative study of microcystin-LR degradation by electrogenerated oxidants at BDD and MMO anodes," *Chemosphere*, 2016, doi: 10.1016/j.chemosphere.2016.09.057.

[182] A. Kapałka, G. Fóti, and C. Comninellis, "Basic principles of the electrochemical mineralization of organic pollutants for wastewater treatment," in *Electrochemistry for the Environment*, 2010.

[183] L. C. Chiang, J. E. Chang, and T. C. Wen, "Indirect oxidation effect in electrochemical oxidation treatment of landfill leachate," *Water Res.*, 1995, doi: 10.1016/0043-1354(94)00146-X.

[184] J. R. Baker, M. W. Milke, and J. R. Mihelcic, "Relationship between chemical and theoretical oxygen demand for specific classes of organic chemicals," *Water Res.*, 1999, doi: 10.1016/S0043-1354(98)00231-0.

[185] A. K. Stoddart and G. A. Gagnon, "Application of photoelectrochemical chemical oxygen demand to drinking water," *J. Am. Water Works Assoc.*, 2014, doi: 10.5942/jawwa.2014.106.0106.

[186] W. He, S. Chen, X. Liu, and J. Chen, "Water quality monitoring in a slightly-polluted inland water body through remote sensing - Case study of the Guanting Reservoir in Beijing, China," *Front. Environ. Sci. Eng. China*, 2008, doi: 10.1007/s11783-008-0027-7.

[187] H. Särkkä, M. Vepsäläinen, M. Pulliainen, and M. Sillanpää, "Electrochemical inactivation of paper mill bacteria with mixed metal oxide electrode," *J. Hazard. Mater.*, 2008, doi: 10.1016/j.jhazmat.2007.12.011.

[188] N. Ates, M. Kitis, and U. Yetis, "Formation of chlorination by-products in waters with low SUVA-correlations with SUVA and differential UV spectroscopy," *Water Res.*, 2007, doi: 10.1016/j.watres.2007.05.042.

[189] H. Wong, K. M. Mok, and X. J. Fan, "Natural organic matter and formation of trihalomethanes in two water treatment processes," *Desalination*, 2007, doi: 10.1016/j.desal.2006.05.031.

[190] *IUPAC Compendium of Chemical Terminology*. 2009.

[191] O. M. Schneider *et al.*, "Photocatalytic degradation of microcystins by TiO 2 using UV-LED controlled periodic illumination," *Catalysts*, 2019, doi: 10.3390/catal9020181.

[192] R. Liang *et al.*, "Utilizing UV-LED pulse width modulation on TiO2 advanced oxidation processes to enhance the decomposition efficiency of pharmaceutical micropollutants," *Chem. Eng. J.*, 2019, doi: 10.1016/j.cej.2018.12.065.

[193] B. K. Körbahti, N. Aktaş, and A. Tanyolaç, “Optimization of electrochemical treatment of industrial paint wastewater with response surface methodology,” *J. Hazard. Mater.*, 2007, doi: 10.1016/j.jhazmat.2007.02.005.

[194] D. Rajkumar, B. J. Song, and J. G. Kim, “Electrochemical degradation of Reactive Blue 19 in chloride medium for the treatment of textile dyeing wastewater with identification of intermediate compounds,” *Dye. Pigment.*, 2007, doi: 10.1016/j.dyepig.2005.07.015.

[195] D. Ghernaout, “Electrocoagulation and Electrooxidation for Disinfecting Water: New Breakthroughs and Implied Mechanisms,” *Appl. Eng.*, 2019, doi: 10.11648/j.ae.20190302.18.

[196] M. Panizza, E. Brillas, and C. Comninellis, “Application of Boron-Doped Diamond Electrodes for Wastewater Treatment,” *J. Environ. Eng. Manag.*, 2008.

[197] M. Zhou, Z. Wu, and D. Wang, “Electrocatalytic degradation of phenol in acidic and saline wastewater,” *J. Environ. Sci. Heal. - Part A Toxic/Hazardous Subst. Environ. Eng.*, 2002, doi: 10.1081/ESE-120005985.

[198] A. F. Ashery, K. Radwan, and M. I. Gar Alalm, “The effect of pH control on turbidity and NOM removal in conventional water treatment,” *Int. water Technol. J.*, 2010.

[199] M. E. H. Bergmann, A. S. Koparal, and T. Iourtchouk, “Electrochemical Advanced oxidation processes, formation of halogenate and perhalogenate species: A critical review,” *Crit. Rev. Environ. Sci. Technol.*, 2014, doi: 10.1080/10643389.2012.718948.

[200] Y. J. Liu, C. Y. Hu, and S. L. Lo, “Direct and indirect electrochemical oxidation of amine-containing pharmaceuticals using graphite electrodes,” *J. Hazard. Mater.*, 2019, doi: 10.1016/j.jhazmat.2018.12.037.

[201] X. Hua, X. Song, M. Yuan, and D. Donga, “The factors affecting relationship between COD and TOC of typical papermaking wastewater,” *Adv. Intell. Soft Comput.*, 2011, doi: 10.1007/978-3-642-23756-0_39.

Appendices

5.3. Appendix A: Chapter 3 raw data

Table 0-1: Tabulated values of NOM removal, TOC Efficiency (%) of M1, M2, and M3.

			Treatment Conditions 6.5 pH, 10 mA cm^{-2}
Time [mins]	***M1 [%]***	***M2 [%]***	***M3 [%]***
0	0.0	0.0	0.0
30	-3.0	-2.8	54.0
60	-12.5	-7.1	63.3
120	2.4	-0.7	65.8

			Treatment Conditions 6.5 pH, 20 mA cm^{-2}
Time [mins]	***M1 [%]***	***M2 [%]***	***M3 [%]***
0	0	0	0
30	-2.3	-5.5	15.4
60	-10.2	-4.5	35.1
120	1.9	8.8	43.2

			Treatment Conditions 8.5 pH, 10 mA cm^{-2}
Time [mins]	***M1 [%]***	***M2 [%]***	***M3 [%]***
0	0.0	0.0	0.0
30	15.3	10.5	22.9
60	4.7	-6.6	27.9
120	33.6	-23.2	30.8

			Treatment Conditions 8.5 pH, 20 mA cm^{-2}
Time [mins]	***M1 [%]***	***M2 [%]***	***M3 [%]***

0	0.0	0.0	0.0
30	37.5	37.6	30.5
60	39.7	38.3	34.3
120	40.2	40.2	35.0

Table 0-2: Tabulated values of NOM removal, COD Efficiency (%) of M1, M2, and M3.

			Treatment Conditions 6.5 pH, 10 mA cm^{-2}
Time [mins]	***M1 [%]***	***M2 [%]***	***M3 [%]***
0	0.0	0.0	0.0
30	-14.4	-42.4	23.8
60	-9.9	-36.1	58.4
120	11.2	-22.6	91.6

			Treatment Conditions 6.5 pH, 20 mA cm^{-2}
Time [mins]	***M1 [%]***	***M2 [%]***	***M3 [%]***
0	0.0	0.0	0.0
30	15.8	8.5	30.8
60	15.8	-0.4	39.3
120	43.8	52.3	54.8

			Treatment Conditions 8.5 pH, 10 mA cm^{-2}
Time [mins]	***M1 [%]***	***M2 [%]***	***M3 [%]***
0.0	0.0	0.0	0.0
30.0	-34.4	-28.1	89.3
60.0	-48.2	-35.7	90.2
120.0	52.7	52.2	90.2

			Treatment Conditions 8.5 pH, 20 mA cm^{-2}
Time [mins]	***M1 [%]***	***M2 [%]***	***M3 [%]***
0.0	0.0	0.0	0.0
30.0	50.4	51.8	54.0
60.0	60.3	55.4	77.2
120.0	57.6	75.4	68.8

Table 0-3: Tabulated values of COD/TOC of M1, M2, and M3.

			Treatment Conditions 6.5 pH, 10 mA cm^{-2}
Time [mins]	***M1***	***M2***	***M3***
0	2.8	2.8	2.8
30	3.0	3.8	4.5
60	2.7	3.5	3.1
120	2.6	3.5	0.7

			Treatment Conditions 6.5 pH, 20 mA cm^{-2}
Time [mins]	***M1***	***M2***	***M3***
0	2.7	2.7	2.7
30	2.1	2.0	2.0
60	1.8	1.8	2.3
120	1.6	1.1	2.3

			Treatment Conditions 8.5 pH, 10 mA cm^{-2}
Time [mins]	***M1***	***M2***	***M3***
0	3.1	3.1	3.1
30	5.2	5.2	1.9
60	6.7	5.3	0.7
120	1.9	1.4	0.9

			Treatment Conditions 8.5 pH, 20 mA cm^{-2}
Time [mins]	***M1***	***M2***	***M3***
0	2.9	2.9	2.9
30	4.7	3.5	3.0
60	7.0	6.1	3.7
120	1.5	1.1	1.2

Table 0-4: Tabulated values of SUVA (L mg-M^{-1}) of M1, M2, and M3.

			Treatment Conditions 6.5 pH, 10 mA cm^{-2}
Time [mins]	***M1 [L mg-M^{-1}]***	***M2 [L mg-M^{-1}]***	***M3 [L mg-M^{-1}]***
0	2.9	2.9	2.9
30	2.7	2.9	6.1
60	2.4	2.4	9.5
120	3.4	2.7	14.4

			Treatment Conditions 6.5 pH, 20 mA cm^{-2}
Time [mins]	***M1 [L mg-M^{-1}]***	***M2 [L mg-M^{-1}]***	***M3 [L mg-M^{-1}]***
0	2.5	2.5	2.5
30	2.7	2.9	3.8
60	2.7	3.3	3.8
120	3.8	3.6	4.7

			Treatment Conditions 8.5 pH, 10 mA cm^{-2}
Time [mins]	***M1 [L mg-M^{-1}]***	***M2 [L mg-M^{-1}]***	***M3 [L mg-M^{-1}]***
0	2.3	2.3	2.3
30	3.2	3.2	4.0
60	3.6	2.7	2.6

120	4.6	3.4	6.7

			Treatment Conditions 8.5 pH, 20 mA cm^{-2}
Time [mins]	***M1 [L mg-M^{-1}]***	***M2 [L mg-M^{-1}]***	***M3 [L mg-M^{-1}]***
0	2.3	2.3	2.3
30	3.4	5.1	3.6
60	4.7	4.6	4.8
120	5.0	6.3	5.6

Table 0-5: Tabulated values of COD/TOC efficiency of M1, M2, and M3.

			Treatment Conditions 6.5 pH, 10 mA cm^{-2}
Time [mins]	***M1***	***M2***	***M3***
0	0.0	0.0	0.0
30	-9.7	-39.4	-62.1
60	2.9	-27.3	-12.5
120	5.8	-26.0	73.9

			Treatment Conditions 6.5 pH, 20 mA cm^{-2}
Time [mins]	***M1***	***M2***	***M3***
0	0.0	0.0	0.0
30	24.7	25.5	26.5
60	33.7	35.6	16.1
120	41.9	60.8	16.7

			Treatment Conditions 8.5 pH, 10 mA cm^{-2}
Time [mins]	***M1***	***M2***	***M3***
0	0.0	0.0	0.0
30	-66.7	-67.9	38.5

60	-117.2	-71.8	76.6
120	38.8	54.8	70.6

			Treatment Conditions 8.5 pH, 20 mA cm^{-2}
Time [mins]	***M1***	***M2***	***M3***
0	0.0	0.0	0.0
30	-61.8	-21.6	-4.2
60	-143.1	-112.8	-27.5
120	49.1	60.3	59.1

Electrical Energy per Order

Table 0-6: Tabulated values of Electrical Energy per Order (kWh order^{-1} m^{-3}) of M1, M2, and M3.

			Treatment Conditions 6.5 pH, 10 mA cm^{-2}
Time [mins]	***M1 [kWh order^{-1} m^{-3}]***	***M2 [kWh order^{-1} m^{-3}]***	***M3 [kWh order^{-1} m^{-3}]***
30	-37.1	-11.6	0.9
60	-19.2	-12.4	1.5
120	-131.6	-5183.2	2.7

			Treatment Conditions 6.5 pH, 20 mA cm^{-2}
Time [mins]	***M1 [kWh order^{-1} m^{-3}]***	***M2 [kWh order^{-1} m^{-3}]***	***M3 [kWh order^{-1} m^{-3}]***
30	-39.9	-7.2	4.5
60	-14.4	0.7	3.9
120	-10.8	-1.9	6.5

			Treatment Conditions 8.5 pH, 10 mA cm^{-2}
Time [mins]	***M1 [kWh order^{-1} m^{-3}]***	***M2 [kWh order^{-1} m^{-3}]***	***M3 [kWh order^{-1} m^{-3}]***

30	7.5	5.2	13.1
60	17.2	67.7	18.2
120	22.0	-2.9	38.9

Treatment Conditions 8.5 pH, 20 mA cm^{-2}

Time [mins]	***M1 [kWh order^{-1} m^{-3}]***	***M2 [kWh order^{-1} m^{-3}]***	***M3 [kWh order^{-1} m^{-3}]***
30	35.9	12.8	20.7
60	50.1	-88.5	34.2
120	86.7	66.4	141.1

Table 0-7: Tabulated TOC removal vs. specific energy consumption

TOC Removal [%]	***Energy Consumption [kWh dm^{-3}]***
10 mA cm^{-2}	
-12.5	0.0008
-10.2	0.0008
-3.0	0.0004
-2.3	0.0004
1.9	0.0014
2.4	0.0016
20 mA cm^{-2}	
4.7	0.0024
15.3	0.0012
33.6	0.0048
37.5	0.0010
39.7	0.0021
40.2	0.0040
30 mA cm^{-2}	
79.4	0.007

81.2	0.004
88.6	0.014
96.6	0.029

TOC Removal [%]	*Energy Consumption [kWh dm^{-3}]*
10 mA cm^{-2}	
-7.1	0.00022
-5.5	0.00012
-4.5	0.00035
-2.8	0.00015
-0.7	0.00042
0.0	0.00043
20 mA cm^{-2}	
-23.2	0.0015
-6.6	0.0006
10.5	0.0003
37.6	0.0010
38.3	0.0014
40.2	0.0033
30 mA cm^{-2}	
79.4	0.000
75.5	0.004
81.6	0.007
87.7	0.014

TOC Removal [%]	*Energy Consumption [kWh dm^{-3}]*
10 mA cm^{-2}	
15.4	0.0005

35.1	0.0007
43.2	0.0013
54.0	0.0004
63.3	0.0006
65.8	0.0017
20 mA cm^{-2}	
22.9	0.0010
27.9	0.0021
30.5	0.0010
30.8	0.0036
34.3	0.0021
35.0	0.0041
30 mA cm^{-2}	
24.6	0.004
48.2	0.007
58.6	0.014
58.5	0.029

Table 0-8: Tabulated COD removal vs. specific energy consumption

COD Removal [%]	***Energy Consumption [kWh dm^{-3}]***
10 mA cm^{-2}	
-14.4	0.0004
-9.9	0.0008
11.2	0.0014
15.8	0.0012
15.8	0.0024
43.8	0.0048
20 mA cm^{-2}	

-48.2	0.0024
-34.4	0.0012
50.4	0.0010
52.7	0.0048
57.6	0.0040
60.3	0.0021
30 mA cm^{-2}	
-23.5	0.004
40.8	0.007
49.0	0.014
98.0	0.029

COD Removal [%]	***Energy Consumption [kWh dm^{-3}]***
10 mA cm^{-2}	
-42.4	0.00015
-36.1	0.00022
-22.6	0.00042
-0.4	0.00035
8.5	0.00012
52.3	0.00043
20 mA cm^{-2}	
-35.7	0.0006
-28.1	0.0003
51.8	0.0010
52.2	0.0015
55.4	0.0014
75.4	0.0033

30 mA cm^{-2}	
32.7	0.004
54.1	0.007
54.1	0.014
93.9	0.029

COD Removal [%]	***Energy Consumption [kWh dm^{-3}]***
10 mA cm^{-2}	
23.8	0.0004
30.8	0.0005
39.3	0.0007
54.8	0.0013
58.4	0.0006
91.6	0.0017
20 mA cm^{-2}	
54.0	0.0010
68.8	0.0041
77.2	0.0021
89.3	0.0010
90.2	0.0021
90.2	0.0036
30 mA cm^{-2}	
95.9	0.007
95.9	0.029
98.0	0.004
98.0	0.014

Table 0-9: Tabulated specific energy consumption of M1, M2, and M3

	Electrolysis Conditions: pH 8.5, time 120 mins		
Current Density [mA cm^{-2}]	***M1 [kWh dm^{-3}]***	***M2 [kWh dm^{-3}]***	***M3 [kWh dm^{-3}]***
10	0.0014	0.0004	0.0013
20	0.004	0.0018	0.0041
30	0.012	0.0223	0.0064

	Electrolysis Conditions: 10 mA cm^{-2}, time 120 mins		
pH	***M1 [kWh dm^{-3}]***	***M2 [kWh dm^{-3}]***	***M3 [kWh dm^{-3}]***
6.5	0.004	0.0018	0.0041
8.5	0.0044	0.0027	0.0036

5.4. Appendix B: BBD design experimental data

Table 0-10: Box-Behnken experimental design matrix with experimental and predicted response values for M1

Run	***Initial pH***	***Time [min]***	***Current [mA cm^{-2}]***	***TOC Removal [%]***	***COD Removal [%]***	***SUVA [L mg-M^{-1}]***
1	7.5	60	20	-43.9	-46.4	3.1
2	7.5	30	10	-60.5	7.8	2.5
3	7.5	60	20	-43.9	-50.0	3.1
4	6.5	30	20	13.5	-8.1	2.7
5	6.5	60	10	6.3	-9.1	3.0
6	8.5	60	10	2.8	42.0	3.1
7	7.5	30	30	82.5	84.8	14.2
8	7.5	120	30	99.2	91.9	39.4
9	7.5	120	10	56.8	59.7	3.9
10	8.5	60	30	84.4	83.1	14.3
11	6.5	60	30	81.2	38.8	14.2

12	8.5	120	20	6.6	60.7	3.1
13	8.5	30	20	3.9	50.0	2.7
14	7.5	60	20	-43.9	-46.4	3.1
15	7.5	60	20	-43.9	-50.0	3.1
16	6.5	120	20	56.2	74.7	6.1
17	7.5	60	20	-43.9	-50.0	3.1

Table 0-11: Box-Behnken experimental design matrix with experimental and predicted response values for M2

Run	***Initial pH***	***Time [min]***	***Current [mA cm^{-2}]***	***TOC Removal [%]***	***COD Removal [%]***	***SUVA [L $mg\text{-}M^{-1}$]***
1	7.5	120	10	-4.8	-15.6	2.6
2	8.5	60	10	-8.6	97.3	6.6
3	6.5	60	30	77.0	51.0	12.7
4	7.5	60	20	-24.2	-36.6	2.6
5	7.5	60	20	-24.2	-34.8	2.6
6	6.5	60	10	1.1	-47.5	2.8
7	6.5	120	20	-35.1	69.7	2.9
8	8.5	60	30	81.6	46.1	10.7
9	7.5	120	30	97.0	84.8	13.8
10	8.5	30	20	5.2	50.9	3.0
11	7.5	30	30	78.6	57.6	9.5
12	7.5	30	10	28.5	-57.1	5.1
13	6.5	30	20	11.5	-6.1	2.8
14	7.5	60	20	-24.2	-34.8	2.6
15	7.5	60	20	-24.2	-36.6	2.6
16	8.5	120	20	3.9	81.3	2.6
17	7.5	60	20	-24.2	-34.8	2.6

Chapter 6.

Table 0-12: Box-Behnken experimental design matrix with experimental and predicted response values for M3

Run	***Initial pH***	***Time [min]***	***Current [mA cm-2]***	***TOC Removal [%]***	***COD Removal [%]***	***SUVA [L mg-M^{-1}]***
1	7.5	60	20	51.1	89.3	1.3
2	7.5	60	20	51.1	91.1	1.3
3	7.5	30	30	54.9	77.8	2.9
4	8.5	30	20	4.6	53.6	2.5
5	6.5	30	20	12.5	14.1	2.6
6	6.5	60	10	68.9	59.6	13.8
7	6.5	120	20	13.5	68.7	4.5
8	7.5	30	10	54.6	88.3	2.8
9	7.5	120	30	82.2	98.0	3.8
10	7.5	60	20	51.1	89.3	1.3
11	7.5	120	10	37.8	-5.2	11.9
12	6.5	60	30	42.8	95.9	4.5
13	7.5	60	20	51.1	91.1	1.3
14	8.5	120	20	2.6	69.6	2.3
15	8.5	60	10	1.8	61.6	2.9
16	8.5	60	30	37.3	69.7	8.1
17	7.5	60	20	51.1	91.1	1.3

7.3. Appendix C: Actual vs. predicted values of Stat-ease models

Table 0-13: Tabulated values of Actual and predicted values M1 TOC efficiency

Actual	*Predicted*
-43.90	-43.90
-60.54	-39.57
-43.90	-43.90
13.53	5.08

6.33	4.63
2.83	-10.27
82.49	83.72
99.24	83.21
56.82	50.66
84.41	82.78
81.23	97.67
6.56	35.04
3.93	-9.82
-43.90	-43.90
-43.90	-43.90
56.22	49.94
-43.90	-43.90

Table 0-14: Tabulated values of Actual and predicted values M2 TOC efficiency

Actual	*Predicted*
-46.43	-48.57
7.79	9.03
-50.00	-48.57
-8.08	-8.08
-9.09	-8.34
41.96	32.89
84.85	74.98
91.92	93.46
59.74	66.83
83.15	85.74
38.78	44.50

60.71	58.56
50.00	58.63
-46.43	-48.57
-50.00	-48.57
74.75	68.27
-50.00	-48.57

Table 0-15 Tabulated values of Actual and predicted values M1 SUVA

Actual	*Predicted*
3.14	2.75
2.54	5.24
3.14	2.75
2.67	0.0011
3.03	3.56
3.13	3.56
14.20	11.56
39.43	33.10
3.87	0.2066
14.33	18.74
14.18	18.74
3.12	8.25
2.71	0.0011
3.14	2.75
3.14	2.75
6.06	8.25
3.14	2.75

Table 0-16 Tabulated values of Actual and predicted values M2 TOC Efficiency

Actual	*Predicted*
-4.78	-9.15
-8.63	-0.8542
76.96	71.90
-24.22	-22.42
-24.22	-22.42
1.14	-3.69
-35.13	-31.45
81.64	74.74
97.00	97.60
5.24	-4.74
78.60	89.95
28.51	29.93
11.53	8.73
-24.22	-22.42
-24.22	-22.42
3.93	4.01
-24.22	-22.42

Table 0-17 Tabulated values of Actual and predicted values M2 COD Efficiency

Actual	*Predicted*
-15.58	-4.23
97.32	56.69
51.02	70.20
-36.61	-26.96
-34.82	-26.96
-47.47	-70.27

69.70	55.49
46.07	47.42
84.85	61.37
50.89	63.84
57.58	17.63
-57.14	-47.97
-6.06	11.76
-34.82	-26.96
-36.61	-26.96
81.25	107.58
-34.82	-26.96

Table 0-18 Tabulated values of Actual and predicted values M2 SUVA

Actual	*Predicted*
2.64	2.53
6.58	6.17
12.69	12.62
2.63	2.69
2.63	2.69
2.79	2.85
2.90	2.71
10.69	10.15
13.83	13.82
3.02	2.79
9.53	10.17
5.06	5.51
2.82	2.37
2.63	2.69

2.63	2.69
2.59	3.13
2.63	2.69

Table 0-19 Tabulated values of Actual and predicted values M3 TOC efficiency

Actual	*Predicted*
51.09	51.09
51.09	51.09
54.89	53.10
4.61	-4.30
12.55	18.57
68.88	59.75
13.54	20.95
54.62	59.28
82.21	79.16
51.09	51.09
37.82	37.99
42.82	38.52
51.09	51.09
2.61	-1.92
1.76	6.05
37.34	46.48
51.09	51.09

Table 0-20 Tabulated values of Actual and predicted values M3 COD Efficiency

Actual	*Predicted*
89.29	89.21
91.07	89.21

77.78	59.59
53.57	52.43
14.14	48.39
59.60	58.79
68.69	47.72
88.31	73.39
97.98	116.59
89.29	89.21
-5.19	15.05
95.92	83.43
91.07	89.21
69.64	51.76
61.61	62.83
69.66	87.47
91.07	89.21

Table 0-21 Tabulated values of Actual and predicted values M3 SUVA

Actual	*Predicted*
1.25	1.00
1.25	1.00
2.87	4.50
2.47	0.7061
2.57	3.10
13.82	13.03
4.53	5.84
2.81	4.08
3.82	3.09
1.25	1.00

11.87	10.96
4.45	3.40
1.25	1.00
2.27	3.44
2.92	3.35
8.13	8.29
1.25	1.00

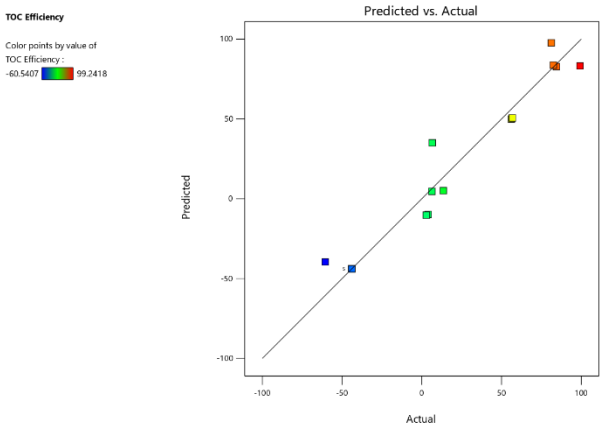

Figure 0-1: Actual versus predicted plots for the model adequacy testing M1 TOC efficiency

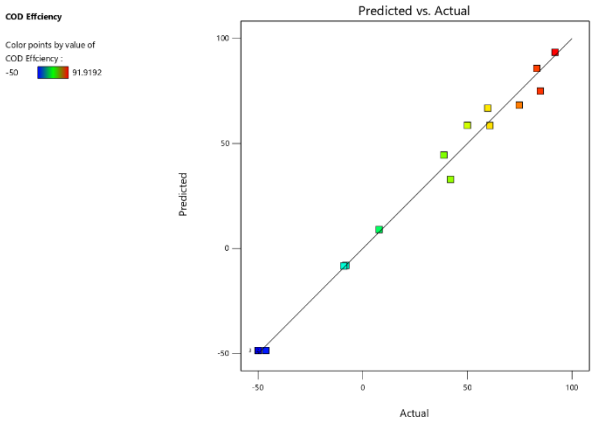

Figure 0-2: Actual versus predicted plots for the model adequacy testing M1 COD efficiency

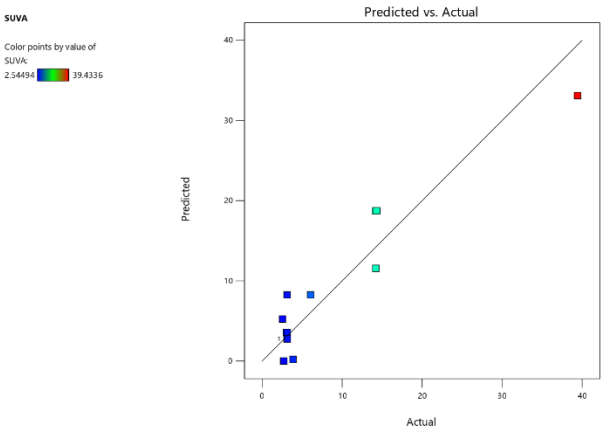

Figure 0-3 Actual versus predicted plots for the model adequacy testing M1 SUVA

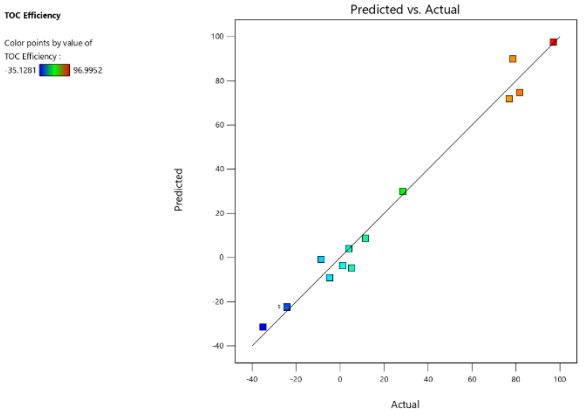

Figure 0-4 Actual versus predicted plots for the model adequacy testing M2 TOC Efficiency

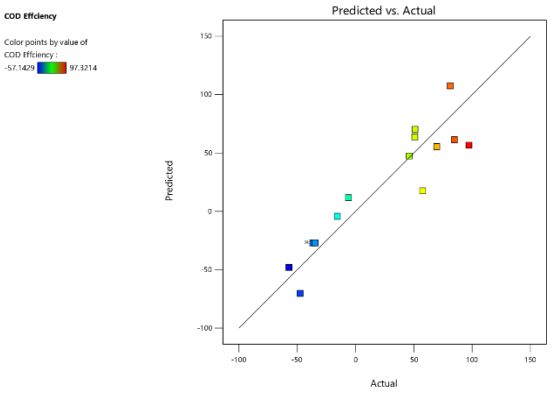

Figure 0-5 Actual versus predicted plots for the model adequacy testing M2 COD Efficiency

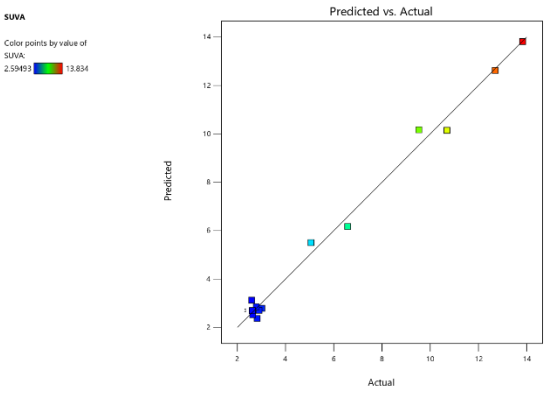

Figure 0-6 Actual versus predicted plots for the model adequacy testing M2 SUVA

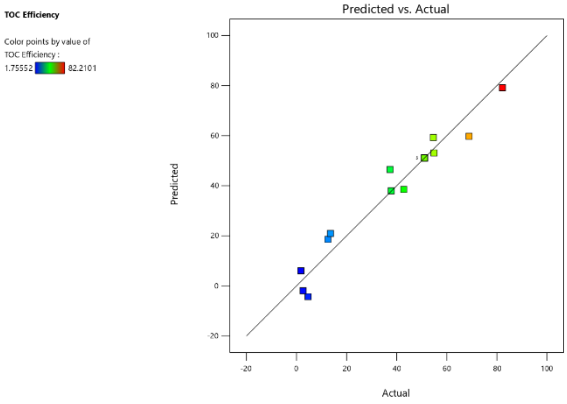

Figure 0-7 Actual versus predicted plots for the model adequacy testing M3 TOC efficiency

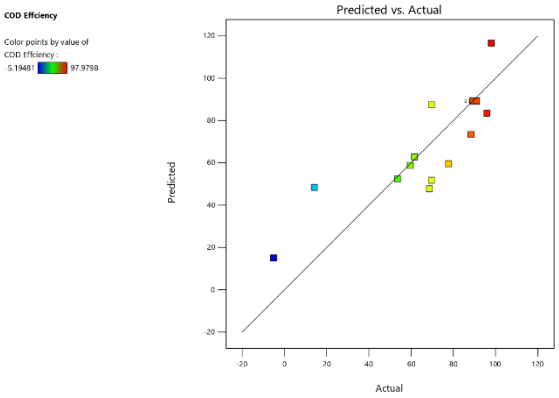

Figure 0-8 Actual versus predicted plots for the model adequacy testing M3 COD efficiency

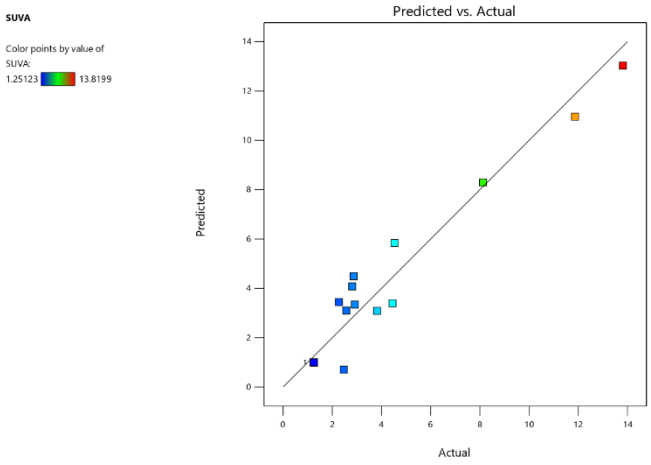

Figure 0-9 Actual versus predicted plots for the model adequacy testing M3 SUVA

7.4. Appendix D: ANOVA Tables

Table 0-22: ANOVA analysis and statistical parameters of the responses M1 TOC efficiency

Source	*Sum of Squares*	*Df*	*Mean Square*	*F-value*	*P-value*	
Model	45382.39	7	6483.20	25.43	< 0.0001	significant
A-Initial pH	443.66	1	443.66	1.74	0.2197	
B-Time	4024.83	1	4024.83	15.79	0.0032	
C-Current	11536.31	1	11536.31	45.25	< 0.0001	
BC	2172.75	1	2172.75	8.52	0.0171	
A^2	4199.48	1	4199.48	16.47	0.0028	
B^2	2467.51	1	2467.51	9.68	0.0125	
C^2	13215.67	1	13215.67	51.84	< 0.0001	
Residual	2294.51	9	254.95			
Lack of Fit	2294.51	5	458.90			
Pure Error	0.0000	4	0.0000			
Cor Total	47676.90	16				

The model f-value of 25.43 indicated the model is significant. In this case, time and current density were determined to be significant model terms. Initial pH was not a significant factor, however, included for the requirements of a hierarchical model.

Table 0-23 ANOVA analysis and statistical parameters of the responses M1 COD efficiency

Source	*Sum of Squares*	*Df*	*Mean Square*	*F-value*	*P-value*	
Model	46231.00	8	5778.87	112.69	< 0.0001	significant
A-Initial pH	1543.18	1	1543.18	30.09	0.0006	
B-Time	2909.37	1	2909.37	56.73	< 0.0001	
C-Current	4071.87	1	4071.87	79.40	< 0.0001	
AB	1541.55	1	1541.55	30.06	0.0006	
BC	408.15	1	408.15	7.96	0.0225	
A^2	5237.84	1	5237.84	102.14	< 0.0001	
B^2	10464.42	1	10464.42	204.05	< 0.0001	
C^2	11385.26	1	11385.26	222.01	< 0.0001	
Residual	410.26	8	51.28			
Lack of Fit	394.96	4	98.74	25.80	0.0041	significant
Pure Error	15.31	4	3.83			
Cor Total	46641.26	16				

Model f-value of 112.69 implied the model is significant. Unlike M1 TOC ANOVA for the quadratic model, all three operating factors played a significant role in COD efficiency. However, the lack of fit was significant for COD efficiency models, which foreshadowed an inadequate M1 COD efficiency regression model.

Table 0-24: ANOVA analysis and statistical parameters of the responses SUVA

Source	*Sum of Squares*	*Df*	*Mean Square*	*F-value*	*P-value*	
Model	1239.92	4	309.98	24.01	< 0.0001	significant
B-Time	144.22	1	144.22	11.17	0.0059	
C-Current	730.48	1	730.48	56.57	< 0.0001	
BC	186.36	1	186.36	14.43	0.0025	
C^2	298.79	1	298.79	23.14	0.0004	

Residual	154.95	12	12.91			
Lack of Fit	154.95	8	19.37			
Pure Error	0.0000	4	0.0000			
Cor Total	1394.87	16				

Model f-value of 24.1 determined the model is significant. Initial pH, once again, is determined not to be a significant factor for SUVA.

Table 0-25: ANOVA analysis and statistical parameters of the responses M2 TOC efficiency

Source	*Sum of Squares*	*Df*	*Mean Square*	*F-value*	*P-value*	
Model	30267.34	7	4323.91	87.57	< 0.0001	significant
A-Initial pH	229.76	1	229.76	4.65	0.0593	
B-Time	493.98	1	493.98	10.00	0.0115	
C-Current	13209.77	1	13209.77	267.54	< 0.0001	
AB	631.97	1	631.97	12.80	0.0060	
BC	576.08	1	576.08	11.67	0.0077	
B^2	1467.10	1	1467.10	29.71	0.0004	
C^2	14175.96	1	14175.96	287.11	< 0.0001	
Residual	444.37	9	49.37			
Lack of Fit	444.37	5	88.87			
Pure Error	0.0000	4	0.0000			
Cor Total	30711.71	16				

The model f-value of 87.57 suggested the model is significant. Identical to M1 TOC efficiency quadratic model, initial pH is not a significant model term but included to support hierarchy.

Table 0-26: ANOVA analysis and statistical parameters of the responses M2 COD efficiency

Source	*Sum of Squares*	*Df*	*Mean Square*	*F-value*	*P-value*	
Model	40983.58	6	6830.60	10.27	0.0009	significant
A-Initial pH	5426.20	1	5426.20	8.16	0.0171	
B-Time	3825.76	1	3825.76	5.75	0.0374	
C-Current	8606.24	1	8606.24	12.94	0.0049	
AC	5606.20	1	5606.20	8.43	0.0158	
A^2	11845.59	1	11845.59	17.81	0.0018	
B^2	2773.08	1	2773.08	4.17	0.0684	
Residual	6652.11	10	665.21			
Lack of Fit	6648.29	6	1108.05	1158.28	< 0.0001	significant
Pure Error	3.83	4	0.9566			
Cor Total	47635.69	16				

The model f-value of 10.27 implied that the model is significant. Initial pH is significant for COD efficiency, like M1 COD efficiency. However, the lack of a fit f-value of 1158.28 is significant and showed a high degree of uncertainty in the model. Similar to M1, lack of fit was significant for COD efficiency models, which foreshadowed an inadequate M2 COD efficiency regression model.

Table 0-27: c

Model f-value of 244.20 determined the model is significant. SUVA, with consistency, was not a significant response of initial pH and electrolysis time.

Table 0-28: ANOVA analysis and statistical parameters of the responses M3 TOC efficiency

Source	*Sum of Squares*	*Df*	*Mean Square*	*F-value*	*P-value*	
Model	8817.02	8	1102.13	20.54	0.0001	significant
A-Initial pH	1046.19	1	1046.19	19.50	0.0022	

B-Time	11.33	1	11.33	0.2111	0.6582	
C-Current	581.28	1	581.28	10.83	0.0110	
AC	950.03	1	950.03	17.71	0.0030	
BC	591.60	1	591.60	11.03	0.0105	
A^2	4104.77	1	4104.77	76.50	< 0.0001	
B^2	566.79	1	566.79	10.56	0.0117	
C^2	1339.47	1	1339.47	24.96	0.0011	
Residual	429.27	8	53.66			
Lack of Fit	429.27	4	107.32			
Pure Error	0.0000	4	0.0000			
Cor Total	9246.29	16				

The model f-value of 20.54 indicated the model is significant. However, unlike M1 and M2, electrolysis time is not a significant factor for TOC efficiency but included in the model for hierarchy. Initial pH played a significant role.

Table 0-29: ANOVA analysis and statistical parameters of the responses M3 COD efficiency

Source	*Sum of Squares*	*Df*	*Mean Square*	*F-value*	*P-value*	
Model	9411.67	6	1568.61	4.21	0.0226	significant
A-Initial pH	32.57	1	32.57	0.0873	0.7736	
B-Time	0.9029	1	0.9029	0.0024	0.9617	
C-Current	3656.15	1	3656.15	9.80	0.0107	
BC	3510.86	1	3510.86	9.42	0.0119	
A^2	1091.45	1	1091.45	2.93	0.1179	
B^2	2099.48	1	2099.48	5.63	0.0391	
Residual	3728.95	10	372.90			
Lack of Fit	3725.13	6	620.85	649.00	< 0.0001	significant
Pure Error	3.83	4	0.9566			

Cor Total	13140.62	16				

The model f-value of 4.21 implied that the model is significant. Time and initial pH were determined to be non-significant factors. Lastly, a lack-of-fit value of 649 determined there is considerable uncertainty in the quadratic fit.

Table 0-30: ANOVA analysis and statistical parameters of the responses M3 SUVA

Source	*Sum of Squares*	*Df*	*Mean Square*	*F-value*	*P-value*	
Model	210.63	7	30.09	18.90	0.0001	significant
A-Initial pH	11.49	1	11.49	7.22	0.0249	
B-Time	15.86	1	15.86	9.96	0.0116	
C-Current	26.38	1	26.38	16.57	0.0028	
AC	53.17	1	53.17	33.39	0.0003	
BC	18.11	1	18.11	11.37	0.0082	
A^2	13.92	1	13.92	8.74	0.0160	
C^2	74.47	1	74.47	46.76	< 0.0001	
Residual	14.33	9	1.59			
Lack of Fit	14.33	5	2.87			
Pure Error	0.0000	4	0.0000			
Cor Total	224.96	16				

The model f-value of 18.90 suggested the model is significant. All three factors played a significant role in determining SUVA.

7.5. Appendix E: Multi-factor tables to supplement 3D contour plots

Table 0-31: Multi-factor analysis tables to identify trends for M1 TOC efficiency

30 % decrease →

Initial pH

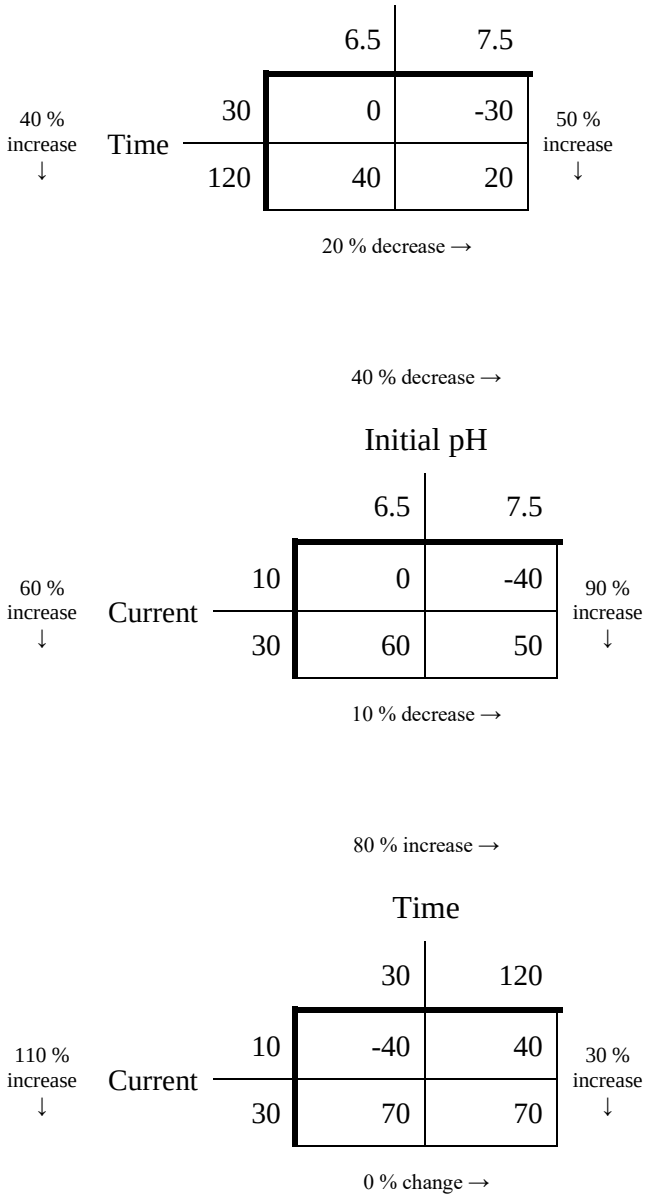

From 6.5 to 7.5 pH, TOC efficiency decreased from 0 to -30 % at 30 mins as opposed to 40 to 20 % at 120 mins at the same pH range. Whereas, at 10 mA cm2, TOC efficiency decreased from 0 to -40 % from 6.5 to 7.5. The reduction was minimized at higher current at 30 mA cm2, where TOC efficiency decreased from 40 to 20%.

From 30 to 120 mins, the TOC efficiency increased from -40 to 40 % at 10 mA cm2; however, at 30 mA cm2, there was no change and remained at 70 %.

From 10 to 30 mA cm2, TOC efficiency increased from 0 to 60 at 6.5 pH and -40 to 50 at 7.5 pH. On the other hand, TOC efficiency increased from -40 to 70 at 30 mins and 40 to 70 at 120 mins.

Table 0-32 Multi-factor analysis tables to identify trends for M1 TOC efficiency

0 % change →

Initial pH

		6.5	7.5	
80 % increase ↓	Time 30	-20	-20	40 % increase ↓
	120	60	20	

40 % decrease →

0 % change →

Initial pH

		6.5	7.5	
80 % increase ↓	Current 10	-20	-20	50 % increase ↓
	30	60	30	

30 % decrease →

50 % increase →

Time

		30	120	
50 % increase ↓	Current 10	0	50	10 % increase ↓
	30	50	60	

10 % increase →

From 6.5 to 8.5 pH, COD efficiency increased from -20 to 40 % at 30 mins; however, at 120 mins COD efficiency remained constant at 60 %. The trend was paralleled by current density,

as COD efficiency increased from -20 to 20 at 10 mA cm2 and 40 to 80 at 30 mA cm2, from 6.5 to 8.5 pH. Additionally, the lowest COD efficiency was experienced at neutral pH.

At 10 ma cm2, increasing the time from 30 to 120 mins increased COD efficiency from 0 to 50 %. On the other hand, at 30 ma cm2, the COD efficiency stabilized at 60 % despite the time elapsed.

Increasing the applied current from 10 to 30 mA cm2, at 30 mins, the COD efficiency increased from 0 to 50 %, whereas at 120 mins, the increase was lower from 50 to 60 %.

Table 0-33 Multi-factor analysis tables to identify trends for M1 SUVA

0 SUVA change →

Initial pH

		6.5	7.5	
7 SUVA increase ↓	Time 30	1	1	7 SUVA increase ↓
	120	8	8	

0 SUVA change →

0 SUVA change →

Initial pH

		6.5	7.5	
15 SUVA increase ↓	Current 10	2	2	15 SUVA increase ↓
	30	17	17	

0 SUVA change →

0 SUVA change →

Time

			30	120	
0 SUVA change↓	Current	10	10	10	20 SUVA increase ↓
		30	10	30	

20 SUVA increase →

From 10 to 30 mA cm2, SUVA increased from 10 to 30 L/mg-M at 120 mins. However, there was no increase at 30 mins.

Table 0-34 Multi-factor analysis tables to identify trends for M2 TOC efficiency

10 % decrease→

Initial pH

			6.5	8.5	
30 % decrease ↓	Time	30	0	-10	10 % increase ↓
		120	-30	0	

30 % increase →

0 % change →

Initial pH

			6.5	7.5	
100 % increase ↓	Current	10	-30	-30	100 % increase ↓
		30	70	70	

0 % change →

40 % decrease →

Time

		30	120
Current	10	20	-20

60 % increase ↓	30	80	80	100 % increase ↓

0 % change →

From 6.5 to 8.5 pH, there was a minimal decrease in TOC efficiency from 0 to -10 % at 30 mins, and an increase from -30 to 0 % at 120 mins. On the other hand, increasing pH from 6.5 to 8.5 did not affect TOC efficiency when the current density was kept constant at 10 and 30 mA cm2, where TOC efficiency was -30 and 70 %, respectively.

Table 0-35 Multi-factor analysis tables to identify trends for M2 COD efficiency

60 % increase →

Initial pH

		6.5	8.5	
40 % increase ↓	Time 30	0	60	30 % increase ↓
	120	40	90	

50 % increase →

100 % increase →

Initial pH

		6.5	8.5	
100 % increase ↓	Current 10	-50	50	0 % change ↓
	30	50	50	

0 % change →

40 % increase →

Time

		30	120	
60 % increase ↓	Current 10	-40	0	60 % increase ↓
	30	20	60	

40 % increase →

From 6.5 to 8.5 pH, at 30 mins, COD efficiency increased from 0 to 60%. The same magnitude of increase was seen at 120 mins, from 40 to 90 %. On the other hand, at 10 mA cm2, the COD efficiency increased from -50 to 50. Whereas, no effect was discovered at 30 mA cm2.

At 6.5 pH, from 30 – 120 mins, the COD efficiency increased from 0 to 40 %, whereas at 8.5, the increase was from 60-75 % within the same timeframe. Additionally, from 30 – 120 mins, at 10 mA cm2, there was an increase in COD efficiency from -40 to 0 %. The same magnitude of increase at 30 mA cm2, from 20 to 60.

Table 0-36 Multi-factor analysis tables to identify trends for M2 SUVA

0.2 SUVA increase→

Initial pH

		6.5	8.5	
0.1 SUVA increase ↓	Time 30	2.4	2.6	0.9 SUVA increase ↓
	120	2.5	3.5	

1 SUVA increase →

4 SUVA increase →

Initial pH

		6.5	8.5	
10 SUVA increase ↓	Current 10	2	6	4 SUVA increase ↓
	30	12	10	

2 SUVA increase →

1 SUVA decrease →

		Time	
		30	120
7 SUVA increase ↓	Current 10	3	2
	30	10	12

10 SUVA increase ↓

2 SUVA increase →

From 6.5 to 8.8 pH, at 30 mins, SUVA increased from 2.4 to 2.6. At 120 mins, there was an increase from 2.5 to 3.5. At 10 mA cm2, SUVA increased from 2 to 6, and at 30 mA cm2, SUVA decreased from 12 to 10. Although there seemed to an interaction effect between current and initial pH, the reactions were minimal.

From 30 to 120 mins, at 6.5 pH, SUVA increased from 2.4 to 2.5, and at 8.5 pH, SUVA increased from 2.6 to 3.5. On the other hand, at 10 mA cm2, SUVA increased from 3 to 2, and at 30 mA cm2, SUVA decreased from 10 to 12.

With a higher current density, it is possible to form more oxidants. From 10 to 30 mA cm2, at 6.5, SUVA increased from 2 to 12. At 8.5 pH, SUVA increased from 6 to 10. Whereas at 30 mins, SUVA increased from 3 to 10 and at 120 mins, SUVA increased from 2 to 12

Table 0-37 Multi-factor analysis tables to identify trends for M3 TOC efficiency

20 % decrease →

		Initial pH	
		6.5	8.5
10 % increase ↓	Time 30	20	0
	120	30	10

10 % increase ↓

20 % decrease →

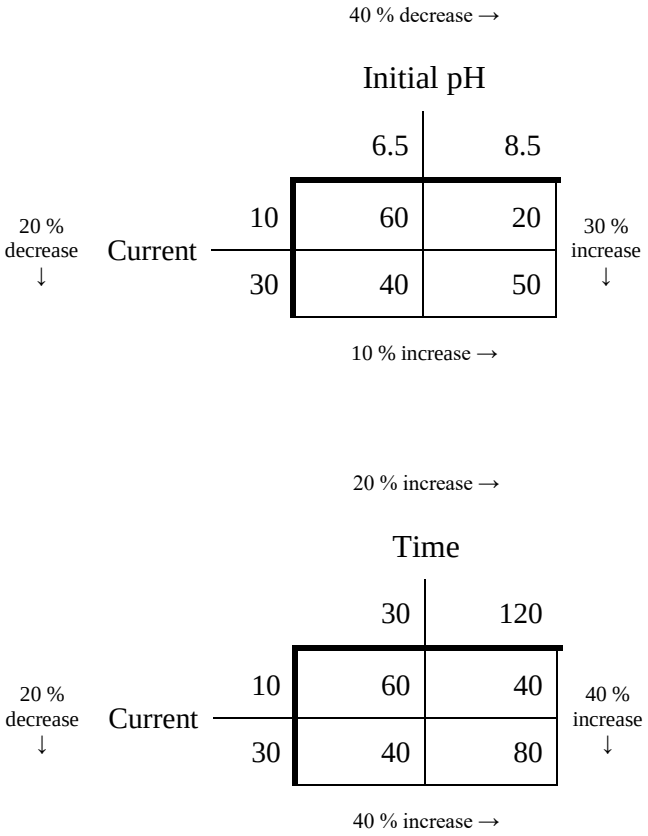

From 6.5 to 8.5, at 30 mins, TOC efficiency decreased from 20 to 0 %. Whereas at 120 mins, the TOC efficiency changed from 30 to 10 %. From the same pH range, at 10 mA cm2, the TOC efficiency decreased from 60 to 20 %. Whereas, at 30 mA cm2, TOC efficiency increased from 40 to 50 %.

From 30 to 120 mins, at 6.5 pH, TOC efficiency increased from 20 to 30 %. Similarly, at 8.5 pH, the increase was minimal from 0 to 10 %. Additionally, at 10 mA cm2, increasing time from 30 to 120, saw a TOC efficiency decrease from 60 to 40 %. Whereas, at 30 mA cm2, there was a recorded increase from 40 to 80 %.

From 10 mA cm2 to 30 mA cm2, at 6.5 pH, the TOC efficiency changed from 60 to 40 %. At 8.5 pH, current density had a positive effect, from 20 to 50 %. Likewise, at 30 mins, TOC

efficiency decreased from 60 to 40 %. Whereas, at 120 mins, there was an increase from 40 to 80 %.

Table 0-38 Multi-factor analysis tables to identify trends for M3 COD efficiency

5 % increase →

	Initial pH		
		6.5	8.5
0 % change ↓	Time 30	50	55
	120	50	55

0 % change ↓

5 % increase →

0 % change →

	Initial pH		
		6.5	8.5
20 % increase ↓	Current 10	60	60
	30	80	80

20 % increase ↓

0 % change →

30 % decrease →

	Time		
		30	120
10 % decrease ↓	Current 10	70	40
	30	60	99

59 % increase ↓

39 % increase →

From 6.5 to 8.5, at 30 mins, the COD efficiency increased minimally from 50 to 55%. At 120 mins, the efficiency goes through an identical trend from 50 to 55%. From the same pH range, at 10 mA cm2 and 30 mA cm2, there were no changes in COD efficiency.

From 30 to 120 mins, at both 6.5 and 8.5 pH, there was no increase in COD removal. At 10 mA cm2, COD efficiency was decreased from 70 to 40 %. Whereas, at 30 mA cm2, there was an increase from 60 to 99.

From 10 mA cm2 to 30 mA cm2, at both 6.5 and 8.5 pH, COD efficiency increased from 60 to 80 %. At 30 mins, COD efficiency decreased from 70 to 60 %. Whereas, at 120 mins, increasing current increased COD efficiency drastically from 40 to 99%.

Table 0-39 Multi-factor analysis tables to identify trends for M3 SUVA

0 % change →

		Initial pH		
		6.5	8.5	
3 SUVA increase ↓	Time 30	3	1	3 SUVA increase ↓
	120	6	4	

2 SUVA decrease →

8 SUVA decrease →

		Initial pH		
		6.5	8.5	
8 SUVA decrease ↓	Current 10	12	4	2 SUVA increase ↓
	30	4	6	

2 SUVA increase→

6 SUVA increase →

		Time		
		30	120	
	Current 10	4	10	6 SUVA

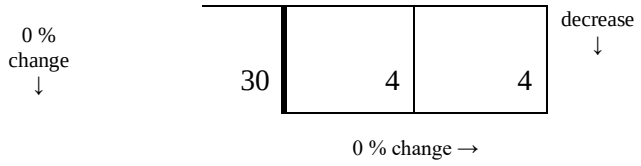

At 30 mins, SUVA decreased from 3 to 1. Whereas at 120 mins, SUVA decreased from 6 to 4. At 10 mA cm2, SUVA decreased significantly from 12 to 4. However, at 30 mA cm2, SUVA increased from 6 to 4.

From 30 to 120 mins, at 6.5 pH, SUVA increased from 3 to 6, whereas at 8.5 pH, SUVA increased from 1 to 4. On the other hand, at 10 mA cm2, SUVA increased from 4 to 10. However, there was no increase in SUVA at 30 mA cm2.

From 10 to 30 mA cm2, at 6.5 pH, SUVA decreased from 12 to 4. At 8.5 pH, SUVA increased minimally from 4 to 6. Increasing current at 30 mins, did not affect SUVA. However, at 120 mins, SUVA decreased from 10 to 4.